A Thesis on

CFD Analysis for Heat Transfer Augmentation Inside Plain and Finned Circular Tubes with Twisted Tape Inserts

Submitted

by

TALAKALA DHANI BABU

(Roll No: 211CH1257)

In partial fulfillment of the requirements for the degree of

Master of Technology

in

Chemical Engineering

Under the guidance of

Prof. S. K. Agarwal

Department of Chemical Engineering

National Institute of Technology Rourkela

May, 2013

NATIONAL INSTITUTE OF TECHNOLOGY, ROURKELA

DEPARTMENT OF CHEMICAL ENGINEERING

CERTIFICATE

This is to certify that the thesis entitled "**CFD ANALYSIS FOR HEAT TRANSFER AUGMENTATION INSIDE PLAIN AND FINNED CIRCULAR TUBES WITH TWISTED TAPE INSERTS"** submitted to the National Institute of Technology, Rourkela by **TALAKALA DHANI BABU**, Roll No. **211CH1257** in partial fulfillment of the requirements for the award of the degree of **Master of Technology** in **Chemical Engineering**, is a bona fide record of research work carried out by him under my supervision and guidance. The thesis, which is based on candidate's own work, has not been submitted elsewhere for any degree/diploma.

Date: 25/05/2013

_____

Prof. S.K. Agarwal

Department of Chemical Engineering

National Institute of Technology

Rourkela – 769008

ACKNOWLEDGEMENT

I take this opportunity to express my sense of gratitude and indebtedness to Prof**. S.K.Agarwal** for helping me a lot to complete the project, without whose sincere and kind effort, this project would not have been success.

I am also thankful to all the staff and faculty members of Chemical Engineering Department, National Institute of Technology, Rourkela for their consistent encouragement.

I would like to thank Mr. Akhilesh Khapre and Mr. Sambhurish Mishra Ph.D. Students of the department, for their assistance in learning ANSYS

Date: 25/05/2013

TALAKALA DHANI BABU

Roll No. 211CH1257

4th Semester M. TECH

Chemical Engineering Department

National Institute of Technology, Rourkela

ABSTRACT

Computational fluid dynamic (CFD) studies were carried out by using the ANSYS FLUENT 13.0 to find the effects of twisted tape insert on heat transfer, friction loss and thermal performance factor characteristics in a circular tube at constant wall temperature. Simulation was performed with Reynolds number in a range from 800 to 10,000 using water as a working fluid. Four turbulent models are examined such as a standard k-ϵ, RNG k-ϵ, standard k-ω and SST k-ω and those compared with standard twisted tape correlations developed by Manglik and Bergles. Plain tube with four different full width twisted tape inserts (FWTT) of twist ratios (y = 2, 3, 4 and 5) were examined, based on constant flow rate. The heat transfer coefficient were found to be 2.67 to 3.35, 2.43 to 2.19, 2.10 to 2.64, and 1.87 to 2.35 times respectively in laminar region, and 1.92 to 1.56, 1.74 to 1.41, 1.65 to 1.34, and 1.6 to 1.3 times of that in the plain tube in the turbulent region. For the same twist ratio (H/w) three different reduced width twisted tapes (RWTT) (of width 12, 14 and 16 mm), were examined in the finned tube. The simulation results revealed that both heat transfer rate and friction factor in the finned tube equipped with twisted tapes were significantly higher than those in the plain tube. Over the range of Reynolds number investigated, based on overall thermal performance factor (η) it is revealed that the plain tube with FWTT (η = 1.12-1.51 in laminar regime & 0.91 – 1.08 in turbulent regime) are suitable in laminar flow region and finned tube with RWTT (η = 0.58-0.91 in laminar regime & 0.83 – 1.31 in turbulent regime) are suitable for turbulent regime.

Key words: CFD, Heat transfer agumentation, Twisted tape, Reduced width twisted tape, Thermal performance

CONTENTS

List of figures

List of tables

NOMENCLATURE

C_p	Specific heat capacity, J/Kg.K
D	ID of the tube, m
d	Internal diameter of the tube, m
E	Energy per unit mass, J/kg
F	External body force, N/m^3
f_0	Friction factor for smooth tube, Dimensionless
f_a	Friction factor for the tube with inserts, Dimensionless
Gz	Graetz Number, (Re x Pr x D/L), Dimensionless
H	Pitch of twisted tape for 180°rotation
h	Heat transfer coefficient, $W/m^2°C$
I	Unit tensor, Dimensionless
J	Diffusion flux, m^2/sec
k	Thermal conductivity, W/m K
k	Turbulence kinetic energy
k_{eff}	Effective conductivity, W/m^2 K
L	Length of the tube, m
Nu_0	Nusselt number for plain tube, Dimensionless
Nu_a	Nusselt number for the tube with inserts, Dimensionless
Pr	Prandtl number, Dimensionless
Re	Reynolds number, Dimensionless
S_W	Swirl parameter, Dimensionless
v	Velocity, m/s
w	Width of the twisted tape, m
y	Twist ratio (H/w), Dimensionless
Δp	Pressure difference, Pa
P	Static pressure, Pa

Greek letters

μ	Viscosity, kg/ m. s
η	Thermal Performance factor, Dimensionless
δ	Thickness of twisted tape, m
ϵ	Turbulence dissipation rate
μ_t	Turbulent viscosity
ρ	Density, kg/m^3
ω	Specific dissipation rate
τ	Stress tensor

CHAPTER 1

INTRODUCTION

Effective utilization, conservation and recovery of heat are critical engineering problems faced by the process industry. The economic design and operation of process plants are often governed by the effective usage of heat. A majority of heat exchangers used in thermal power plants, chemical processing plants, air conditioning equipment, and refrigerators, petrochemical, biomedical and food processing plants serve to heat and cool different types of fluids. Both the mass and overall dimensions of heat exchangers employed are continuously increasing with the unit power and the volume of production. This involves huge investments annually for both operation and capital costs. Hence it is an urgent problem to reduce the overall dimension characteristics of heat exchangers. The need to optimize and conserve these expenditures has promoted the development of efficient heat exchangers. Different techniques are employed to enhance the heat transfer rates, which are generally referred to as heat transfer enhancement, augmentation or intensification technique.

1.1. Heat transfer enhancement[1]

Heat transfer enhancement is one of the key issues of saving energies and compact designs for mechanical and chemical devices and plants. In the recent years, considerable emphasis has been placed on the development of various augmented heat transfer surfaces and devices. Energy and materials saving considerations, space considerations as well as economic incentives have led to the increased efforts aimed at producing more efficient heat exchange equipment through the augmentation of heat transfer.

The heat exchanger industry has been striving for enhanced heat transfer coefficient and reduced pumping power in order to improve the thermo hydraulic efficiency of heat exchangers. A good heat exchanger design should have an efficient thermodynamic performance, i.e. minimum generation of entropy or minimum destruction of energy in a system incorporating a heat exchanger. It is almost impossible to stop energy loss completely, but it can be minimized through an efficient design. The major challenge in designing a heat exchanger is to make the equipment compact and to achieve a high heat transfer rate using minimum pumping power.

Heat transfer enhancements can improve the heat exchanger effectiveness of internal and external flows. They increase fluid mixing by increasing flow vorticity, unsteadiness, or

turbulence or by limiting the growth of fluid boundary layers close to the heat transfer surfaces. In some specific applications, such as heat exchangers dealing with fluids of low thermal conductivity like gases or oils, it is necessary to increase the heat transfer rates. This is further compounded by the fact that viscous fluids are usually characterized by laminar flow conditions with low Reynolds numbers, whose heat transfer coefficient is relatively low and thus becomes the dominant thermal resistance in a heat exchanger. The adverse impact of low heat transfer coefficients of such flows on the size and cost of heat exchangers adds to excessive energy, material, and monetary expenditures. As the heat exchanger becomes older, the resistance to heat transfer increases owing to fouling or scaling.

Augmented surfaces can create one or more combinations of the following conditions that are indicative of the improvement of performance of heat exchangers

- Decrease in heat transfer surface area, size, and hence the weight of a heat exchanger for a given heat duty and pressure drop or pumping power
- Increase in heat transfer rate for a given size, flow rate, and pressure drop.
- Reduction in pumping power for a given size and heat duty
- Reduction in fouling of heat exchangers

1.2. Heat transfer augmentation techniques[2]

Heat transfer augmentation techniques are generally classified into three categories namely: Active techniques, Passive techniques and Compound techniques.

1.2.1. Active techniques

As the name indicates, these techniques involve some external power input for enhancement of heat transfer. These has not shown much potential due to complexity in design.

They are classified as below:

- Mechanical aids

- Surface vibrations
- Fluid vibration
- Electrostatic fields (DC or AC)
- Jet impingement

1.2.2. Passive techniques

Passive techniques do not require any direct input of external power. They generally use geometrical or surface modifications to the flow channel by incorporating inserts or additional devices. Except for the case of extended surfaces, they promote higher heat transfer coefficients by disturbing or altering the existing flow behaviour.

Passive techniques are classified as below:

- Treated surfaces
- Rough surfaces
- Extended surfaces
- Displaced enhancement devices.
- Swirl flow devices
- Coiled tubes
- Surface-tension devices
- Additives for gases
- Additives for liquids.

1.2.3. Compound techniques

Two or more of the above techniques may be utilized simultaneously to produce an enhancement that is larger than the individual technique applied separately.

Some examples of compound techniques are given below:

- Rough tube wall with twisted tape
- Rough cylinder with acoustic vibrations
- Internally finned tube with twisted tape insert

- Finned tubes in fluidized beds
- Externally finned tubes subjected to vibrations
- Gas-solid suspension with an electrical field
- Fluidized bed with pulsations of air

1.3. Performance evaluation criteria [3]

In most of the practical applications of enhancement techniques, the following performance objectives, along with a set of operating constraints and conditions, are usually considered for evaluating the thermo hydraulic performance of a heat exchanger:

- Increase in the heat duty of an existing heat exchanger without altering the pumping power or flow rate requirements.
- Reduction in the approach temperature difference between the two heat exchanging fluid streams for a specified heat load and size of exchanger.
- Reduction in the size or heat transfer surface area requirements for a specified heat duty and pressure drop.
- Reduction in the process stream pumping power requirements for a given heat load and exchanger surface area.

Different Criteria used for evaluating the performance of a single - phase flows are:

1.3.1. Fixed Geometry (FG) Criteria: The area of flow cross-section (N and d) and tube length L are kept constant. This criterion is typically applicable for retrofitting the smooth tubes of an existing exchanger with enhanced tubes, thereby maintaining the same basic geometry and size (N, d, L). The objectives then could be to increase the heat load Q for the same approach temperature ΔT_i and mass flow rate *m* or pumping power P; or decrease ΔT_i or P for fixed Q and m or P; or reduce P for fixed Q.

1.3.2. Fixed Number (FN) Criteria: The flow cross sectional area (N and d_i) is kept constant, and the heat exchanger length is allowed to vary. Here the objectives are to seek a reduction in either the heat transfer area ($A \rightarrow L$) or the pumping power P for a fixed heat load.

1.3.3. Variable Geometry (VN) Criteria: The flow frontal area (N and L) is kept constant, but their diameter can change. A heat exchanger is often sized to meet a specified heat duty Q for a

fixed process fluid flow rate *m*. Because the tube side velocity reduces in such cases so as to accommodate the higher friction losses in the enhanced surface tubes, it becomes necessary to increase the flow area to maintain constant *m*. This is usually accomplished by using a greater number of parallel flow circuits.

Table 1.1 Performance Evaluation Criteria [3]

Case	Geometry	m	P	Q	ΔT_i	Objective
FG-1a	N, L, d	x			x	Q↑
FG-1b	N, L, d	x		x		ΔTi↓
FG-2a	N, L, d		x		x	Q↑
FG-2b	N, L, d		x	x		ΔTi↓
FG-3	N, L, d			x	x	P↓
FN-1	N, d		x	x	x	L↓
FN-2	N, d	x		x	x	L↓
FN-3	N, d	x		x	x	P↓
VG-1	-------	x	x	x	x	NL) ↓
VG-2a	N, L,	x	x		x	Q↑
VG-2b	N, L,	x	x	x		Δ Ti↓
VG-3	N, L,	x		x	x	P↓

Bergles et al [4] suggested a set of eight (R_1-R_8) numbers of performance evaluation criteria as shown in Table 1.2.

Table 1.2 Performance Evaluation Criteria of Bergles et al [4]

		Criterion number							
		R_1	R_2	R_3	R_4	R_5	R_6	R_7	R_8
Fixed	Basic Geometry	x	x	x	x				
	Flow Rate	x						x	x
	Pressure Drop		x				x		x
	Pumping Power			x		x			
	Heat Duty				x	x	x	x	x
Objective	Increase Heat Transfer	x	x	x					
	Reduce pumping power				x				
	Reduce Exchange Size					x	x	x	x

1.3.4. Thermal Performance factor (η): This is defined by equation 1.1 as follows and is similar to enhancement of heat transfer at constant pumping power is criteria FG-2a

$$\eta = \frac{(Nu_a/Nu_0)}{(f_a/f_0)^{(1/3)}} \quad (1.1)$$

Where Nu_a, f_a, Nu_0 and f_0 are the Nusselt numbers and friction factors for a duct configuration with and without inserts respectively.

It may be noted that FG-1a & FG-2a are similar to R_1 & R_3 respectively. Evaluation criteria R_1 (i.e. Nu_a/Nu_0) & R_3 (i.e. η) have been used for present numerical simulation work to determine heat transfer enhancement for different types of twisted tapes.

1.4. Applications of heat transfer enhancement

The petrochemical and chemical industries are under economic pressure to increase the energy efficiency of their processing plants to compete in today's global market. Hence, these industries must invest in innovative thermal technologies that would significantly reduce unit energy consumption in order to reduce overall cost. In recent years, heat transfer enhancement technology has been widely applied to heat exchanger applications in boiling and refrigeration process industries. Most significantly, the uses of enhancement extend well beyond surface reduction i.e., they can also be used for capital cost reduction, the improvement of exchanger operability, the mitigation of fouling, the improvement of condenser design and the improvement of flow distribution within heat exchangers.

Important applications of heat transfer enhancement are listed below:

- Heating, Ventilating, Refrigeration and air conditioning
- Automotive Industries
- Power sector
- Process Industries
- Industrial Heat Recovery
- Aerospace and others.

1.5. Swirl flow devices

This is coming under category of passive heat transfer enhancement technique. These include a number of geometric arrangements or tube inserts for forced flow that create rotating and/or secondary flow i.e. inlet vortex generators, twisted-tape inserts and axial-core inserts with a screw-type winding etc.

1.5.1. Twisted tape inserts

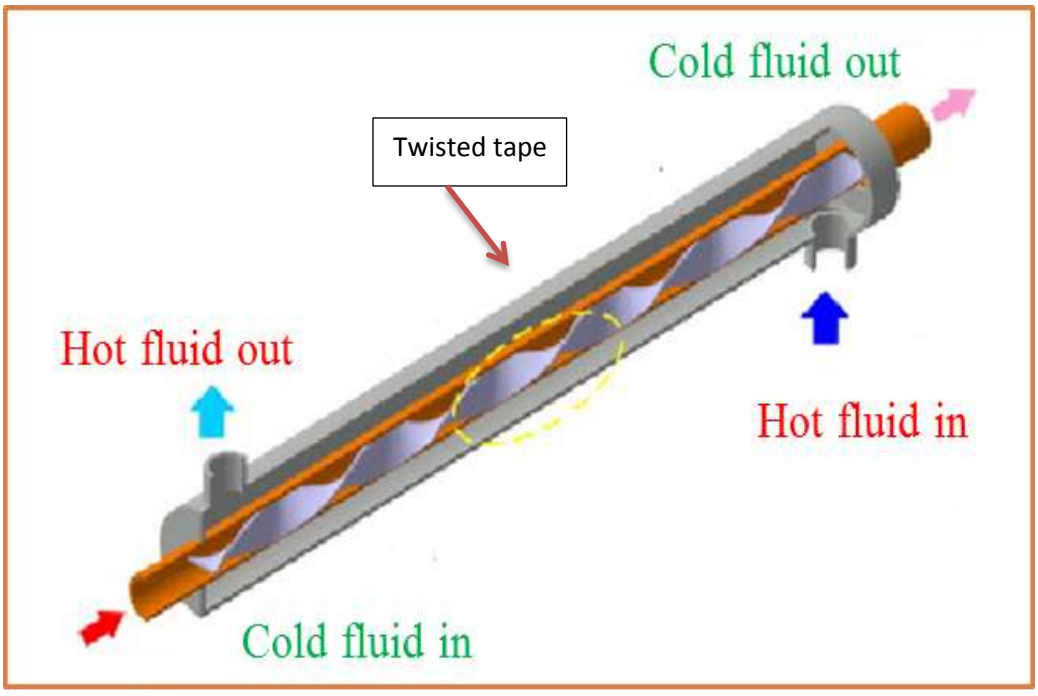

Fig.1.1. View of the twisted tape inside a plain tube

To enhance the heat transfer rate, some kind of insert is placed in the flow passages and they also reduce the hydraulic diameter of the flow passages. Heat transfer enhancement in a tube flow is due to flow blockage, partitioning of the flow and secondary flow. Flow blockages increase the pressure drop and leads to viscous effects, because of a reduced free flow area [5]

The selection of the twisted tape depends on performance and cost. The performance comparison for different tube inserts is a useful complement to the retrofit design of heat exchangers. The development of high performance thermal systems has stimulated interest in methods to improve heat transfer.

1.5.2. Geometry of the twisted tape

A schematic diagram of a twisted tape insert inside a tube is shown in Fig.1.2. The enhancement is defined geometrically in terms of thickness of the tape δ and its twist ratio. The twist ratio (y) is defined as the axial length (H) for a 180^0 turn of the tape divided by the internal diameter (d) of the tube. This is the most common definition used in research literature and that used here.

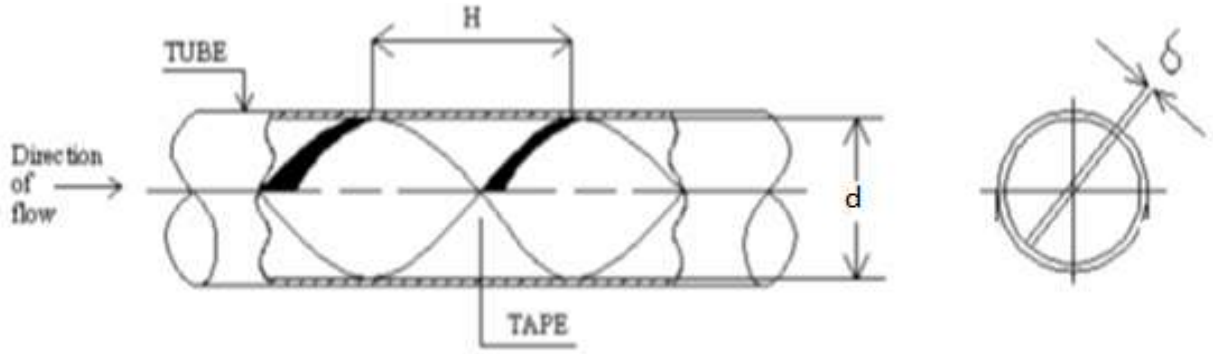

Fig.1.2.Diagram of a twisted tape insert inside a tube

Terms used in twisted tape insert

Pitch (H): Axial distance for 180^0 rotation of the tape

Twist Ratio (y): The twist ratio is defined as the ratio of pitch to inside diameter of the tube.

1.5.3. Different types of twisted tape insert [6]

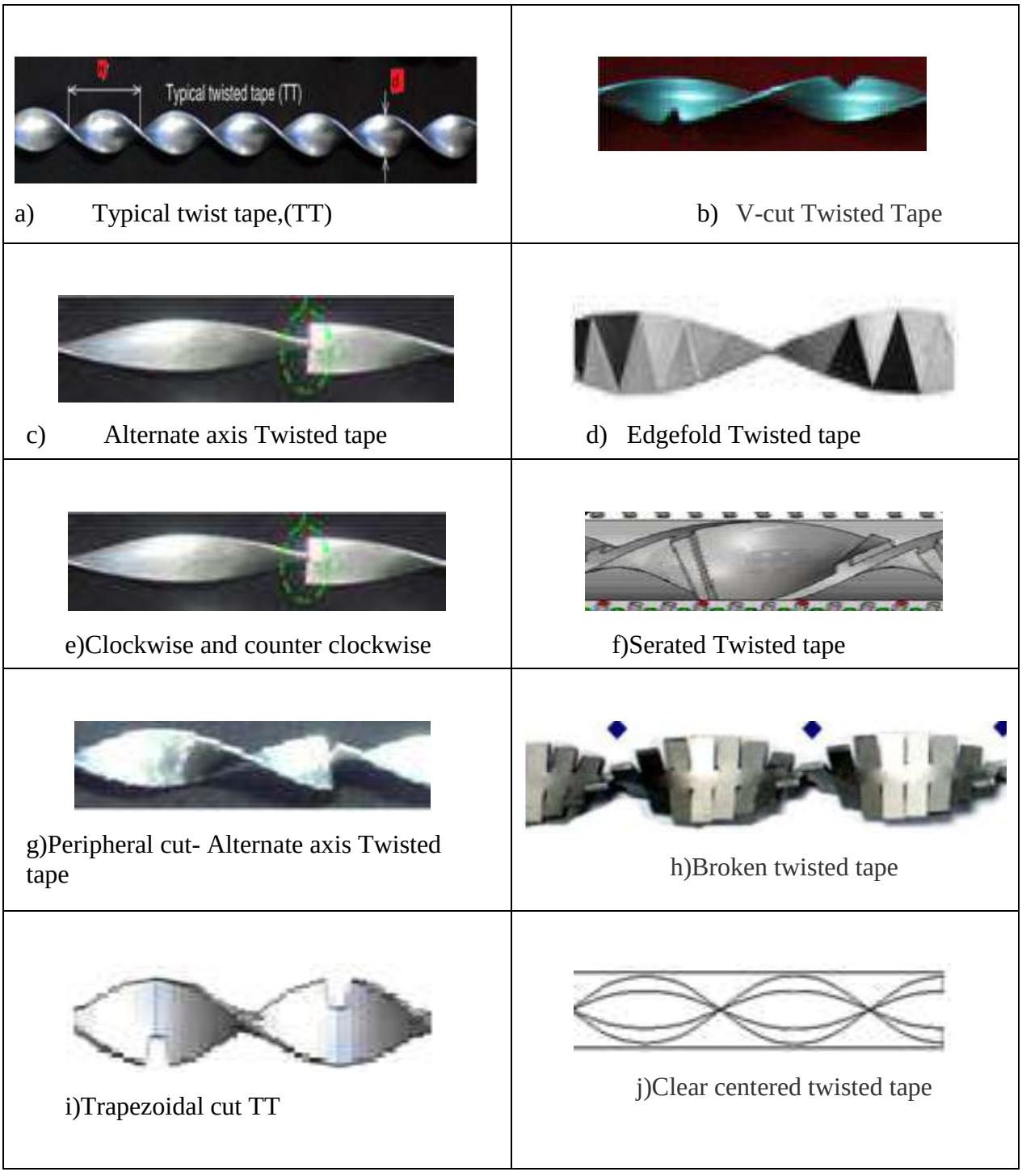

a) Typical twist tape,(TT)

b) V-cut Twisted Tape

c) Alternate axis Twisted tape

d) Edgefold Twisted tape

e)Clockwise and counter clockwise

f)Serated Twisted tape

g)Peripheral cut- Alternate axis Twisted tape

h)Broken twisted tape

i)Trapezoidal cut TT

j)Clear centered twisted tape

Fig.1.3. Different types of twisted tape insert [6]

1.6. Fluid flow in circular tubes

Fluid flow in circular tubes has been a topic of continuing interest because of its applications in number of cases especially in the design of heat exchangers. Passive techniques of heat transfer augmentation can play an important role in the design of heat exchangers if a proper tube insert configuration can be selected according to the heat exchanger working conditions. For generality and simplicity, the present study will focus on a single tube instead of a multi tube heat exchanger as the results obtained by employing inserts inside a horizontal plain tube can be extended to a multi-tube heat exchanger with the similar type of inserts.

1.7. Computational fluid dynamics

Fluid (gas and liquid) flows are governed by partial differential equations (PDE) which represent conservation laws for the mass, momentum and energy. Computational Fluid Dynamics (CFD) is used to replace such PDE systems by a set of algebraic equations which can be solved using digital computers. The basic principle behind CFD modeling method is that the simulated flow region is divided into small cells. Differential equations of mass, momentum and energy balance are discretized and represented in terms of the variables at any predetermined position within or at the center of cell. These equations are solved iteratively until the solution reaches the desired accuracy (ANSYS FLUENT 13.0). CFD provides a qualitative prediction of fluid flows by means of

- Mathematical modeling (partial differential equations)
- Numerical methods (discretization and solution techniques)
- Software tools (solvers, pre- and post-processing utilities)

1.6.1. ANSYS FLUENT 13.0 Software

FLUENT is one of the widely used CFD software package. ANSYS Fluent software contains the wide range of physical modeling capabilities which are needed to model flow, turbulence and heat transfer for industrial applications. Features of ANSYS FLUENT software are:

Turbulence: ANSYS Fluent offers a number of turbulence models to study the effects of turbulence in a wide range of flow regimes.

Mesh flexibility: ANSYS Fluent software provides mesh flexibility. It has the ability to solve flow problems using unstructured meshes. Mesh types that are supported in FLUENT includes triangular, quadrilateral, tetrahedral, hexahedral, pyramid, prism (wedge) and polyhedral. The techniques which are used to create polyhedral meshes save time due to its automatic nature. A polyhedral mesh contains fewer cells than the corresponding tetrahedral mesh. Hence convergence is faster in case of polyhedral mesh.

Dynamic and Moving mesh: The user sets up the initial mesh and instructs the motion, while FLUENT software automatically changes the mesh to follow the motion instructed.

Post-Processing and Data export: Users can post-process their data in FLUENT software, creating among other things contours, path lines, and vectors to display the data.

1.8. Objectives of the present study

Objectives of the present work are given below

- Computational Fluid Dynamics modeling and simulation of a horizontal plain tube with Reynolds number ranging from 800 to 10000 are conducted and the results (Nusselt number and friction factor) are compared with those obtained by using standard correlations available in literature for internal flow.
- Computational Fluid Dynamics modeling and simulation of a horizontal plain tube fitted with twisted tape insert with different twist ratios and identify the geometry of the twisted tape insert that provides the maximum heat transfer enhancement when compared with plain tube
- Computational Fluid Dynamics modeling and simulation of a finned horizontal tube fitted with twisted tape insert of different twist ratios and different tape widths. identify the geometry that provides the maximum heat transfer enhancement when compared with plain tube

1.8. LAYOUT OF THESIS

An introduction to this thesis is provided in Chapter-1, which includes the need and applications of heat transfer enhancement. The various techniques under active and passive heat transfer augmentation techniques, has been cited

Chapter –2 Literature review on experimental and numerical studies with different types of twisted type inserts in horizontal single pipe and Shell and tube heat exchangers under laminar and turbulent flow conditions with special reference to twisted tapes.

Chapter 3: In this chapter, the steps of the CFD analysis procedure are explained, the discretisation technique used by the CFD adopted in this work to discretise each of the terms in the governing equations is explained, and the strategy used to solve the resulting numerical equations is described.

Chapter–4 is related to numerical investigations to determine the heat transfer and friction factor characteristics of fluid flowing inside the horizontal circular tube. The results obtained from numerical investigations are validated by comparing with the available correlations for tube internal flow.

Chapter – 5 is related to numerical investigations with twisted tape inserts of twist ratio, y=2, 3, 4 and 5 fitted inside the horizontal circular tube. Twisted tape inserts of twist ratio = 5 inside the horizontal circular tube are considered for numerical analysis for model verification by comparing with Manglik and Bergles correlation [8]. The numerical results obtained from twisted tape inserts are compared with the plain tube results to estimate the increase of heat transfer coefficient and friction factor in the presence of twisted tape inserts. The effect of the inserts on thermal performance factor (Nu_a/Nu_0) & η are also presented.

Chapter – 6 is related to numerical investigations with twisted tape inserts of twist ratio (y=2, 3, 4 and 5) and varying widths (w = 12mm, 14 mm and 16 mm) fitted inside the finned horizontal circular tube. The numerical results obtained from twisted tape inserts are compared with the plain tube results to estimate the enhancement of heat transfer.

Chapter – 7 deals with the conclusions drawn.

CHAPTER 2

LITERATURE REVIEW

With the desired objectives as explained in the preceding chapter, literature survey is carried out to ascertain the progress in the field of heat transfer enhancement with twisted tape inserts. The literature in enhanced heat transfer is growing faster. At least fifteen percent of the heat transfer literature is directed towards the techniques of heat transfer augmentation now. A lot of research has been done in heat transfer equipment by using twisted tape inserts, both experimentally and numerically.

2.1. Twisted tape in laminar flow

A summary of important investigations of twisted tape in a laminar flow is represented in Table 2.1. Twisted tape increases the heat transfer coefficient with an increase in the pressure drop. Different configurations of twisted tapes, like full-length twisted tape, short length twisted tape, full length twisted tape with varying pitch, reduced width twisted tape and regularly spaced twisted tape have been studied widely by many researchers.

Manglik and Bergles [7] developed the correlation between friction factor and Nusselt number for laminar flows including the swirl parameter, which defined the interaction between viscous, convective inertia and centrifugal forces. These correlations pertain to the constant wall temperature case for fully developed flow, based on both previous data and their own experimental data. The heat transfer correlation as proposed by them is

$$Nu = 0.106(s_w)^{0.767}(Pr)^{0.3}\left(\frac{\mu}{\mu_w}\right)^{0.14} \quad (2.1)$$

Where Sw is the swirl parameter and is defined as $S_W = Re_s/y^{0.5}$. Based on the same data, a correlation for friction factor was given as

$$f_s = \frac{15.767}{Re_s}\left(\frac{\pi+2-\delta/d}{\pi-4\delta/d}\right)^2\left(1+10^{-6}{S_w}^{2.55}\right)^{1/6} \quad (2.2)$$

Where, δ and d are the thickness and the tube inner diameter of the twisted tape respectively.

Table.2.1. Summaries of important investigations of twisted tape in laminar flow

S. No	Authors	Fluid	Configuration of tape	Type of investigation	Observations
1	Saha and Dutta[8]	Water 2.5<Pr <5.18	Short length, Full length, Smoothly varying pitch, Regularly Spaced Twisted tapes	Experimental in a circular tube	• Friction and Nu low for short length tape • Short length tape requires small pumping power • Multiple twist and single twist has no difference on thermohydraulic performance • It was observed that twisted tape is effective in laminar flow
2	Tariq et al.[9]	Air 1300 <Re< 10^4	Twisted tape	Experiment in internally threaded tube	• Efficiency lower for threaded tube than twisted tape, but better than some fluted geometries • Good promoter of turbulence • Heat transfer coefficient in internally threaded tube approximately 20 per cent higher than that in smooth tube
3	Saha and Bhunia[10]	Servotherm medium oil 45<Re<840	Twisted tape (twist ratio 2.5< y< 10)	Experiment in circular tube	• Heat transfer characteristics depend on twist ratio, Re and Pr • Uniform pitch performs better than gradually decreasing pitch

4	Ray and Date[11]	Water 100<Re<3000 Pr<5.0	Full-length twisted tape with width equal to side of duct	Numerical work for square duct	• Proposed correlations for friction and Nu • Higher hydrothermal performance for square duct than circular one • Local Nusselt number peaks at cross-sections where tape aligned with diagonal of duct
5	Lokanath and Misal[12]	Water 3.0 < Pr < 6.5 lube oil (Pr = 418)	Twisted tape	Experiment in plate heat exchanger and shell and tube heat exchanger	• Large value of overall heat transfer coefficient produced in water-to-water mode with oil-to-water mode
6	Saha et al.[13]	Fluids with 2.05<Pr <5.18	Twisted tape (regularly spaced)	Experiment in circular tube	• Pinching of twisted tape gives better results than connecting thin rod for thermohydraulic performance • Reducing tape width gives poor results; larger than zero phase angle not effective
7	Al-Fahed and Chakroun[14]	Oil	Twisted tape with twist ratios 3.6, 5.4,7.1 and microfin	Experiment in single shell and tube heat exchanger	• For low twist ratio resulting low pressure drop, tight fit will increase more heat transfer • For high twist it is different • Microfins are not used for laminar

8	Liao and Xin[15]	Water,Ethylene glycol, Turbine oil 80<Re<50000	Segmented twisted tape and three dimensional extended surfaces	Experiment in tube flow	• In a tube with three-dimensional extended surfaces and twisted tape increases average Stanton number up to 5.8 times compared with empty smooth tube
9	Ujhidy et al.[16]	Water	Twisted tape	Experiment in channel	• Explained flow structure • Proved existence of secondary flow in tubes with helical static elements.
10	Suresh Kumar et al.[17]	Water	Twisted tape	Experiment in large-diameter annulus	• Observed relatively large values of friction factor • Measured heat transfer in annulus with different configurations of twisted tapes
11	Wang and Sunden[18]	Water 0<Re<2000 0.7<Pr<3.0	Twisted tape	Experiment in circular tube flow	• Both inserts effective in enhancing heat transfer in laminar region compared with turbulent flow • Twisted tape has poor overall efficiency if pressure drop is considered
12	Saha and Chakraborty[19]	Water 145<Re<1480 4.5<Pr <5.5	Twisted tape regularly spaced 1.92<y<5.0	Experiment in circular tube flow	• Larger number of turns may yield improved thermohydraulic performance compared with single turn

13	Lokanath[5]	Water 240<Re<2300 2.6< Pr< 5.4	Full-length and half-length twisted tapes	Experimental in horizontal tube	• On unit pressure drop basis and on unit pumping power basis, half-length twisted tape is more effective than full-length twisted tape
14	Ray and Date[6]	Water	Twisted tape	Numerical study in square duct	• Higher Prandtl numbers and lower twist ratios can give good performance
15	Guo et al.[20]	Water	Center –cleared twisted tape Short width	Numerical study in circular tube	• Center-cleared twisted tape is a promising technique for laminar convective heat transfer enhancement.
16	Kumar.et. al[21]	water	Twisted tape	Numerical study in a square ribbed duct with twisted tape	• rib spacing and higher twist ratio for high Prandtl fluids and for low Prandtl fluid rib spacing should be higher and twist ratio should be lower
17	Zhang et al.[22]	water	multiple regularly spaced twisted tapes	Numerical study in circular tube	• The simulation results verify the theory of the core flow heat transfer enhancement which leads to the separation of the velocity boundary layer and the temperature boundary layer, and thus enhances the heat transfer greatly while the flow resistance is not increased very much.

2.2. Twisted tape in turbulent flow

The important investigations of twisted tape in turbulent flow are summarized in Table 2.2. In turbulent flow, the dominant thermal resistance is limited to a thin viscous sublayer. A tube inserted with a twisted tape performs better than a plain tube, and a twisted tape with a tight twist ratio provides an improved heat transfer rate at a cost of increase in pressure drop for low Prandtl number fluids. This is because the thickness of the thermal boundary layer is small for a low Prandtl number fluid and a tighter twist ratio disturbs the entire thermal boundary layer, thereby increasing the heat transfer with increase in the pressure drop.

Manglik and Bergles [23] developed correlations for both turbulent flow and laminar flow. For an isothermal friction factor, the correlation describes most available data for laminar, transitional and turbulent flows within 10 per cent. However, a family of curves is needed to develop correlation for the Nusselt number on account of the non-unique nature of laminar turbulent transition. Their correlations are as follows

$$f = \frac{0.079}{Re^{0.25}}\left(\frac{\pi}{\pi-4\delta/d}\right)^{1.75}\left(\frac{\pi+2-2\delta/d}{\pi-4\delta/d}\right)^{1.25}\left(1+\frac{2.752}{y^{1.29}}\right) \tag{2.3}$$

$$Nu = 0.023Re^{0.8}Pr^{0.4}\left(\frac{\pi}{\pi-4\delta/d}\right)^{0.8}\left(\frac{\pi+2-2\delta/d}{\pi-4\delta/d}\right)^{0.2}\left(\frac{\mu}{\mu_w}\right)^{0.18} \tag{2.4}$$

Table.2.2. Summaries of important investigations of twisted tape in turbulent flow

S. No	Authors	Fluid	Configuration of tape	Type of investigation	Observations
1	Kumar et al.[24]	Water	Twisted tape	Experiment in solar water heater	• Investigated performance of tape inserted solar water heater
2	AI-Fahed et. al. [25]	Water	Full-length twisted tape	Experiment in horizontal isothermal tube	• There is optimum tape width, depending on twist ratio and Re, for best thermohydraulic performance
3	Rao and Sastri[26]	Water	Twisted tape	Experimental study in rotating twisted tape	• Enhancement of heat transfer offsets rise in friction factor due to rotation
4	Sivanshanmugam and Sunduram[27]	Water	Twisted tape	Experiment in circular tube	• Studied thermohydraulic characteristics of tape-generated swirl flow
5	Agarwal and Raja rao[28]	water	Twisted tape	Experiment in circular tube flow	• Studied thermohydraulic characteristics of tape-generated swirl flow
6	Chung and Sung[29]	Air	Transverse curvature	Numerical study in Annulus pipe flow	• Turbulent structure more effective near outer wall compared with inner wall

7	Gupte and Date[30]	Air	Twisted tape	Numerical study in annulus	• Semi-empirically evaluated friction and heat transfer data for tape-generated swirl flow in annulus
8	Rahimi et al.[31]	Air	Modified twisted tapes	Experimental and CFD studies	• Maximum increase of 31% and 22% were observed in the calculated Nusselt and performance of the jagged insert as compared with those obtained for the classic one.
9	Murugesan et al.[32]	water	Twisted Tape Consisting of Wire-nails	Experiment in circular tube flow	• The better performance of wire nails twisted tape is due to combined effects of the following factors: common swirling flow generated by twisted tape additional turbulence offered by the wire nails.
12	Eiamsa-ard et al.[33]	water	loose-fit twisted tapes	Numerical study in circular tube	• The thermal performance factor of the twisted tape is influenced by the clearance ratios and the best thermal performance factor at constant pumping power is found at full width twisted tape
13	Yadav.et al.[34]	Air	Half-length twisted tape	Numerical study in circular tube	• Heat transfer coefficient and the pressure drop were 9–47% and 31–144% higher than those in the plain tube

CHAPTER 3

Computational fluid dynamics model equations

Computational Fluid Dynamics (CFD) is the use of computer-based simulation to analyse systems involving fluid flow, heat transfer and associated phenomena such as chemical reaction. A numerical model is first constructed using a set of mathematical equations that describe the flow. These equations are then solved using a computer programme in order to obtain the flow variables throughout the flow domain. Since the arrival of the digital computer, CFD has received extensive attention and has been widely used to study various aspects of fluid dynamics. The development and application of CFD have undergone considerable growth, and as a result it has become a powerful tool in the design and analysis of engineering and other processes. [35]

3.1. CFD analysis procedure

CFD analysis requires the following information:

- A grid of points at which to store the variables calculated by CFD
- Boundary conditions required for defining the conditions at the boundaries of the flow domain and which enable the boundary values of all variables to be calculated
- Fluid properties such as viscosity, thermal conductivity and density etc.
- Flow models which define the various aspects of the flow, such as turbulence, mass and heat transfer.
- Initial conditions used to provide an initial guess of the solution variables in a steady state simulation.
- Solver control parameters required to control the behaviour of the numerical solution process.

3.2. CFD methodology

The mathematical modelling of a flow problem is achieved through three steps:

- Developing the governing equations which describe the flow
- Discretisation of the governing equations
- Solving the resulting numerical equations.

3.3. Equations describing fluids in motion [36]

The mathematical equations used to describe the flow of fluids are the continuity and momentum equations, which describe the conservation of mass and momentum. The momentum equations are also known as the Navier-Stokes equations. For flows involving heat transfer, another set of equations is required to describe the conservation of energy. The continuity equation is derived by applying the principle of mass conservation to a small differential volume of the fluid. In Cartesian coordinates, three equations of the following form are obtained:

$$\frac{\partial \rho}{\partial t} + \nabla.(\rho \vec{v}) = S_m \tag{3.1}$$

Equation 3.1 is the general form of the mass conservation and valid for incompressible as well as compressible flows. The source S_m is the mass added to the dispersed second phase.

The momentum equations are derived by applying Newton's second law of motion to differential volume of the fluid. According to Newton's second law, the rate of change of momentum over a differential volume of fluid is equal to the sum of all external forces acting on this volume of fluid. The resulting momentum equations in Cartesian coordinates take the general form

$$\frac{\partial}{\partial t}(\rho \vec{v}) + \nabla.(\rho \vec{u} \vec{v}) = -\nabla P + \nabla \bar{\bar{\tau}} + \rho \vec{g} + \vec{F} \tag{3.2}$$

Where P is the static pressure, $\bar{\bar{\tau}}$ is the stress tensor (described below), and $\rho \vec{g}$ and $\vec{F}$ are the gravitational body force and external body force.

$$\bar{\bar{\tau}} = \mu \left[(\nabla \vec{v} + \nabla \vec{v}^T) - \frac{2}{3} \nabla . \vec{v} I \right] \tag{3.3}$$

Where μ is the molecular viscosity, I is the unit tensor, and the second term on the right hand side is the effect of volume dilation.

The Energy equation is derived from the first law of thermodynamics which states that the rate of change of energy of fluid particle is equal to the rate of heat addition to the fluid particle plus the rate of work done on the particle. The resulting energy equation in general form

$$\frac{\partial}{\partial t}(\rho E) + \nabla.\left(\vec{v}(\rho E + P)\right) = \nabla.\left(k_{eff}\nabla T - \sum_j h_j \overrightarrow{J_J} + \left(\bar{\bar{\tau}}_{eff}.\vec{v}\right)\right) + S_h \quad (3.4)$$

Where k_{eff} is the effective conductivity (k + k_i, where k_i is the turbulent thermal conductivity, defined according to the turbulence model being used), and $\overrightarrow{J_j}$ is the diffusion flux of species *j*. the first three terms on the right- hand side of equation (3.4) represent energy transfer due to conduction, species diffusion, and viscous dissipation. S_h includes the heat of chemical reaction, and any other volumetric heat sources

In equation (3.4), Energy *E* per unit mass is defined as:

$$E = h - \frac{P}{\rho} + \frac{u^2}{2} \quad (3.5)$$

3.4. Turbulence modelling [36]

Turbulent flows are characterized by fluctuating velocity fields. These fluctuations mix transported quantities such as momentum, energy, and species concentration, and cause the transported quantities to fluctuate as well. It is an unfortunate fact that no single turbulence model is universally accepted as being superior for all classes of problems. The choice of turbulence model will depend on considerations such as the physics encompassed in the flow, the established practice for a specific class of problem, the level of accuracy required, the available computational resources, and the amount of time available for the simulation.

Boussinesq Approach vs. Reynolds Stress Transport Models

$$\frac{\partial \rho}{\partial t} + \frac{\partial}{\partial x_i}(\rho u_i) = 0 \quad (3.6)$$

$$\frac{\partial}{\partial t}(\rho u_i) + \frac{\partial}{\partial x_j}\left(\rho u_i u_j\right) = -\frac{\partial}{\partial x_i} + \frac{\partial}{\partial x_j}\left[\mu\left(\frac{\partial u_i}{\partial x_j} + \frac{\partial u_j}{\partial x_i} - \frac{2}{3}\delta_{ij}\frac{\partial u_l}{\partial x_l}\right)\right] + \frac{\partial}{\partial x_j}\left(-\rho\overline{u_i' u_j'}\right) \quad (3.7)$$

Equations 3.6 and 3.7 is called Reynolds – averaged Navier -stokes (RANS) equations. They have the same general form as the instantaneous Navier-Stokes equation, with velocities and other solution variables representing time averaged values. Additional terms now appear that represent the effects of turbulence. These Reynolds stresses, $\left(-\rho\overline{u_i' u_j'}\right)$ must be modeled in order to close equation 3.7.

The Reynolds-averaged approach to turbulence modeling requires that the Reynolds stresses in Equation (3.7) is appropriately modeled. A common method employs the Boussinesq hypothesis to relate the Reynolds stresses to the mean velocity gradients:

$$\left(-\rho\overline{u_i'u_j'}\right) = \mu_t\left(\frac{\partial u_i}{\partial x_j}+\frac{\partial u_j}{\partial x_i}\right) - \frac{2}{3}\left(\rho k + \mu_t\frac{\partial u_k}{\partial x_k}\right)\delta_{ij} \qquad (3.8)$$

The Boussinesq hypothesis is used in the Spalart-Allmaras model, the k-ϵ models, and the k-ω models. The advantage of this approach is the relatively low computational cost associated with the computation of the turbulent viscosity, μ_t. In the case of the Spalart-Allmaras model, only one additional transport equation (representing turbulent viscosity) is solved. In the case of the k-ϵ and k-ω models, two additional transport equations (for the turbulence kinetic energy, k, and either the turbulence dissipation rate, ϵ, or the specific dissipation rate, ω are solved, and μ_t is computed as a function of k and ϵ or k and ω.

3.4.1. k- ϵ model [36]

1. Standard k-ϵ model

The simplest complete models of turbulence are the two-equation models in which the solution of two separate transport equations allows the turbulent velocity and length scales to be independently determined. The standard k-ϵ model in ANSYS FLUENT falls within this class of models and has become the workhorse of practical engineering flow calculations in the time since it was proposed at 1972. Robustness, economy, and reasonable accuracy for a wide range of turbulent flows explain its popularity in industrial flow and heat transfer simulations. It is a semi-empirical model, and the derivation of the model equations relies on phenomenological considerations and empiricism.

As the strengths and weaknesses of the standard k-ϵ model have become known, improvements have been made to the model to improve its performance. Two of these variants are available in ANSYS FLUENT: the RNG k-ϵ model and the realizable k-ϵ model

Transport Equations for the Standard k-ϵ models

The turbulence kinetic energy, k, and its rate of dissipation, ϵ, are obtained from the following transport equations:

$$\frac{\partial}{\partial t}(\rho k) + \frac{\partial}{\partial x_i}(\rho k u_i) = \frac{\partial}{\partial x_j}\left[\left(\mu + \frac{\mu_t}{\sigma_k}\right)\frac{\partial k}{\partial x_j}\right] + G_k + G_b - \rho\epsilon - Y_M + S_k \quad (3.9)$$

$$\frac{\partial}{\partial t}(\rho \in) + \frac{\partial}{\partial x_i}(\rho \in u_i) = \frac{\partial}{\partial x_j}\left[\left(\mu + \frac{\mu_t}{\sigma_k}\right)\frac{\partial \in}{\partial x_j}\right] + C_{1\in}\frac{\in}{k}(G_k + C_{3\in}G_b) - C_{2\in}\frac{\in^2}{k} + S_\in \quad (3.10)$$

Modeling the Turbulent Viscosity

The turbulent (or eddy) viscosity, μ_t, is computed by combining k and ϵ as follows:

$$\mu_t = \rho C_\mu \frac{k^2}{\epsilon} \quad (3.11)$$

Model Constants

The model constants $C_{1\epsilon}$, $C_{2\epsilon}$, C_μ, σ_k, and σ_ϵ have the following default values

$C_{1\epsilon} = 1.44$, $C_{2\epsilon} = 1.92$, $C_\mu = 0.09$, $\sigma_k = 1.0$, $\sigma_\epsilon = 1.3$

These default values have been determined from experiments with air and water for fundamental turbulent shear flows including homogeneous shear flows and decaying isotropic grid turbulence. They have been found to work fairly well for a wide range of wall bounded and free shear flows.

2. RNG k-ϵ Model

- The RNG k-ϵ model was derived using a rigorous statistical technique (called renormalization group theory). It is similar in form to the standard k-ϵ model, but includes the following refinements:
- The RNG model has an additional term in its ϵ equation that significantly improves the accuracy for rapidly strained flows.
- The effect of swirl on turbulence is included in the RNG model, enhancing accuracy for swirling flows.
- The RNG theory provides an analytical formula for turbulent Prandtl numbers, while the standard k-ϵ model uses user-specified, constant values.

- While the standard k-ϵ model is a high-Reynolds-number model, the RNG theory provides an analytically-derived differential formula for effective viscosity that accounts for low-Reynolds-number effects. Effective use of this feature does, however, depend on an appropriate treatment of the near-wall region.

These features make the RNG k-ϵ model more accurate and reliable for a wider class of flows than the standard k-ϵ model.

3.4.2. k- ω model [36]

1. Standard k-ω model

The standard k-ω model in ANSYS FLUENT is based on the Wilcox k-ω model, which incorporates modifications for low-Reynolds-number effects, compressibility, and shear flow spreading. The Wilcox model predicts free shear flow spreading rates that are in close agreement with measurements for far wakes, mixing layers, and plane, round, and radial jets, and is thus applicable to wall-bounded flows and free shear flows. A variation of the standard k-ω model called the SST k-ω model is also available in ANSYS FLUENT

Transport Equations for the Standard k-ω Model

$$\frac{\partial}{\partial t}(\rho k) + \frac{\partial}{\partial x_i}(\rho k u_i) = \frac{\partial}{\partial x_j}\left[\left(\mu + \frac{\mu_t}{\sigma_k}\right)\frac{\partial k}{\partial x_j}\right] + G_k - Y_k + S_k \quad (3.12)$$

$$\frac{\partial}{\partial t}(\rho \omega) + \frac{\partial}{\partial x_i}(\rho \omega u_i) = \frac{\partial}{\partial x_j}\left[\Gamma_\omega \frac{\partial \omega}{\partial x_j}\right] + G_\omega - Y_\omega + S_\omega \quad (3.13)$$

In these equations, G_k represents the generation of turbulence kinetic energy due to mean velocity gradients. G_ω represents the generation of ω. Γ_k and Γ_ω represent the effective diffusivity of k and ω, respectively. Y_k and Y_ω represent the dissipation of k and ω due to turbulence. All of the above terms are calculated as described below. S_k and S_ω are user-defined source terms.

2. Shear-Stress Transport (SST) k-ω Model [36]

The shear-stress transport (SST) k-ω model was developed by Menter [37] to effectively blend the robust and accurate formulation of the k-ω model in the near-wall region with the free-stream independence of the k-ϵ model in the far field. To achieve this, the k-ϵ model is converted into a

k-ω formulation. The SST k-ω model is similar to the standard k-ω model, but includes the following refinements:

- The standard k-ω model and the transformed k-ϵ model are both multiplied by a blending function and both models are added together. The blending function is designed to be one in the near-wall region, which activates the standard k-ω model, and zero away from the surface, which activates the transformed k- model.
- The SST model incorporates a damped cross-diffusion derivative term in the ω equation.
- The definition of the turbulent viscosity is modified to account for the transport of the turbulent shear stress.
- The modeling constants are different.

These features make the SST k-ω model more accurate and reliable for a wider class of flows (e.g., adverse pressure gradient flows, airfoils, transonic shock waves) than the standard k-ω model. Other modifications include the addition of a cross-diffusion term in the ω equation and a blending function to ensure that the model equations behave appropriately in both the near-wall and far-field zones.

3.5. Discretisation of the governing equations [36]

The governing equations shown above are partial differential equations (PDEs). Since digital computers can only recognise and manipulate numerical data, these equations cannot be solved directly. Therefore, the PDEs must be transformed into numerical equations containing only numbers and no derivates. This process of producing a numerical analogue to the PDEs is called numerical discretisation. The discretisation process involves an error since the numerical terms are only approximations to the original partial differential terms. This error, however, can be minimised to very low, and therefore acceptable, levels.

The major technique used for discretisation is finite volume method.

The finite volume method is probably the most popular method used for numerical discretisation in CFD. This method is similar in some ways to the finite difference method but some of its implementations draw on features taken from the finite element method. This approach involves the discretisation of the spatial domain into finite control volumes. A control volume overlaps

with many mesh elements and can therefore be divided into sectors each of which belongs to a different mesh element, as shown in Fig. 3.1.

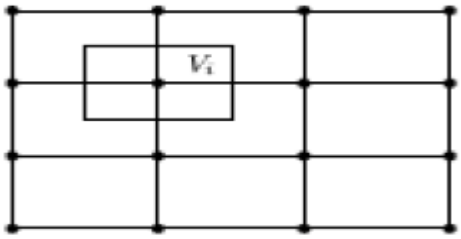

Fig. 3.1. A control volume (V_i) surrounded by mesh elements.

The governing equations in their differential form are integrated over each control volume. The resulting integral conservation laws are exactly satisfied for each control volume and for the entire domain, which is a distinct advantage of the finite volume method. Each integral term is then converted into a discrete form, thus yielding discretised equations at the centroids, or nodal points, of the control volumes

3.5.1. Discretisation methods [36]

In FLUENT, solver variables are stored at the centre of the grid cells (control volumes).
Interpolation schemes for the convection term are:

- **First-Order Upwind** – Easiest to converge, only first-order accurate.
- **Power Law** – More accurate than first-order for flows when $Re_{cell} < 5$ (type. low Re flows)
- **Second-Order Upwind** – Uses larger stencils for 2nd order accuracy, essential with tri/tetra mesh or when flow is not aligned with grid; convergence may be slower.
- Monotone Upstream-Centered Schemes for Conservation Laws (**MUSCL**) – Locally 3rd order convection discretisation scheme for unstructured meshes; more accurate in predicting secondary flows, vortices, forces, etc.
- Quadratic Upwind Interpolation (**QUICK**) – Applies to quad/hex and hybrid meshes, useful for rotating/swirling flows, 3rd-order accurate on uniform mesh.

Interpolation methods for Gradients

Gradients of solution variables are required in order to evaluate diffusive fluxes, velocity derivatives, and for higher-order discretisation schemes.

The gradients of solution variables at cell centers can be determined using three approaches:

- **Green-Gauss Cell-Based** – Least computationally intensive. Solution may have false diffusion.
- **Green-Gauss Node-Based** – More accurate/computationally intensive; minimizes false diffusion; recommended for unstructured meshes.
- **Least-Squares Cell-Based** – Default method; has the same accuracy and properties as Node-based Gradients and is less computationally intensive.

3.6. Solving the resulting numerical equations [37]

There are two kinds of solvers available in FLUENT: **Pressure based, Density based**

The **pressure-based** solvers take momentum and pressure (or pressure correction) as the primary variables. Pressure-velocity coupling algorithms are derived by reformatting the continuity equation

Interpolation Methods for pressure

Interpolation schemes for calculating cell-face pressures when using the pressure-based solver in FLUENT are available as follows: Standard, PRESTO, Linear, Second-Order, Body Force Weighted

Standard – The default scheme, reduced accuracy for flows exhibiting large surface-normal pressure gradients near boundaries

Pressure - velocity coupling

Pressure-velocity coupling refers to the numerical algorithm which uses a combination of continuity and momentum equations to derive an equation for pressure (or pressure correction) when using the pressure-based solver. Five algorithms are available in FLUENT. Semi-implicit Method for Pressure-Linked Equation (SIMPLE) it is robust and default scheme.

CHAPTER 4

NUMERICAL INVESTIGATIONS FOR PLAIN TUBE

This chapter deals with the numerical analysis of water flowing through a horizontal circular tube at constant wall temperature, for estimation of the heat transfer and friction factor characteristics. The results obtained from numerical investigations are validated by comparing with the available correlations

4.1. Physical model

Considered the problem of water flowing through a circular tube with length (L) and inside diameter of 2200 mm and 22 mm respectively.

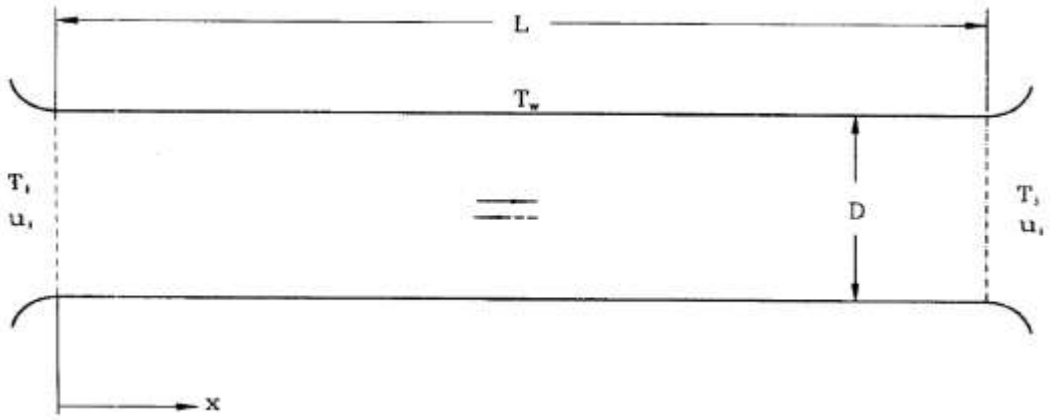

Fig.4.1. Physical geometry of plain tube

4.2. FLUENT Simulation

4.2.1. Geometry Creation and Mesh generation

A circular pipe of diameter 22 mm and length 2200 mm was used as the geometry. A 3-D geometry is created by using ANSYS workbench and schematic view is shown in the Fig. 4.2. Structured meshing method is used for meshing the geometry. It is meshed into 55,806 nodes and 1, 95,569 elements as shown in Fig. 4.3.

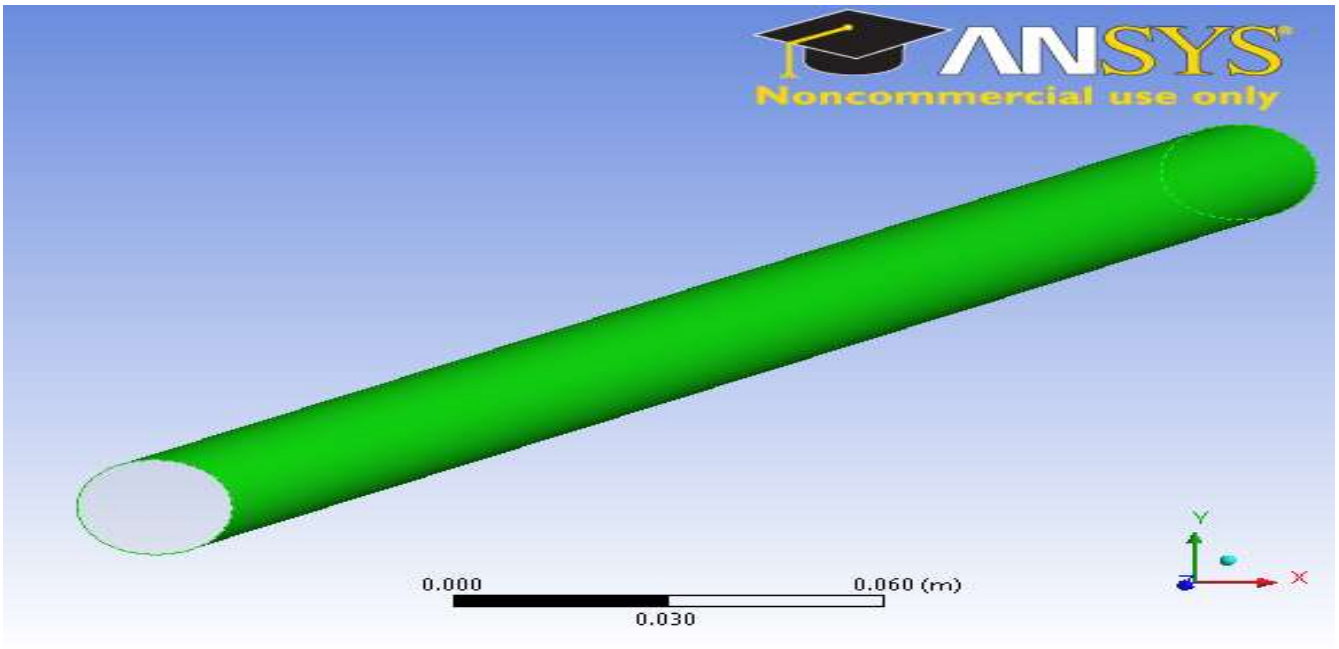

Fig 4.2 Plain tube geometric created by ANSYS workbench

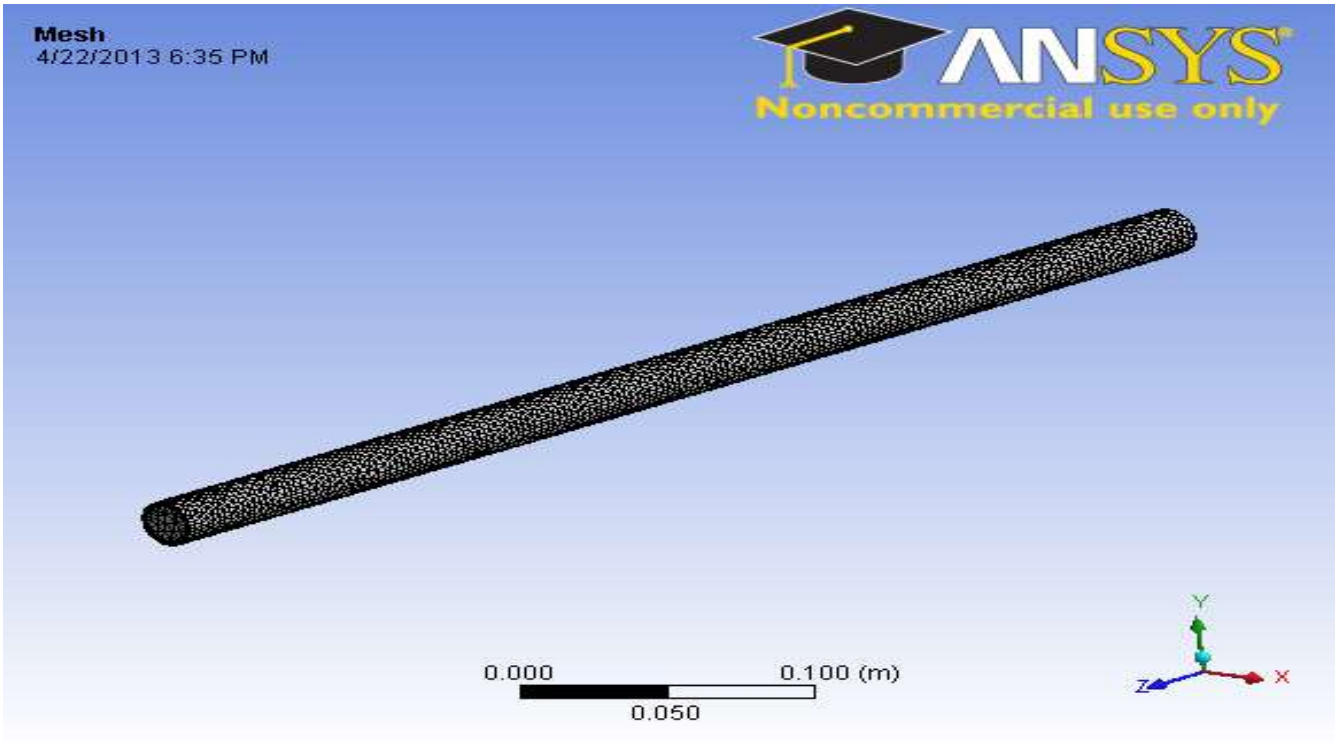

Fig 4.3 Meshing of plain tube geometry

4.2.2. FLUENT Setup

Numerical simulations were carried out using the Commercial CFD software package ANSYS FLUENT 13.0. The first step taken after importing the mesh geometry into FLUENT involves checking the mesh/grid for errors. Checking the grid assures that all zones are present and all dimensions are correct. Once the grid was set, the solver and boundary conditions of the system were then set and cases were run and analyzed.

4.2.3. Defining the Material Properties

This section of the input contains the options for the materials to be chosen. Water is passing in the horizontal tube under constant wall temperature condition in the present work. Under materials Tab in FLUENT, fluid considered is water -liquid. Solid (tube wall) material considered for analysis is copper.

The selection of material is done. Material selected is water-liquid. The properties of water-liquid is taken as follows

Table.4.1. properties of water at 25^0C

S.No.	properties	value
1	Density, ρ	998.2 kg/m^3
2	Specific heat capacity, C_p	4182 J/kg K
3	Thermal conductivity	0.6 W/m K
4	Viscosity, μ	1.003 x 10^{-3} kg/m s

4.2.4 Boundary Conditions [37]

Water at a temperature of 25^0C was used as the working fluid. The numerical studies were carried out with uniform velocity profile at the inlet of the horizontal pipeline. The direction of the flow was defined normal to the boundary. Inlet velocity and temperature were specified. Turbulent intensity, I and the hydraulic diameter, D_h were specified for an initial guess of turbulent (k and ϵ). The Turbulent intensity was estimated for each case based on formula $I = 0.16(Re)^{-1/8}$. Outflow boundary condition was used at pressure-out let boundary. The wall of the

pipe was assumed to be perfectly smooth with zero roughness height and stationary wall, no slip condition. A constant wall temperature of 373K was used at the wall boundary

Velocity- Inlet Boundary: inlet was taken for the pipe inlet section and the velocity values are varying as 0.037 to 0.47 m/s. Initial gauge pressure was taken as zero Pascal. Temperature was taken as 298 K.

4.2.5. Numerical Solution Strategy [37]

The commercial CFD solver FLUENT 13.0 was used to perform the simulations, based on finite volume approach to solve the governing equations with a segregated solver. The second-order upwind scheme was used for discretization of convection terms, energy, and turbulent kinetic and turbulent dissipation energy. This scheme ensures, in general especially for tri or tetrahedral mesh flow domain, satisfactory accuracy, stability and convergence.

SIMPLE algorithm was used to resolve the coupling between velocity and pressure fields. The convergence criterion is based on the residual value of calculated variables such as mass, velocity components, turbulent kinetic (k), turbulent dissipation energies (ε), and energy. In the present calculations, the initial residual values were set to 10^{-4} for all variables, except for energy for which 10^{-6} is used. The under-relaxation factors used for the stability of the converged solutions are set at their default values. The numerical simulation was decided as converged when the sum of normalized residuals for each conservation equation and variables was less than the set residual values.

4.2.6 Executing the FLUENT Code

Each case must be initialized before the FLUENT code begins iterating towards a converged solution. In this study, the option chosen for initialization was to compute from inlet zones. The number of iterations ranged between 100 and 1000 depending on the case being run and how long it took to converge. Iterations were performed with the default under- relaxation factors for all parameters. The computations were performed with Intel (R) Core (TM) i5 CPU 650 @ 3.20 GHz of 4GB RAM.

4.2.7. Data Reduction

The area weighted average temperature and static pressure were noted at the inlet and outlet surfaces of the pipe. The friction factor and average heat transfer coefficients were calculated as follows.

Friction factor, $f = \Delta P/2\left((L/D)\rho V^2\right)$ (4.1)

Nusselt number $Nu = hD/k$ (4.2)

4.3. Standard equations used

I. Heat transfer calculations

i. Laminar flow, for Re < 2100

Nu= f(Gz)

For Gz <100, Hausen's Equation is used.

$$Nu_D = 3.66 + \frac{0.085\,Gz}{1+0.045[Gz]^{2/3}}\left\{\frac{\mu}{\mu_w}\right\}^{0.14} \quad (4.3)$$

For Gz>100, Seider - Tate equation is used.

$$Nu = 1.86\left(\frac{Re_D Pr}{L/D}\right)^{1/3}\left\{\frac{\mu}{\mu_w}\right\}^{0.14} \quad (4.4)$$

ii. Transition Zone:

for 2100 < Re < 10000, Hausen's Equation is used

$$Nu = 0.116(Re^{2/3} - 125)(Pr^{1/3})\left[1 + \left(\frac{D}{L}\right)^{2/3}\right]\left\{\frac{\mu}{\mu_w}\right\}^{0.14} \quad (4.5)$$

iii. Turbulent Zone

Re > 10000 (Dittus - Boelter equation)

$$Nu_D = 0.023 Re_D^{0.8} Pr^{0.4} \quad (4.6)$$

Viscosity correction Factor $\left\{\frac{\mu}{\mu_w}\right\}^{0.14}$ is assumed to be 1.

- Friction factor(f_0) correlation

Laminar region, $Re_D < 2100$

$$f = 16/N_{Re} \quad (4.7)$$

Turbulent flow, $Re_D > 2100$ (Colburn's Equation)

$$f = 0.046 N_{Re}^{-0.2} \quad (4.8)$$

4.4. Results and Discussion

In this section steady state simulation results are discussed. The temperature and pressure distributions of the fluid inside the pipe displayed Fig.4.4 and Fig.4.5. Three dimensional numerical simulations were performed for inlet velocities of 0.037, 0.055, 0.073, 0.091, 0.18, 0.27, 0.37 and 0.46 m/sec of water corresponding to Reynolds numbers of 800, 1200, 1600, 2000, 4000, 6000, 8000, and 10000 respectively. Temperature distribution of water inside the plain tube at Re= 4000 are shown in Fig. 4.4. is subjected to Constant wall temperature boundary condition.

Initially water temperature adjacent to the tube wall is more compared to the center of tube as indicated in the figure. This will increase along the length of horizontal tube. Inlet water temperature is held constant at 298 K for all flow rates. Outlet temperature varied from 340 K to 326 K for the range of Reynolds numbers considered for numerical analysis.

Fig. 4.5 shows the pressure distribution of water while passing through the plain tube. Because of the frictional resistance offered to fluid flow, water pressure drops across flow field. Pressure drop varied from 6.042 Pa to 330.05 Pa for the range of Reynolds numbers considered for numerical analysis.

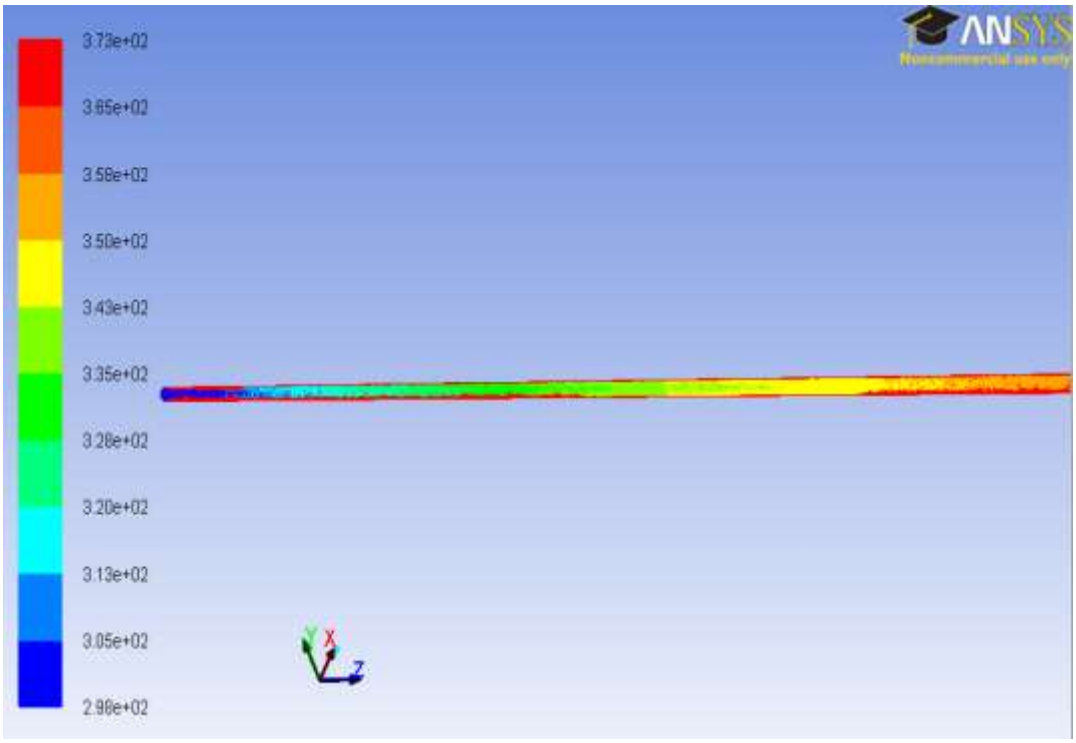

Fig 4.4 Temperature variation along the length of horizontal tube

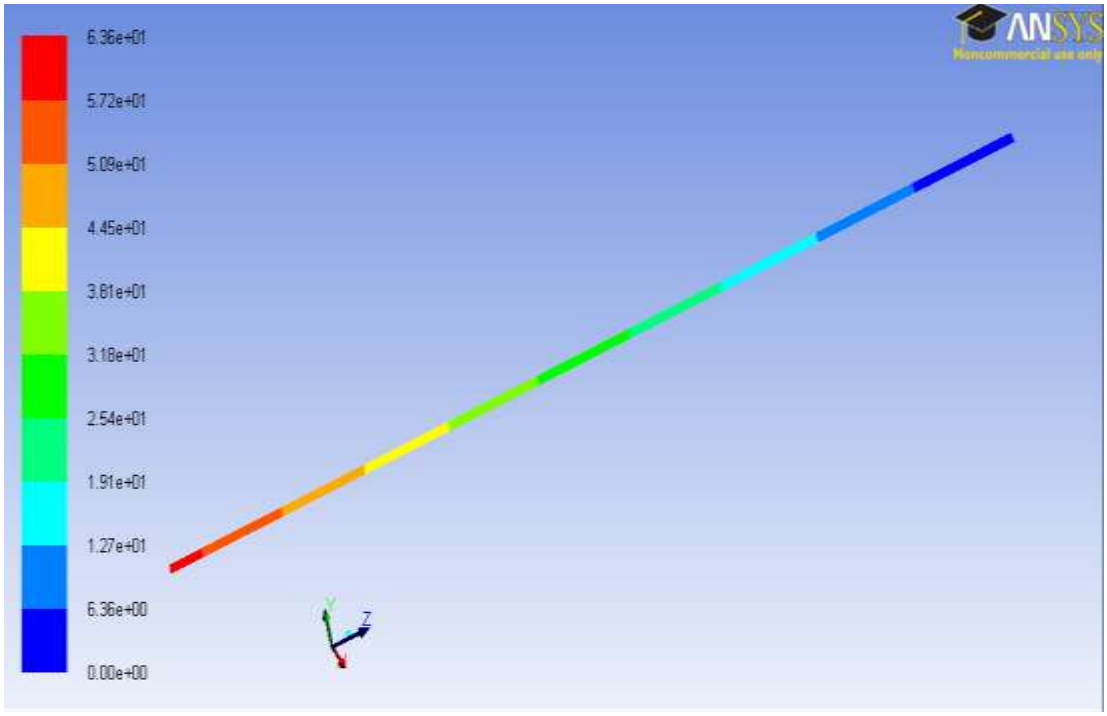

Fig 4.5 Pressure distribution along the length of plain tube

4.5. Validation of Numerical Results

Numerical results were made compared with the standard correlation values under similar condition, in order to evaluate the validity of the plain tube results. Simulated and calculated values are given in Table. A.1 and A.2

4.5.1. Laminar Region

Nusselt number for the base fluid (water) in the laminar region was compared with equations (4.3) and (4.4). It can be seen from Fig.4.6. Friction factor for the base fluid (water) in the laminar region was compared with equation (4.7). It can be seen from Fig.4.7.

4.5.2. Turbulent Region.

Nusselt number for the base fluid (water) in the turbulent region was compared with equation (4.5). It can be seen from Fig.4.8. Friction factor for the base fluid (water) in the turbulent region was compared with equation (4.8). It can be seen from Fig.4.9.

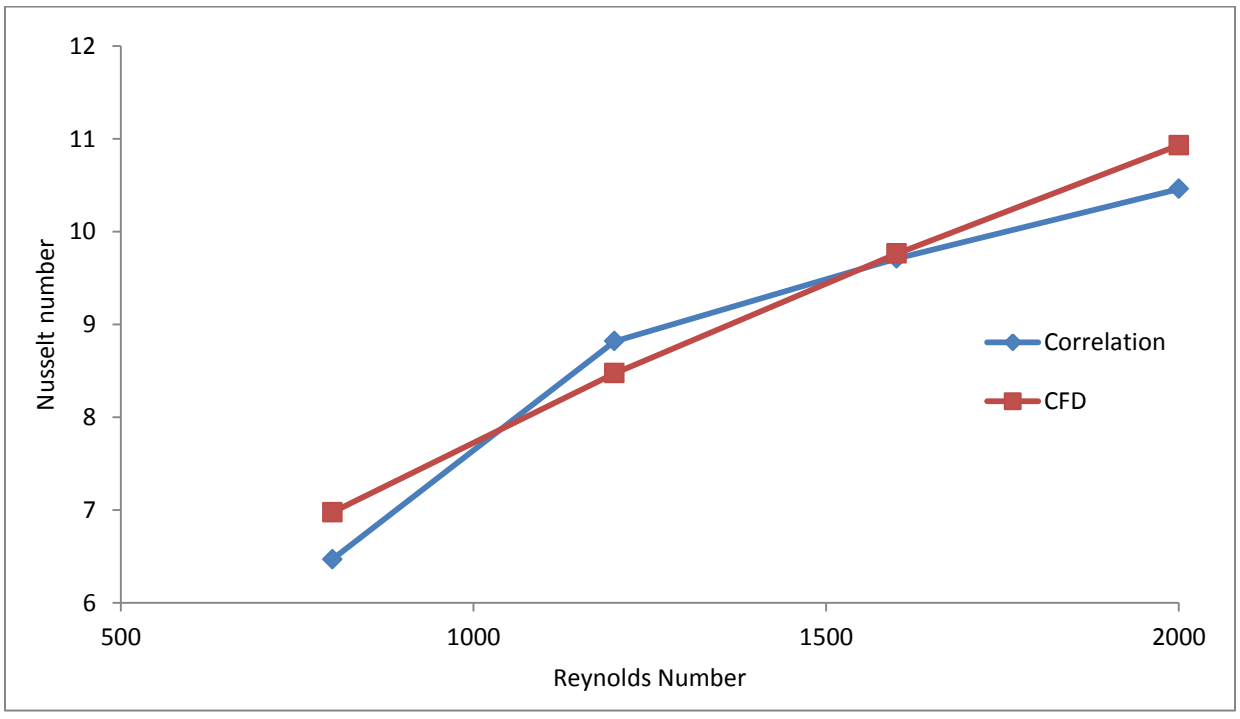

Fig.4.6. Comparison of Numerical Nu with correlations in plain tube at laminar regime

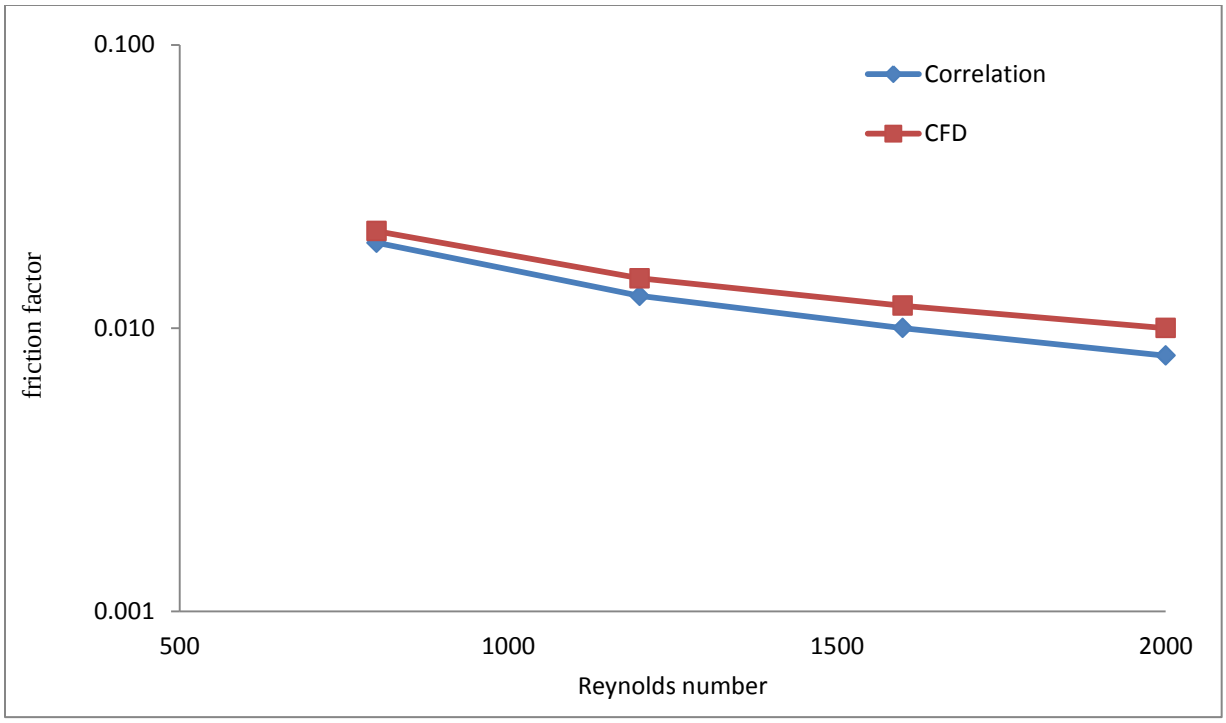

Fig.4.7.Comparison of Numerical friction factor with correlations in plain tube at laminar regime

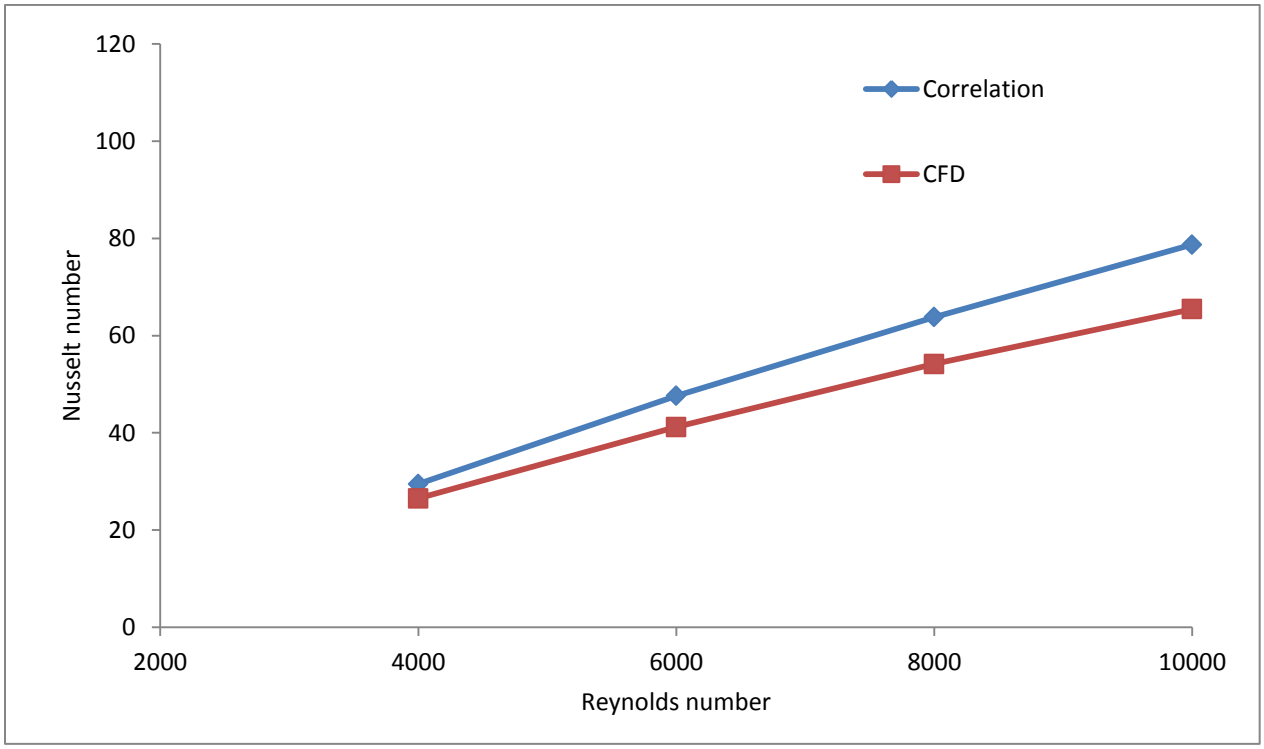

Fig.4.8. Comparison of Numerical Nu with correlations in plain tube at turbulent regime

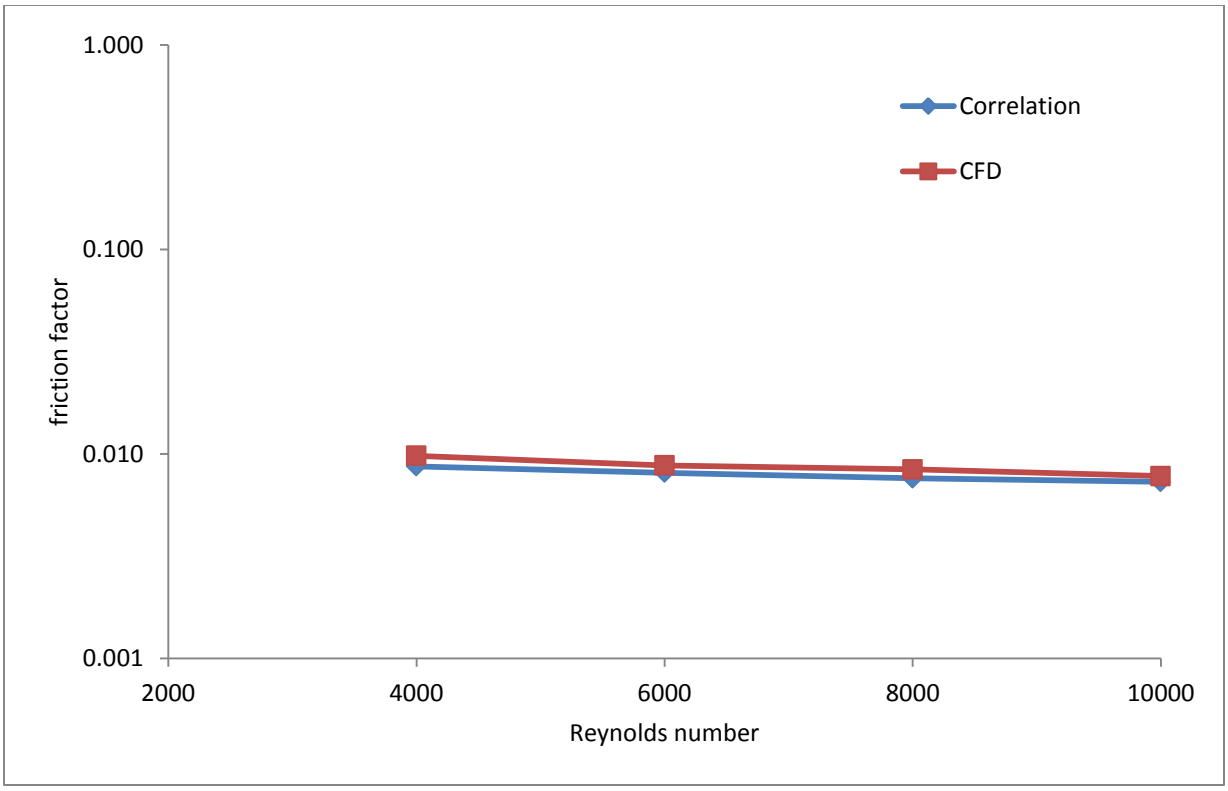

Fig.4.9.Comparison of Numerical friction factor with correlations in plain tube at turbulent regime

4.6. Conclusion

Numerical analysis was conducted initially for plain tube to have an estimate of the heat transfer and friction factor characteristics of water in plain tube. The commercial Computational Fluid Dynamics (CFD) program Fluent 13.0 was used to predict the flow and heat transfer performance in the horizontal tube. The obtained numerical data were, then compared with the standard correlation values under the similar condition, in order to evaluate the validity of CFD results for the plain tube. It is observed that, the simulated data are valid within $\pm$16.82 percentage error limit with measurements for Nusselt number and $\pm$ 25.0 percentage error for friction factor.

CHAPTER 5

FRICTION FACTOR AND HEAT TRANSFER IN PLAIN TUBE WITH TWISTED TAPE INSERTS

Heat transfer augmentation with twisted tape is given extreme importance due to its applicability in various industrial applications. Most of the studies have addressed to the fluid flow and heat transfer characteristics in tubes with twisted tape inserts on the basis of experimental investigations, but the numerical simulations are scarce. The present work, numerical study was made on heat transfer enhancement for water inside the horizontal tube in the presence of twisted tape inserts. Numerical study is done using CFD analysis. The aim of the current study is to report details of the turbulence modeling to help in understanding of the behaviors of the incompressible swirl flows for tube fitted with the twisted tapes in comparison with those for a plain tube. The simulation studies were conducted with the tapes of four different twist ratios, y= 2, 3, 4 and 5, for the Reynolds number ranging from 800 to 10000, The mathematical models including the turbulence models, numerical solution and other computational details are described. Effects of the twist ratio on heat transfer rate (Nu_a), friction factor (f_a) and thermal performance factor (η) are examined under constant wall temperature.

5.1. Physical model of twisted tape

A schematic diagram of a twisted tape insert inside a tube is shown in Fig.5.1. The Twisted tape is defined geometrically by the thickness of the tape δ and its twist ratio. The twist ratio (y) is defined as the axial length (H) for a 180^0 turn of the tape divided by the width (w) of the tube. This is the most common definition used in research literature and that used here.

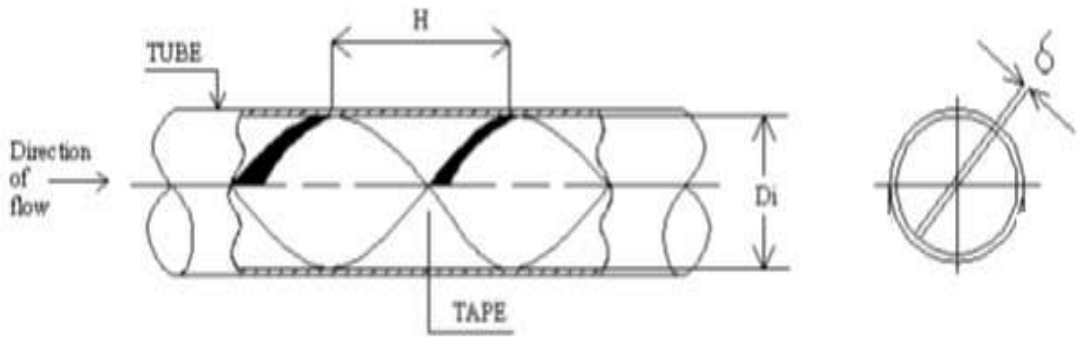

Fig.5.1.Diagram of a twisted tape insert inside a tube

Twisted tapes with thickness (δ) of 1 mm are fitted in the full length of all tubes. The diameter (D) and length (L) of the tube are 22 mm and 2200 mm.

5.2. FLUENT Simulation

The 3D geometry of twisted tape Insert inside a plain tube created by using ANSYS 13.0 software.

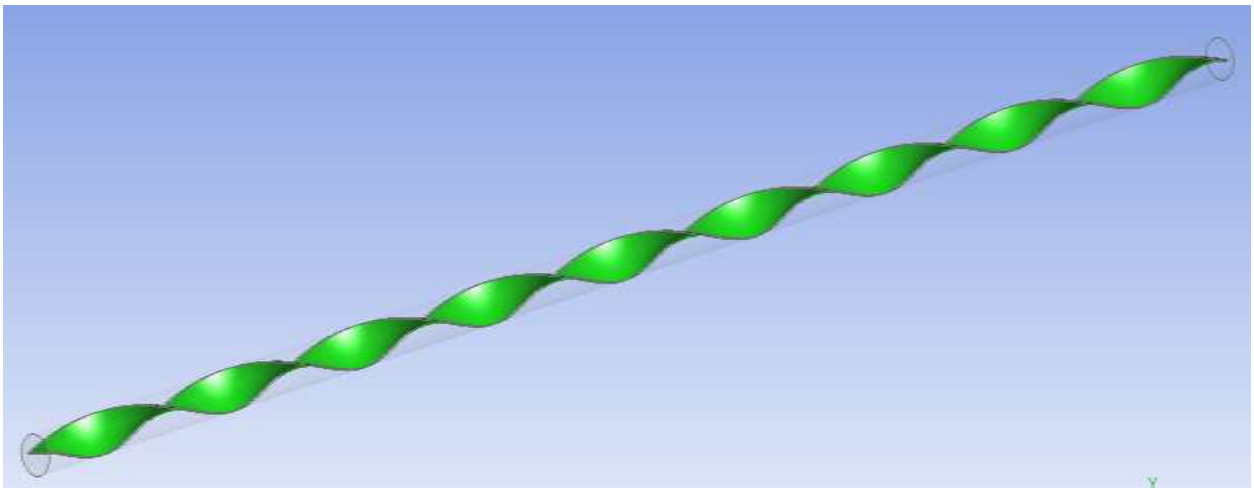

Fig.5.2. Geometry of twisted tape Insert inside a plain tube in ANSYS workbench

The geometry is meshed into smaller cells. The meshing method used is patch independent tetrahedron. The geometry is meshed into 35,348 nodes and 1, 37,668 elements.

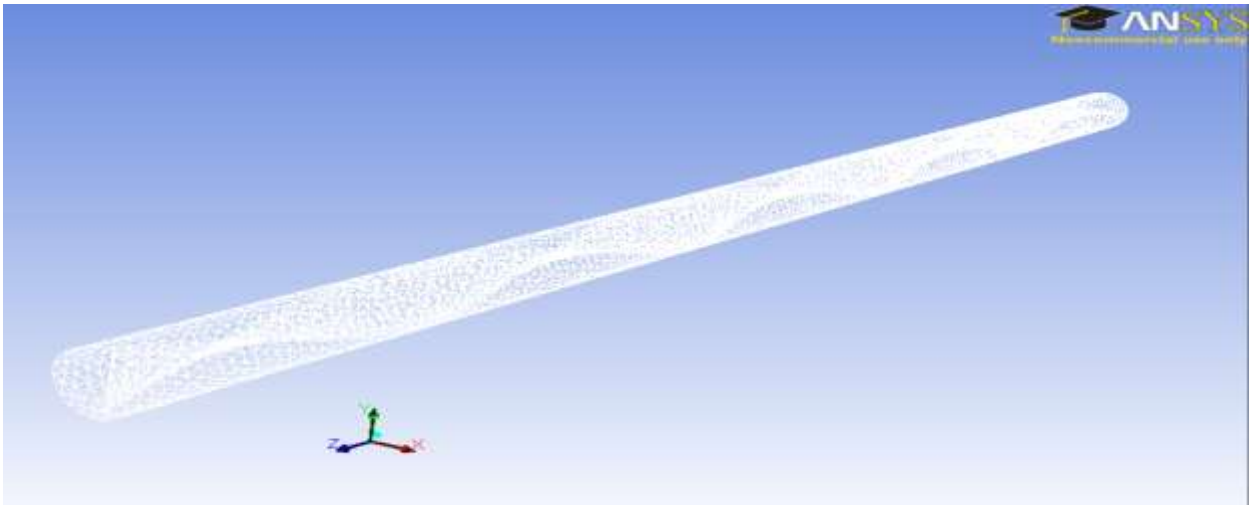

Figure.5.3. Meshing of twisted tape Insert geometry

5.5.2. Mathematical foundation [33]

The mathematical modeling involves the prediction of flow and heat transfer behaviors. The available finite volume procedures for swirling flows and boundary layer are employed to solve the governing partial differential equations. Some simplifying assumptions are required for applying of the conventional flow equations and energy equations to model the heat transfer process in tube with twisted tape.

The major assumptions are:

- The flow through the twisted tape inserted tube is turbulent and incompressible
- The flow is in steady state
- Natural convection and thermal radiation are neglected
- The thermo-physical properties of the fluid are temperature independent

5.2.3. Material Properties

Water is selected as the working fluid which is assumed to be incompressible. The dynamic viscosity (μ), thermal conductivity (k), density (ρ) and specific heat at constant pressure (Cp) of water are given as $\mu = 1.003x10^{-3}$ kgm^{-1} s^{-1}, $k = 0.6$ Wm^{-1} K^{-1}, $\rho = 998.2$ $kg.m^{-3}$ and $Cp = 4182$ J. kg^{-1} K^{-1}.

5.2.4. Model specification

We cannot perfectly represent the effects of turbulence in the CFD simulation. Instead we need a Turbulence Model. There is no one size fits all answer to turbulence modeling. Therefore, selecting a turbulence model accommodated the flow behavior of each application. To attain the accurate aerodynamic prediction in tube with twisted tape insert, the predictive ability of four different turbulence models, including, the standard k–ε turbulence model, the Renormalized Group (RNG) k–ε turbulence model, the standard k–ω turbulence model, and the Shear Stress Transport (SST) k–ω turbulence model.

5.2.5. Boundary conditions

A constant wall temperature is imposed on the tube wall. At the inlet velocity and temperature are specified. At the outlet, a pressure-outlet condition is used. On the surfaces of the tube wall and twisted tape, no slip conditions are applied.

5.2.6. Solution techniques

In the present numerical solution, the time-independent incompressible Navier –Stokes equations and the various turbulence models are discretized using the finite volume technique. A second order upwind scheme is applied for convective and diffusive terms. To evaluate the pressure field, the pressure–velocity coupling algorithm SIMPLE (Semi Implicit Method for Pressure-Linked Equations) is selected. The turbulence intensity is kept at 10% at the inlet.

5.2.7. Flow configurations

The numerical analysis is made for twisted tapes at four different twist ratios, y =2, 3, 4, and 5 detailed dimensions are mention in Table.5.1. The Reynolds numbers used for the computation are referred to the inlet values which are set at 800, 1200, 1600, 2000, 4000, 6000, 8000 and 10,000. The tube wall and inlet temperatures are kept constant at 373 K and 298 K.

Table.5.1.Dimensions of twisted tape inserts

S.No.	Twist ratio, y	Pitch, H mm	Width mm	Thickness, δ mm
1	2	44	22	1
2	3	66	22	1
3	4	88	22	1
4	5	110	22	1

5.3. Results and Discussion

5.3.1. Model verification [33]

The characteristics of swirling turbulent flows in a circular tube fitted with twisted tape insert by means of mathematical equations in association with the standard k–ε turbulence model, the Renormalized Group (RNG) k–ε turbulence model, the standard k–ω turbulence model, and Shear Stress Transport (SST) k–ω turbulence model were determined Twisted tape with twist ratio, (y = 5) was used for model verification. The present results are compared with the correlations obtained suggested Manglik and Bergles [7, 23] as given in Table.A.3 and A.4. Fig. 5.4 and 5.5 shows the comparison of predicted Nusselt number and friction factor results with correlation results in laminar regime. Similarly Fig. 5.6 and Fig.5.7 shows the comparison of predicted Nusselt number and friction factor results with correlation results in turbulent regime.

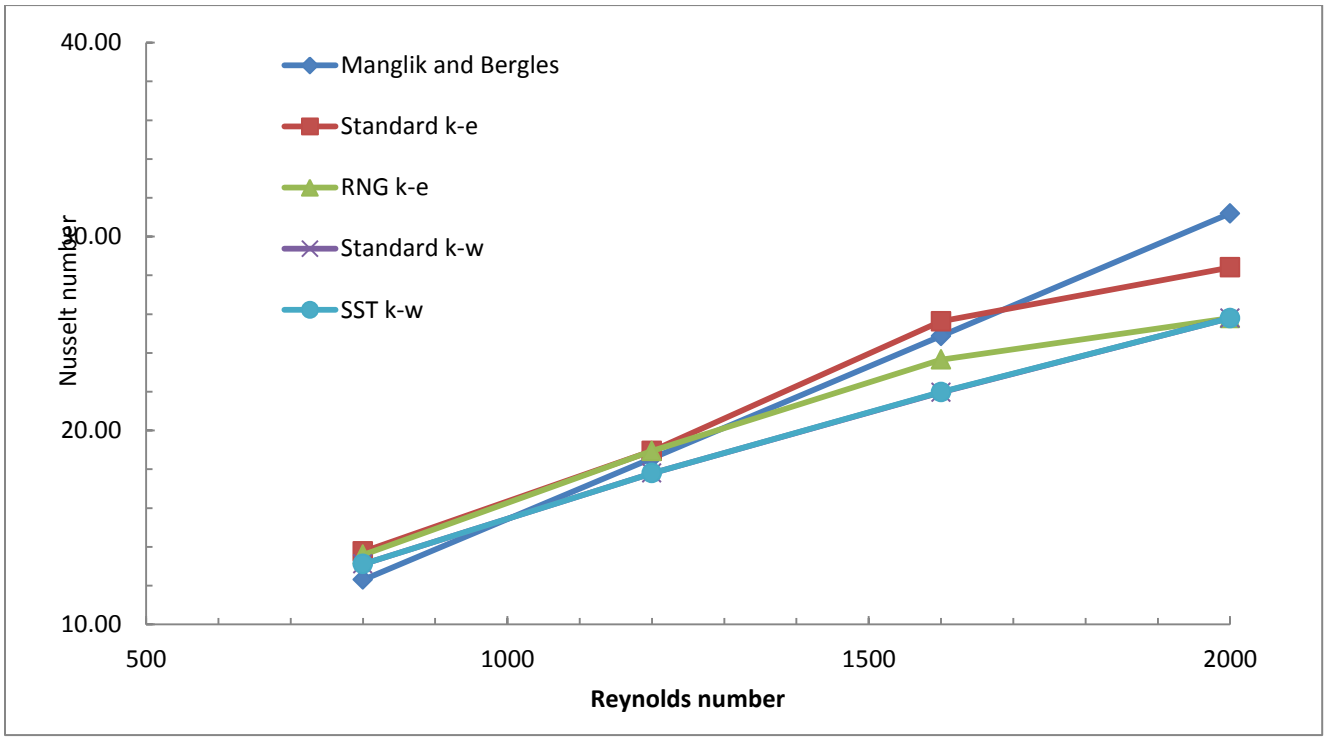

Fig.5.4.Comparison of the predicted Nusselt number with those obtained by Manglik and Bergles [7] for y=5 in the laminar region.

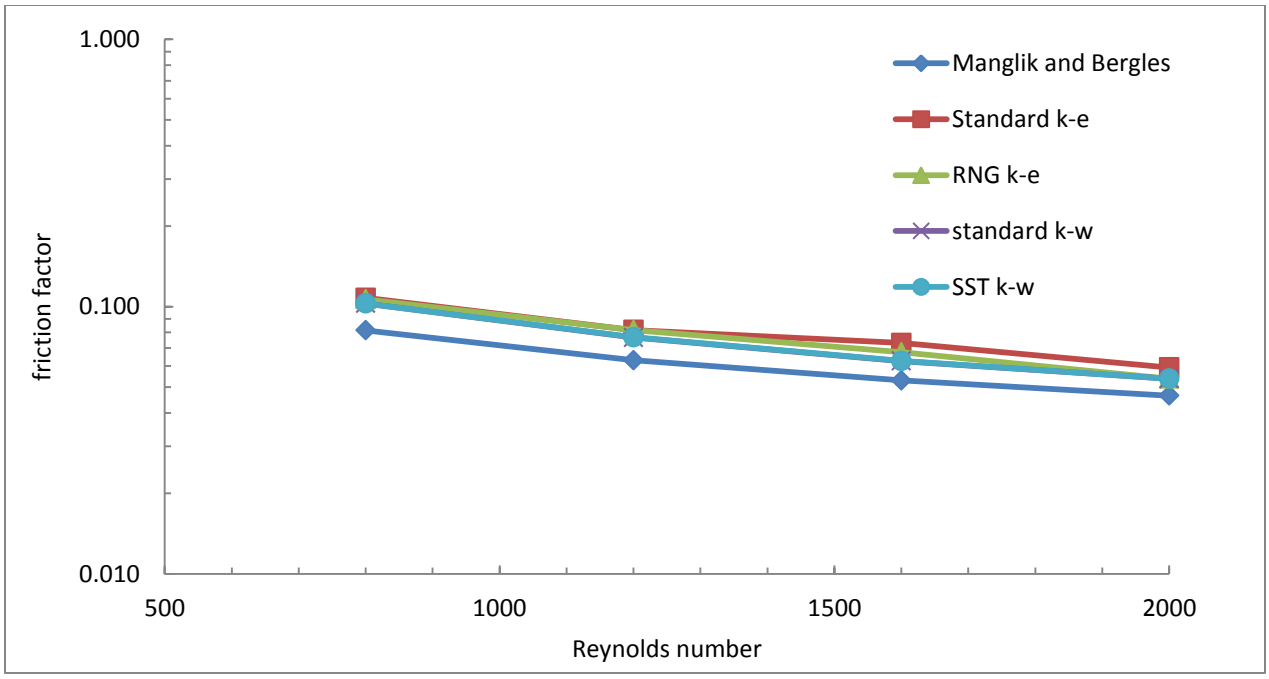

Fig.5.5.Comparison of the predicted friction factor with those obtained by Manglik and Bergles [7] for y=5 in laminar region.

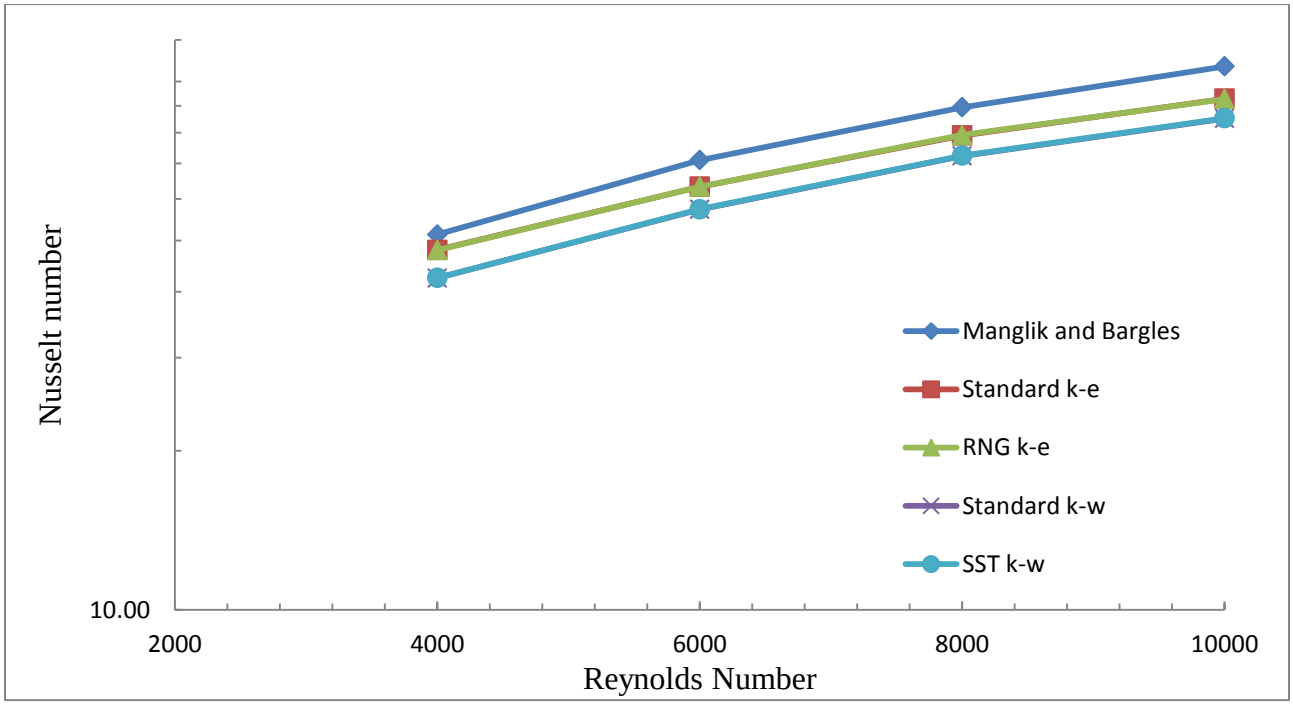

Fig.5.6.Comparison of the predicted Nusselt number with those obtained by Manglik and Bergles [23] for y=5 in turbulent region.

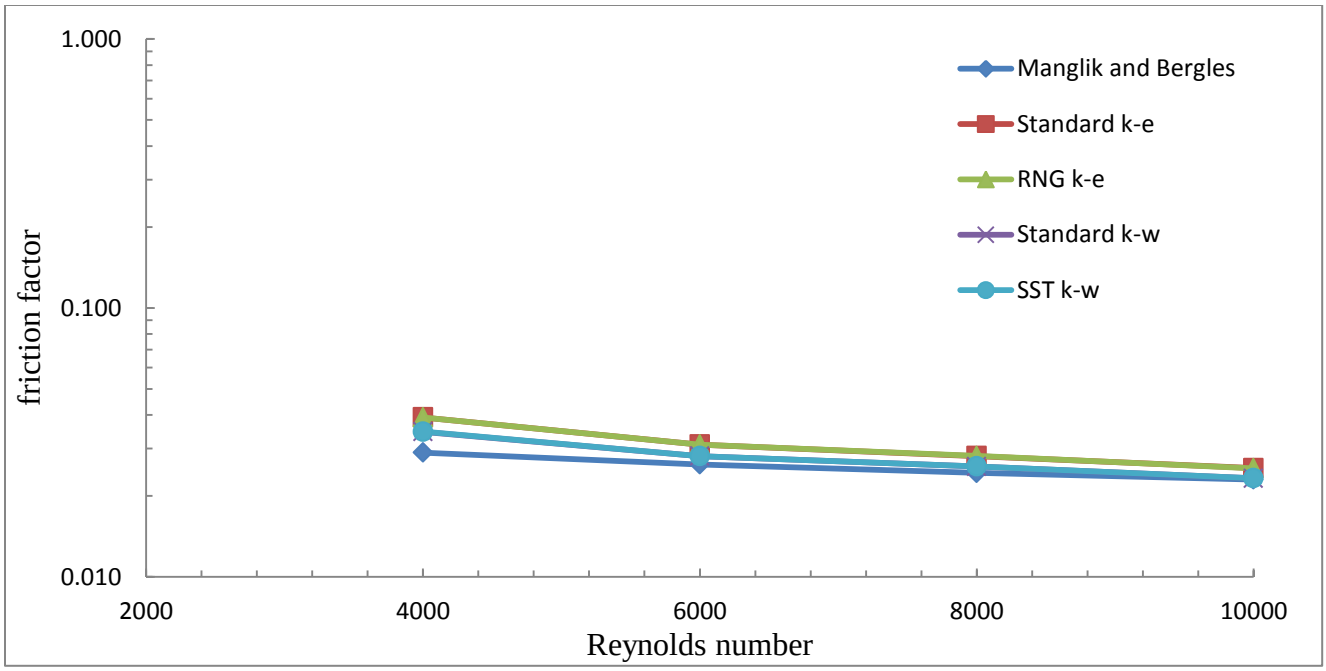

Fig.5.7.Comparison of the predicted friction factor with those obtained by Manglik and Bergles [23] for y=5 in turbulent region.

The predicted results of Nusselt number and friction factor are compared with the obtained by Manglik and Bergles as given in Table 5.1. It is clearly seen that the predicted Nusselt numbers obtained from the SST k–ω turbulence models is in better agreement compared to those from other models. The SST k–ω turbulence model is valid within ±20.2% error limit with measurements for Nusselt number and ±26.4% for friction factor.

5.3.2. Heat transfer Enhancement studies with different twist ratios

The Shear Stress Transport (SST k-ω) model is used in the simulation for finding the Nusselt number and friction factor with twist ratios of 2, 3, 4 and 5. Vector plots of velocity, Pathlines, contour plots of static pressure and Temperature fields shown in figures 5.8, 5.9, 5.10 and 5.11 respectively in the Re = 2000 at twist ratio y=2.Velocity was found increase with decrease in twist ratio

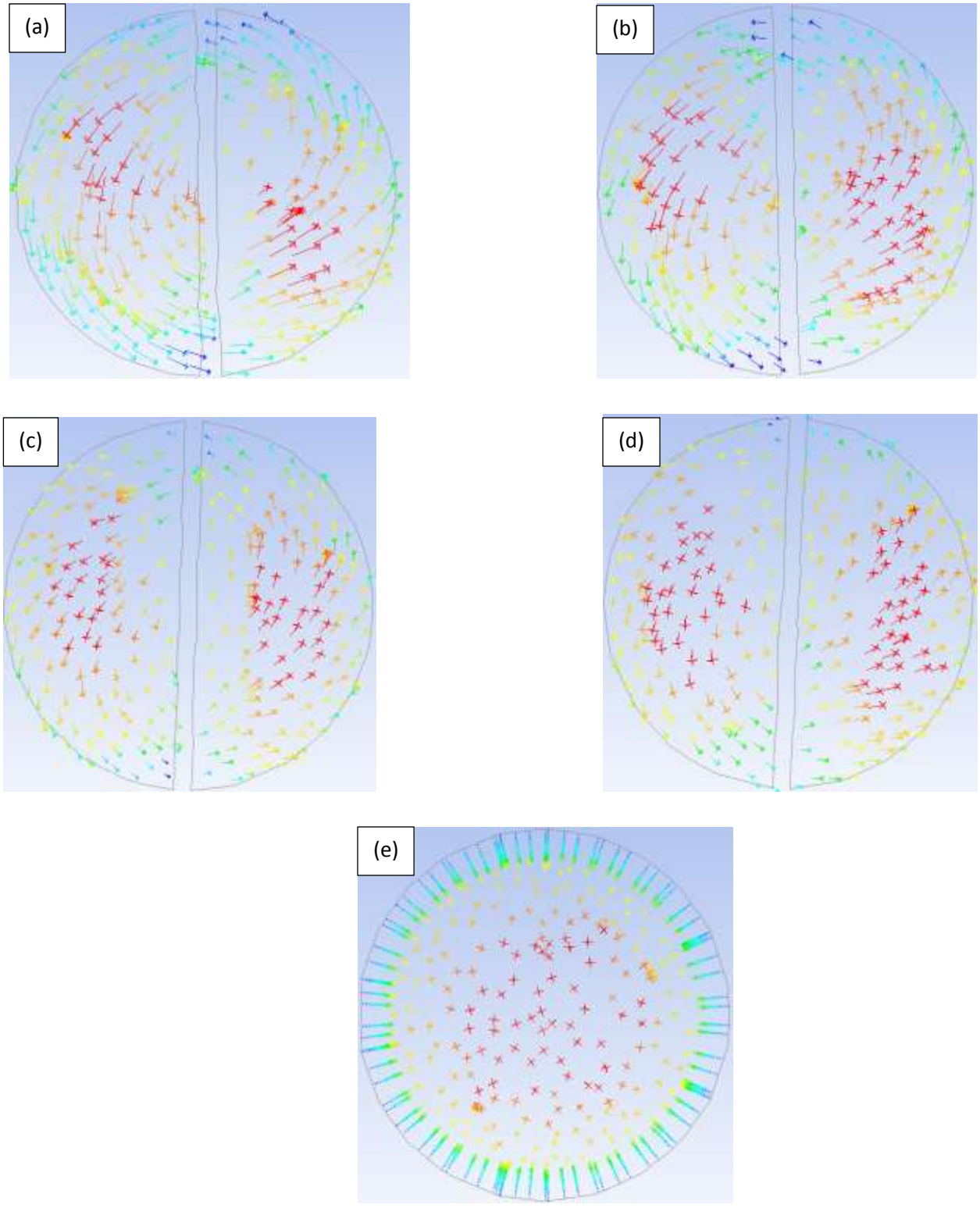

Fig.5.8. Vector plots of velocity at different twist ratios for Re= 2000: (a) y= 2, (b) y=3, (c) y=4, (d) y= 5, (e) plain tube

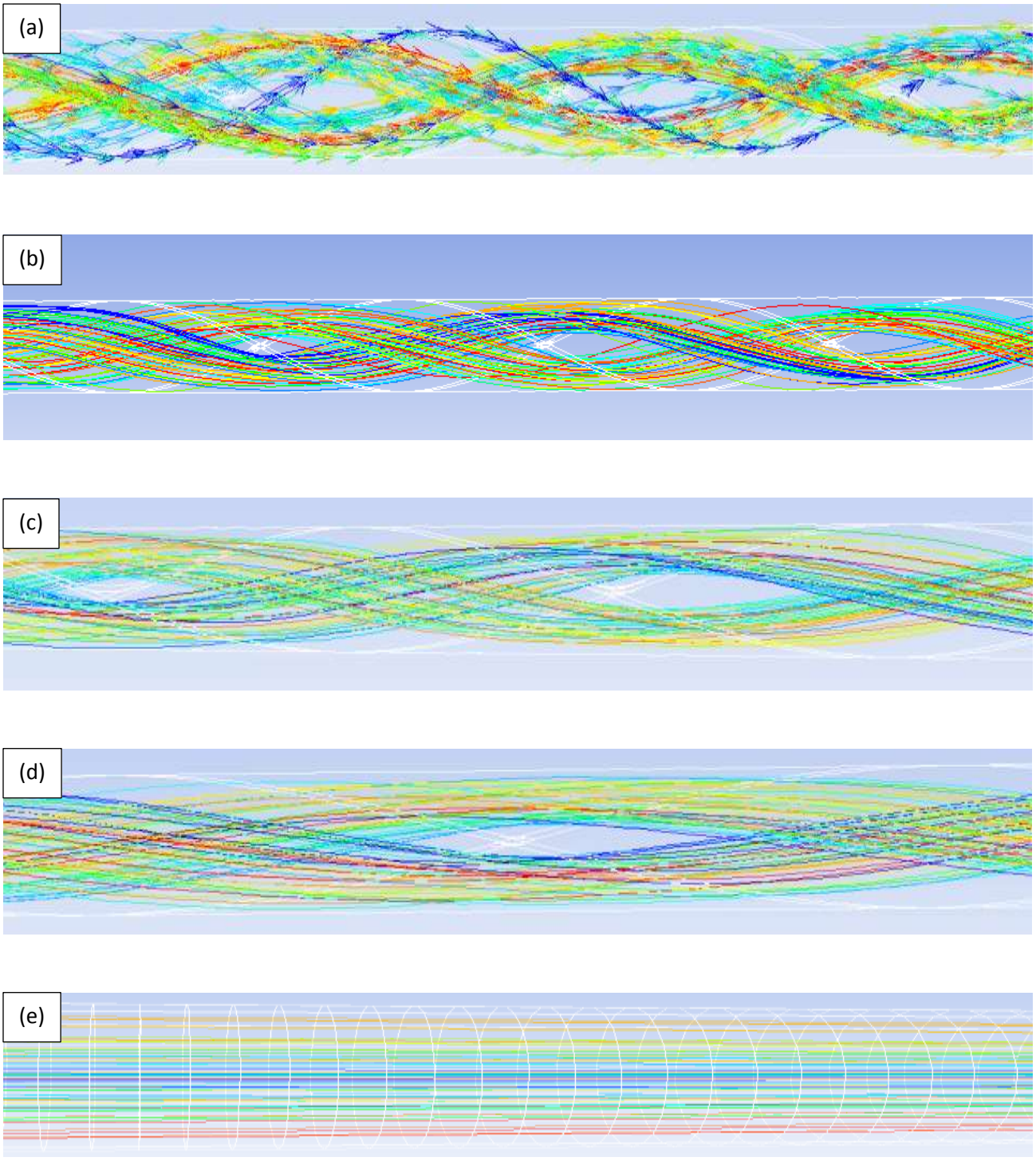

Fig.5.9. Pathlines at different twist ratios for Re= 2000: (a) y= 2, (b) y=3, (c) y=4, (d) y= 5, (e) plain tube

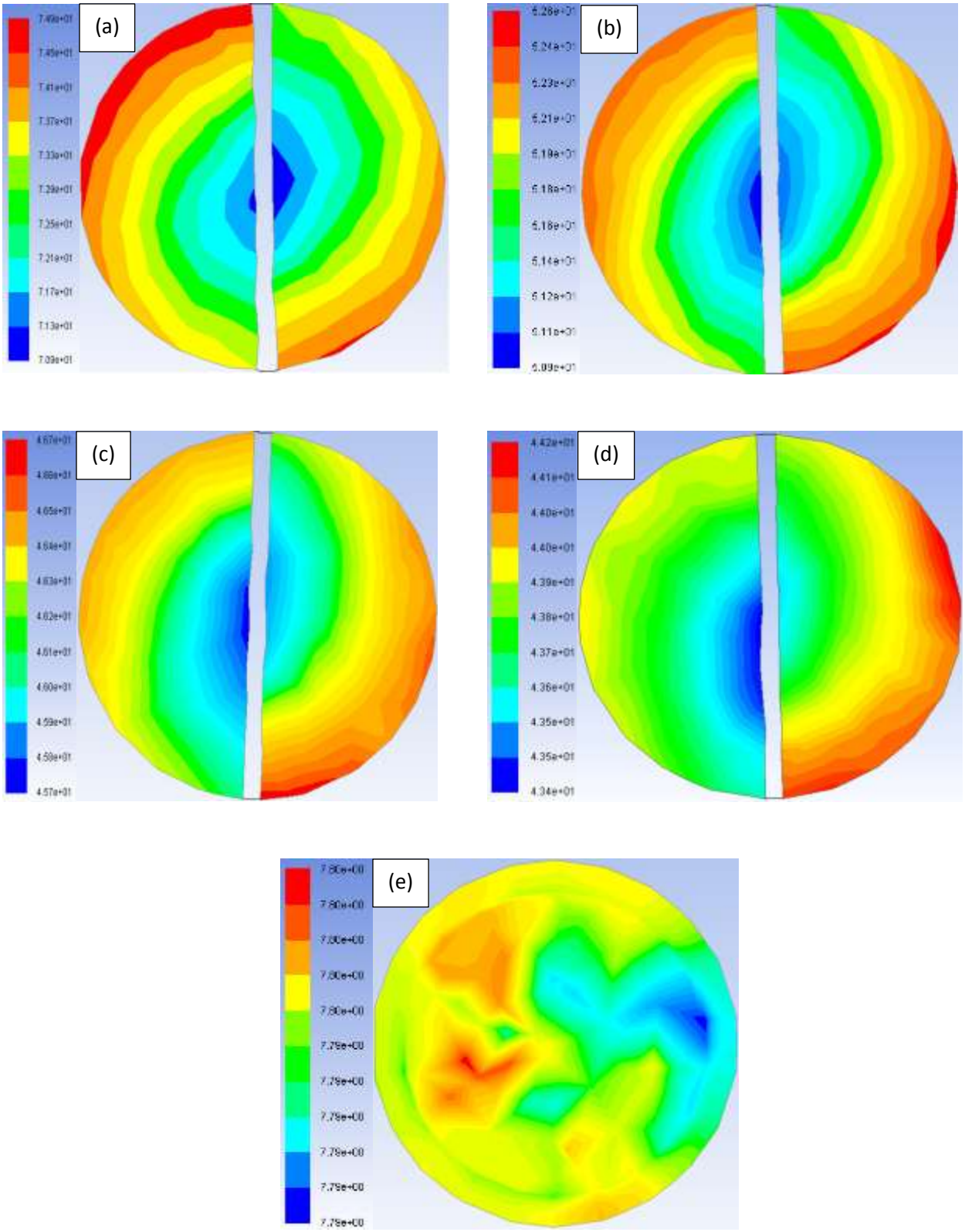

Fig.5.10. Contour plots of static pressure at different twist ratios for Re= 2000: (a) y= 2, (b) y=3, (c) y=4, (d) y= 5, (e) plain tube

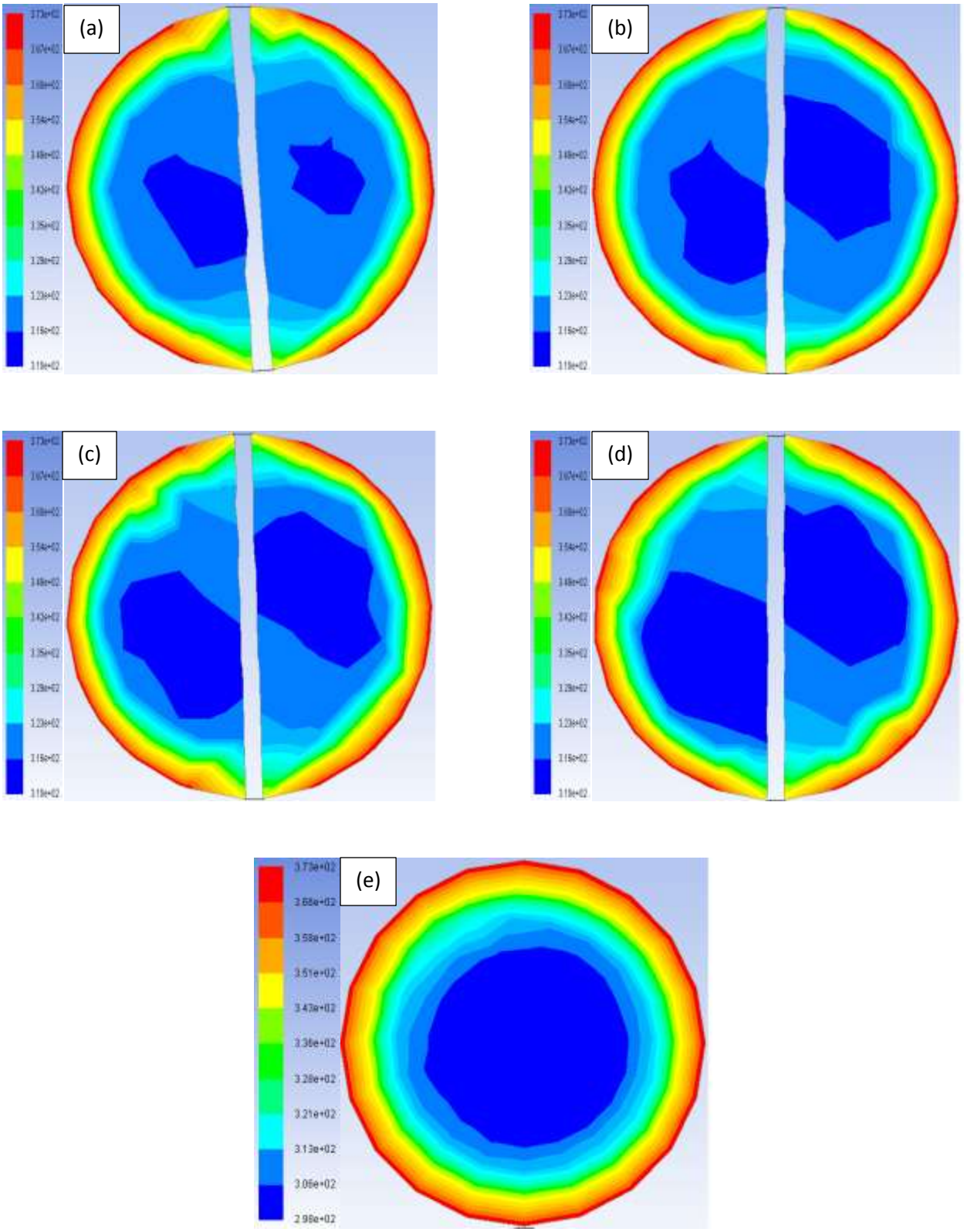

Fig.5.11. Contour plots of temperature field at different twist ratios for Re= 2000: (a) y= 2, (b) y=3, (c) y=4, (d) y= 5, (e) plain tube

5.3.3. Heat transfer results

Effect of the twist ratios on the heat transfer rate is numerically studied; the values are given in Table.A.5. The results for the tube fitted with all twisted tapes are also compared with those for a plain tube under similar operating conditions. The heat transfer rate is considered in terms of Nusselt numbers Fig, 5.12 and 5.13 shows the Nusselt number ratio (Nu_a/Nu_0) with Reynolds number of the tube equipped with four different twist ratios (y = 2, 3, 4 and 5). The Nusselt number in the tube with the twist ratios y= 2, 3, 4 and 5, are around 2.67 to 3.35, 2.43 to 2.19, 2.10 to 2.64, and 1.87 to 2.35 times of that in the plain tube in laminar region. Similarly in turbulent region 1.92 to 1.56, 1.74 to 1.41, 1.65 to 1.34, and 1.6 to 1.3 times of that in the plain tube.

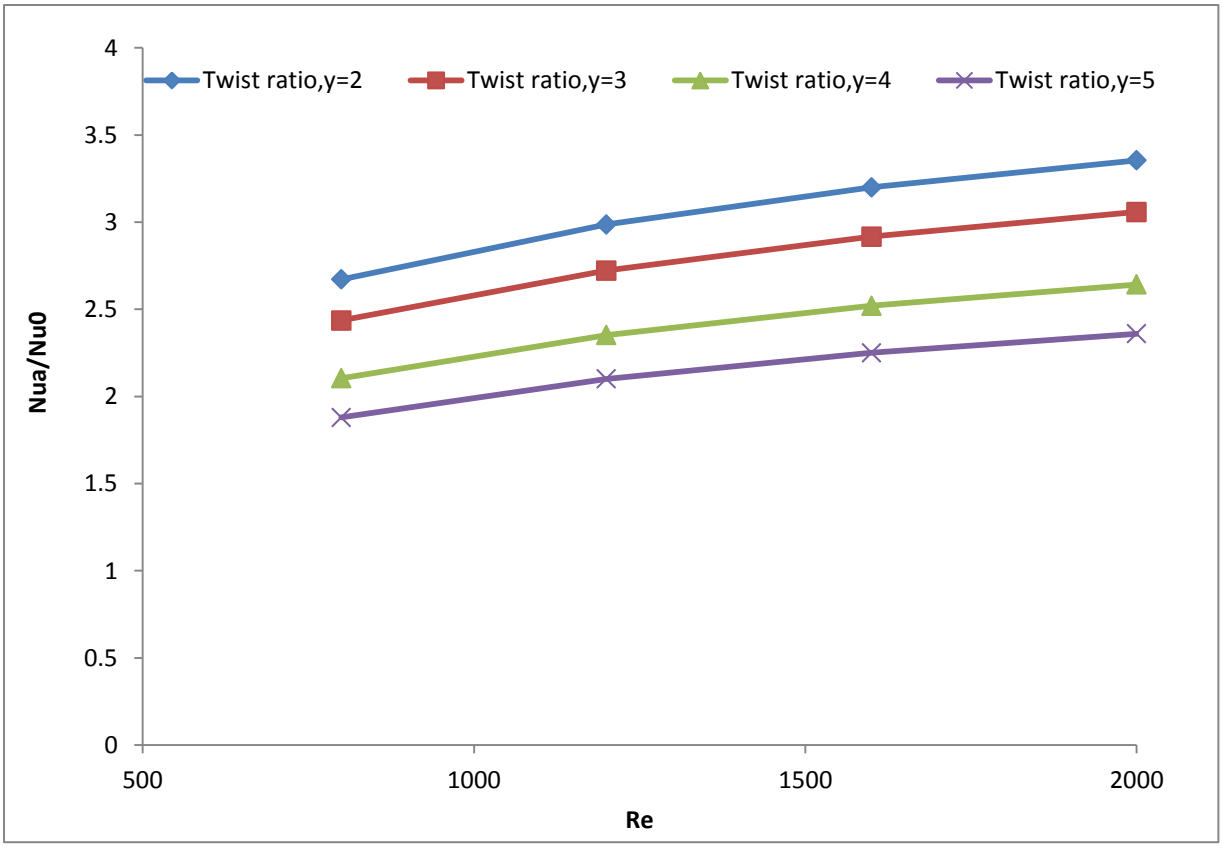

5.12. Variation of Nu_a/Nu_0 with Reynolds number in laminar regime for FWTT

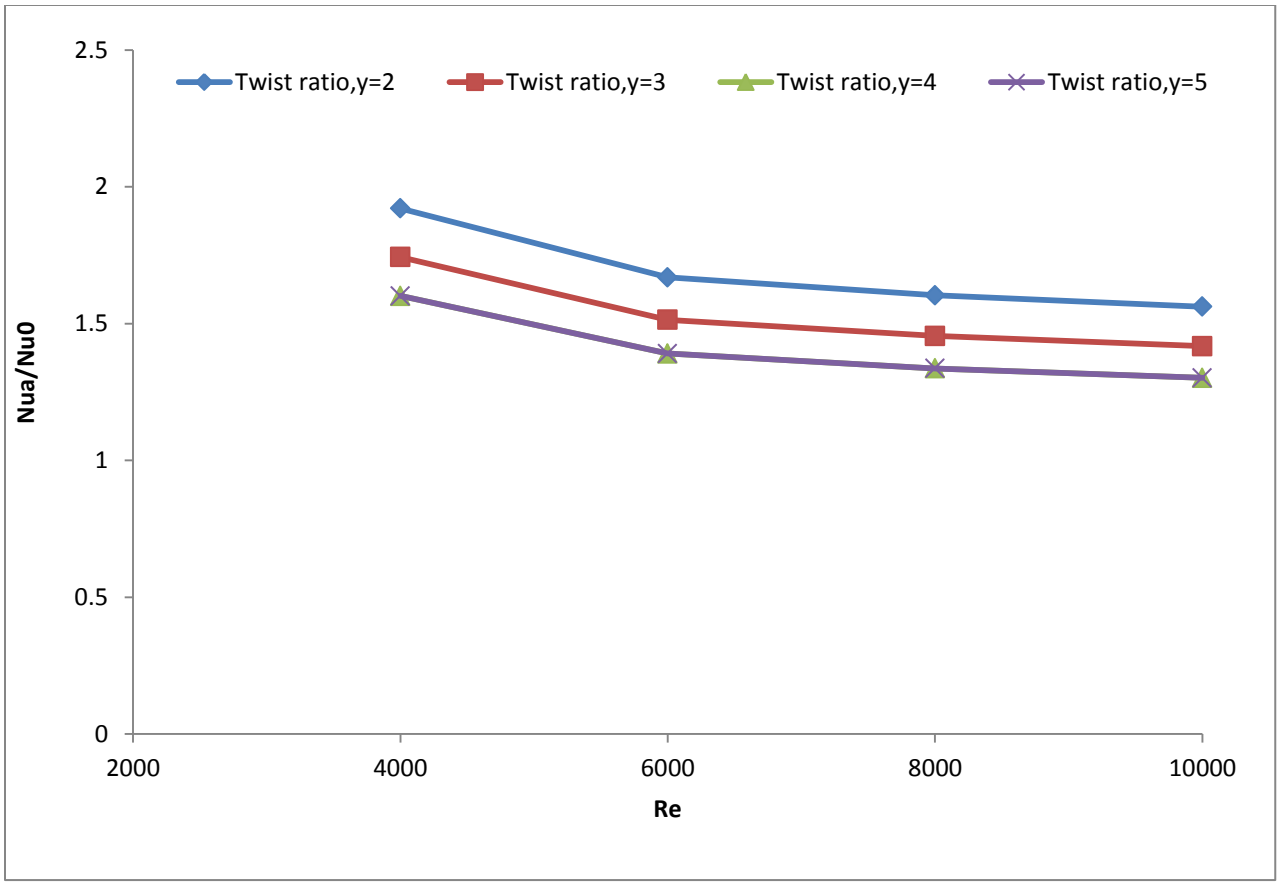

5.13. Variation of Nu_a/Nu_0 with Reynolds number in turbulent regime for FWTT

5.3.4. Friction factor results

Effect of the twist ratios on the friction factor is numerically studied, the values are given in Table.A.6.The friction factor characteristic in a plain tube fitted with twisted tape at various twist ratios is displayed in Fig. 5.14 and Fig. 5.15. Friction factor decreases with increasing twisted ratio. The friction factors in the tube with the twist ratios y= 2, 3, 4 and 5, are around 8.77 to 10.39, 6.09 to 7.15, 5.14 to 5.97, and 4.67 to 5.37 times of that in the plain tube in laminar region. Similarly in turbulent region 5.59 to 4.69, 4.39 to 3.68, 3.84 to 3.22, and 3.54 to 2.97 times of that in the plain tube.

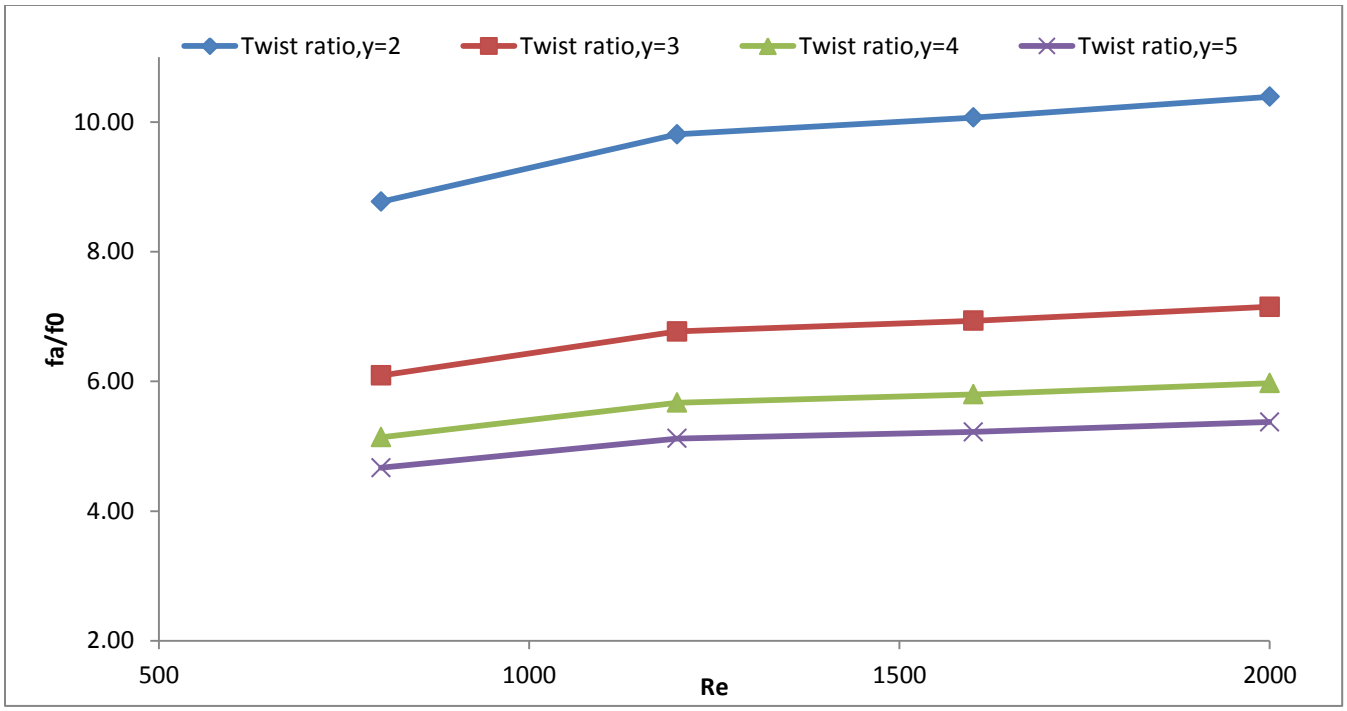

5.14. Variation of f_a/f_0 with Reynolds number in laminar regime for FWTT

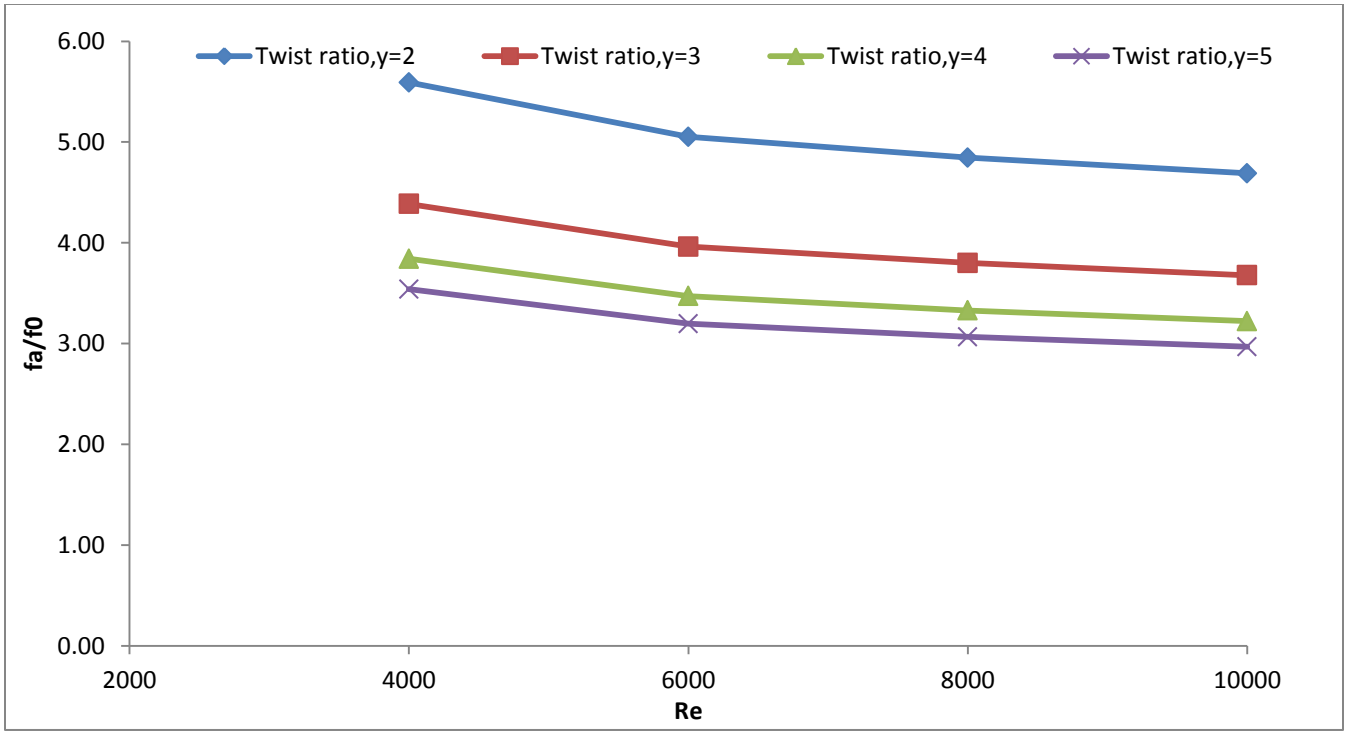

Fig.5.15. Variation of f_a/f_0 with Reynolds number in turbulent regime for FWTT

5.3.5. Thermal performance factor

Thermal performance factor (η) is the ultimate parameter used for evaluating the use of the twisted tape, simulation result are given in Table.A.7. The factor is obtained by considering the effect of heat enhancement and the increase of pressure drop, consideration is based on the same pumping power consumption for tubes with and without a twisted tape insert. The variation of thermal performance factor with Reynolds number of the twist ratios (y=2, 3, 4 and 5) is shown in Fig.5.16 and Fig.5.17. Thermal performance factor increases with increasing Reynolds number in laminar region, decrease with increasing in Reynolds number in turbulent region

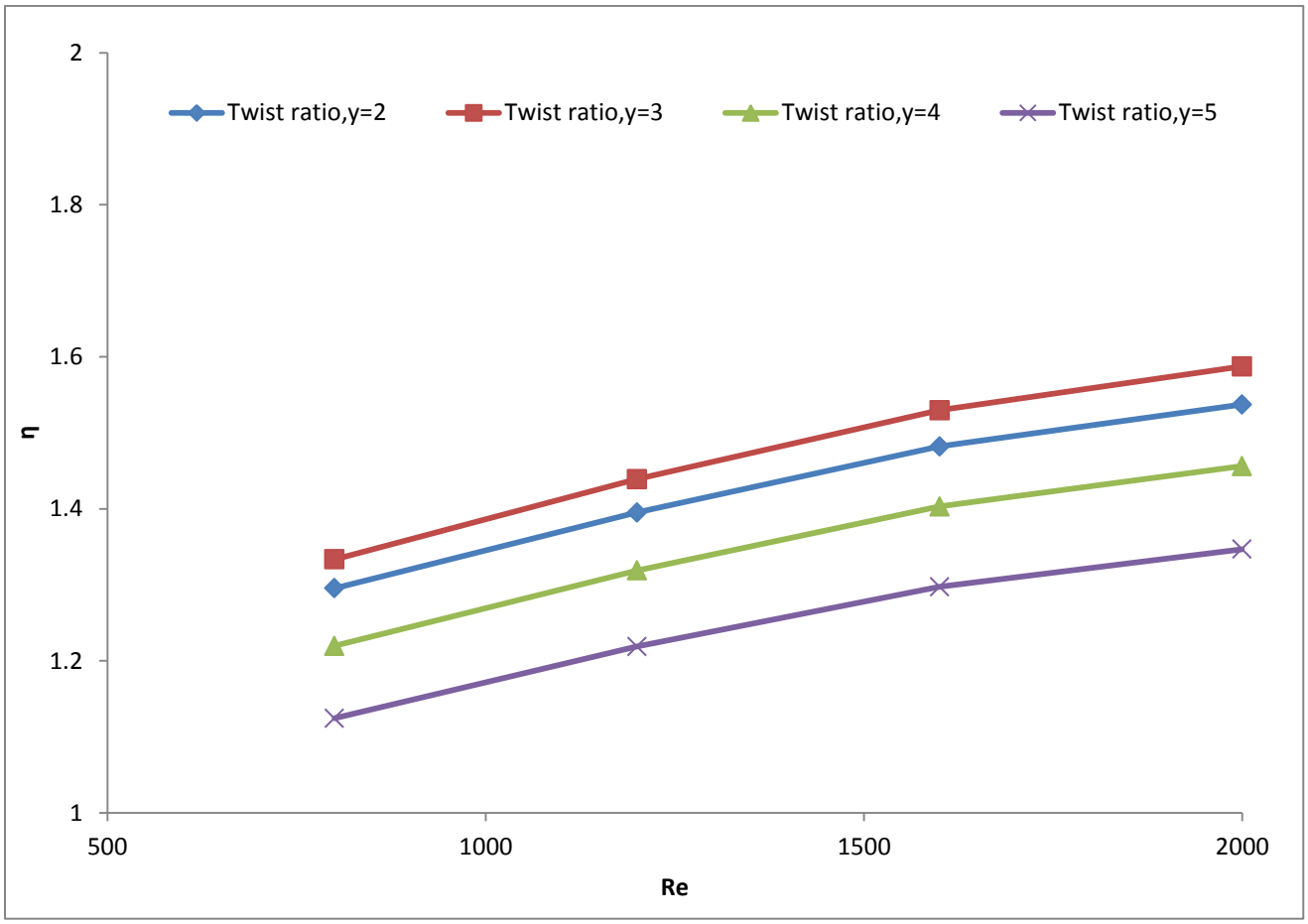

Fig.5.16. Variation of η with Reynolds number in laminar regime for FWTT

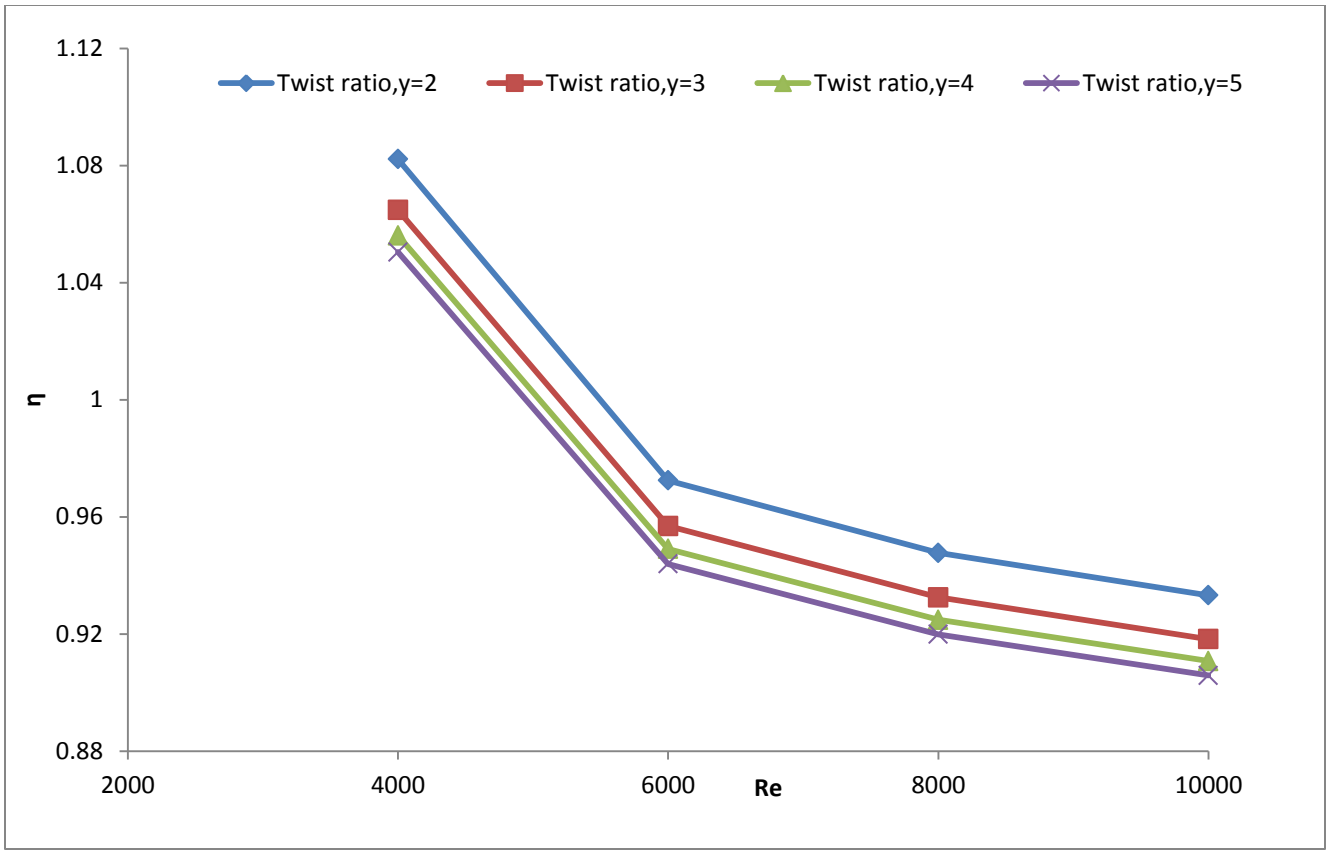

Fig.5.17. Variation of η with Reynolds number in turbulent regime for FWTT

5.4. Conclusion

Nusselt number and friction factor values were found to decrease with increasing in twist ratio. The contour plots of predicted velocity vector, static pressure and temperature are also examined. It is shown that the twisted tape inserts for twist ratio (y=2) can enhance heat transfer rates up to 3.5 times at Reynolds number 2000 and increase in friction factors nearly 9 times in comparison with those of the plain tube. Thermal performance factor (η) was found to increase with increase in Reynolds number in the laminar region and decrease in the turbulent region. The maximum value of the thermal performance factor was found to be 1.6 for Twisted tape (y=3) in plain tube of a Reynolds number of 2000

CHAPTER 6

FRICTION FACTOR AND HEAT TRANSFER IN INTERNAL FINNED TUBE WITH REDUCED WIDTH (RWTT) TWISTED TAPE INSERTS

A numerical solution is carried out for plain tube with four longitudinal internal fins and Reduced width Twisted Tape (RWTT) inserts of twist ratio varying form 2-5. Four longitudinal fins are placed inside the plain tube with equal spacing. Fin thickness is 1 mm and 2 mm height, length of the fin same as the circular tube. Thickness and height of the longitudinal fins are considered as constant values. The SST k–ω turbulence model was considered for finding the Nusselt number and friction factor. Material properties, boundary conditions are same as the previous studies (chapter 5).

6.1. FLUENT Simulation

6.1.1. Geometry and Mesh

The 3D geometry of finned tube with twisted tape inserts was created by using ANSYS 13.0 software. The geometry is meshed into smaller cells. The meshing method used is automatic .The geometry is meshed into 77,230 nodes and 3, 49, 806 elements.

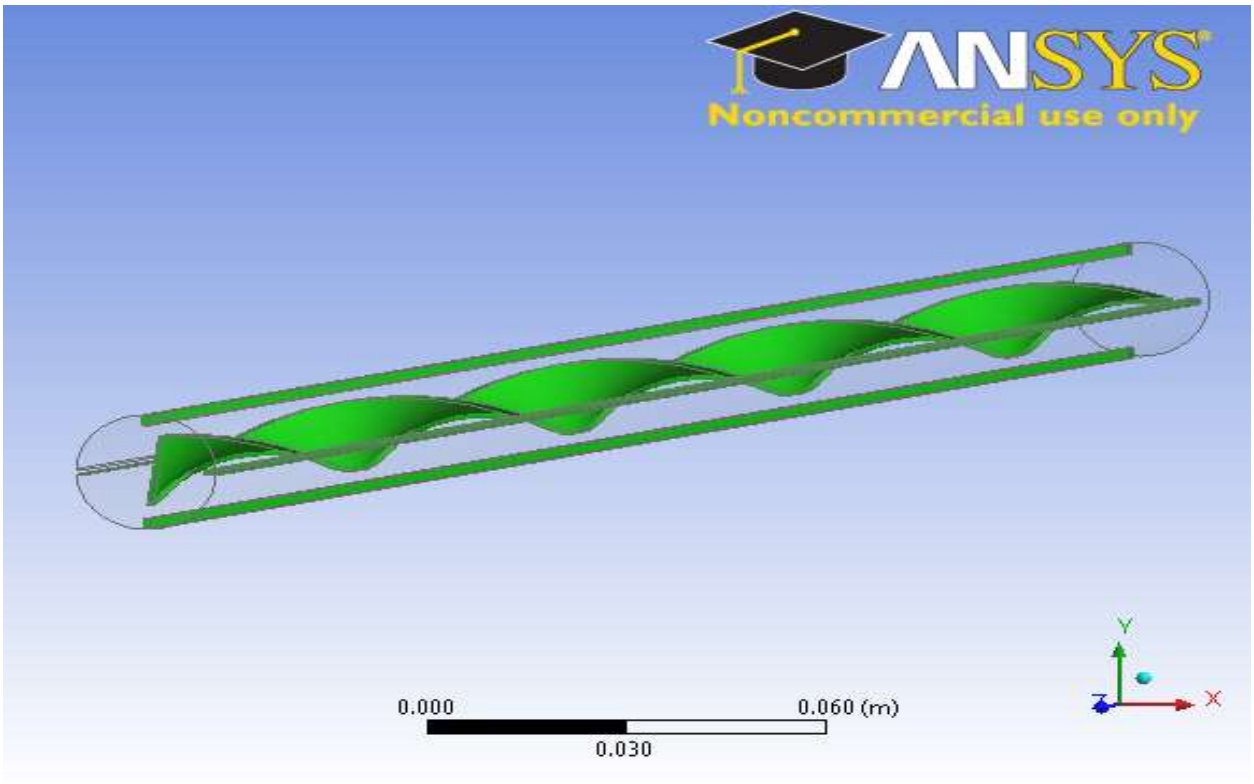

Fig.6.1. Geometry of internal longitudinal finned tube with the twisted tape

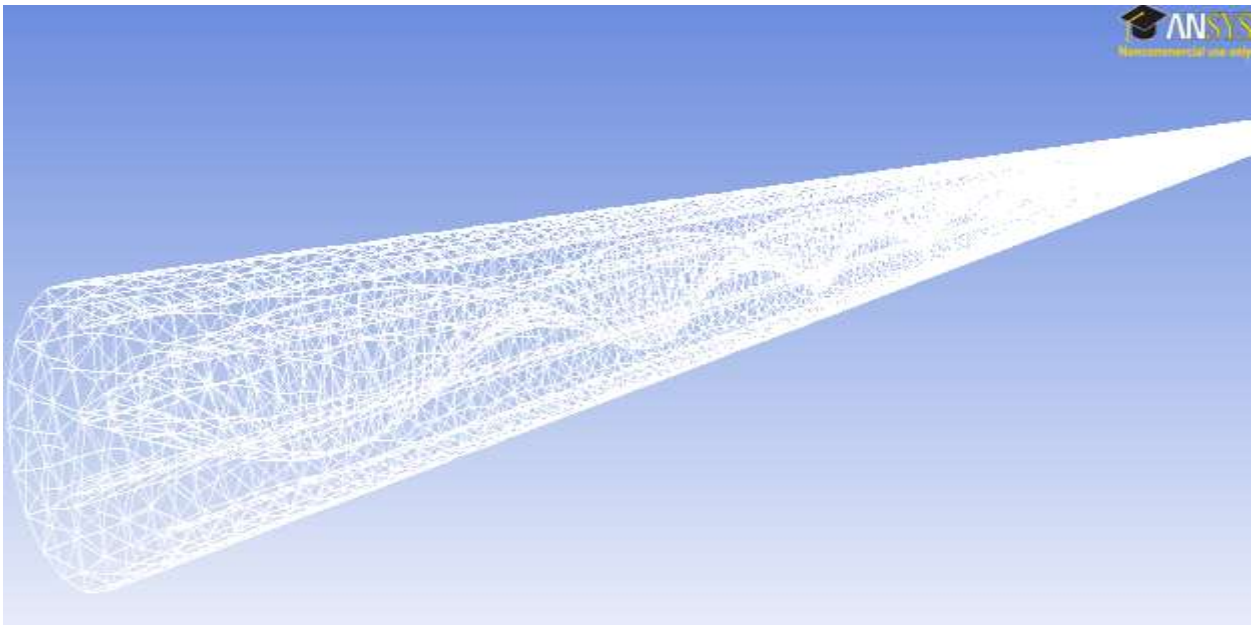

6.2. Meshing of the finned tube geometry

6.1.3. Flow configurations

The numerical analysis is made for finned tube with tapes width of w =12mm, 14mm and 16mm for the twist ratios, y=2, 3, 4, and 5 as detailed in Table.6.1. The Reynolds numbers used for the computation are referred to the inlet values which are set at 800, 1200, 1600, 2000, 4000, 6000, 8000 and 10,000. The tube wall and inlet temperatures are kept constant at 373 K and 298 K.

Table.6.1. Dimensions of twisted tape inserts in finned tube

S. No	Twist ratio, y	Width , w mm	Pitch, H mm
1	2	12	24
		14	28
		16	32
2	3	12	36
		14	48
		16	64
3	4	12	48
		14	56
		16	64
4	5	12	60
		14	70
		16	80

6.2. Results and discussion

6.2.1. Pathlines

Contour plots of pathlines through the tube with twisted tape insert(y=2) at Re = 2000, w ==12 mm, 14 mm and 16 mm are displayed in Fig.6.3. It is clearly seen that the tape with width of 12 mm there is no effect on flow near the wall. This may be because of its smaller width.

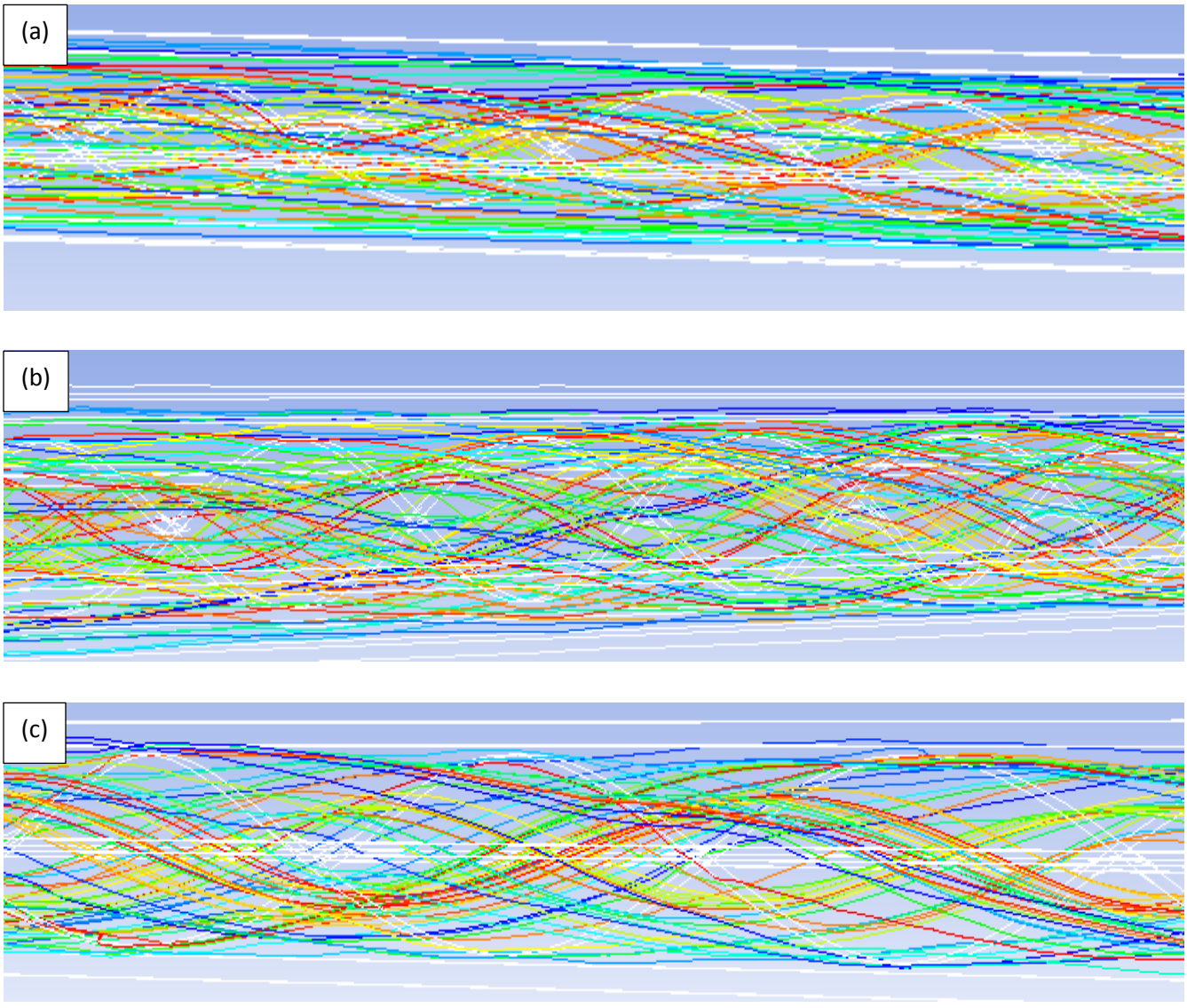

Fig.6.3. pathlines at different tape widths at twist ratio (y=2) of Re = 2000, (a) w= 12 mm, (b) w = 14 mm, (c) w = 16 mm

6.2.2. Heat transfer results

The effectiveness of heat transfer augmentation in terms of R_1 (i.e. Nu_a/Nu_0) in the finned tube with RWTT of various twist ratios (y=2, 3, 4 and 5) and tape widths (w= 12 mm, 14 mm and 16 mm) relative to the plain tube for the various cases is compared in Fig.6.4 to Fig.6.11. The effectiveness is represented by the ratio of the Nusselt number of the finned tube with twisted tape insert to that of the plain tube of the same mass flow rate, in terms of i.e. $Nu_a/Nu_{0,}$ as shown in Table. A.8.

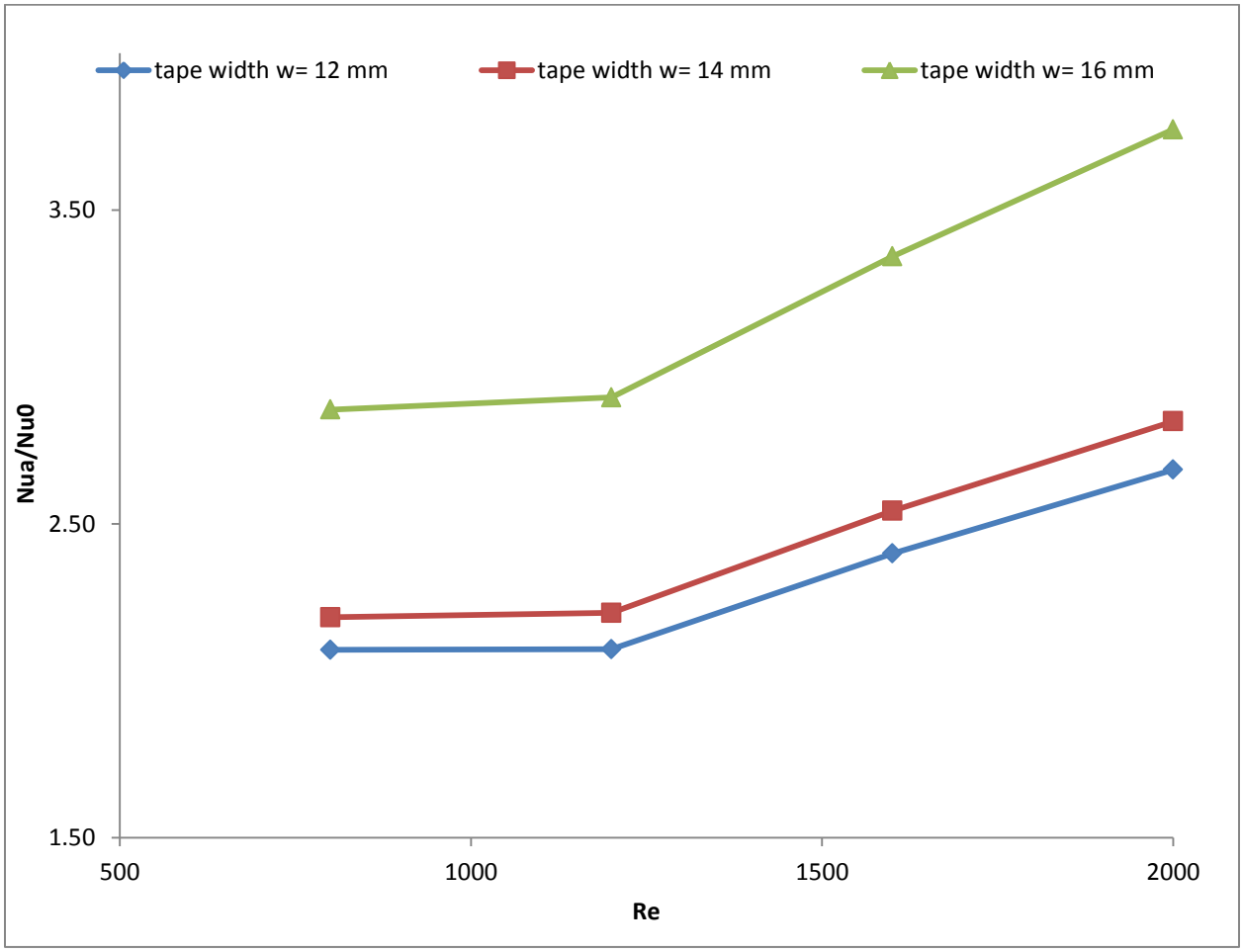

Fig.6.4. Variation of Nu_a/Nu_0 with Reynolds number in laminar regime, twist ratio y=2(RWTT)

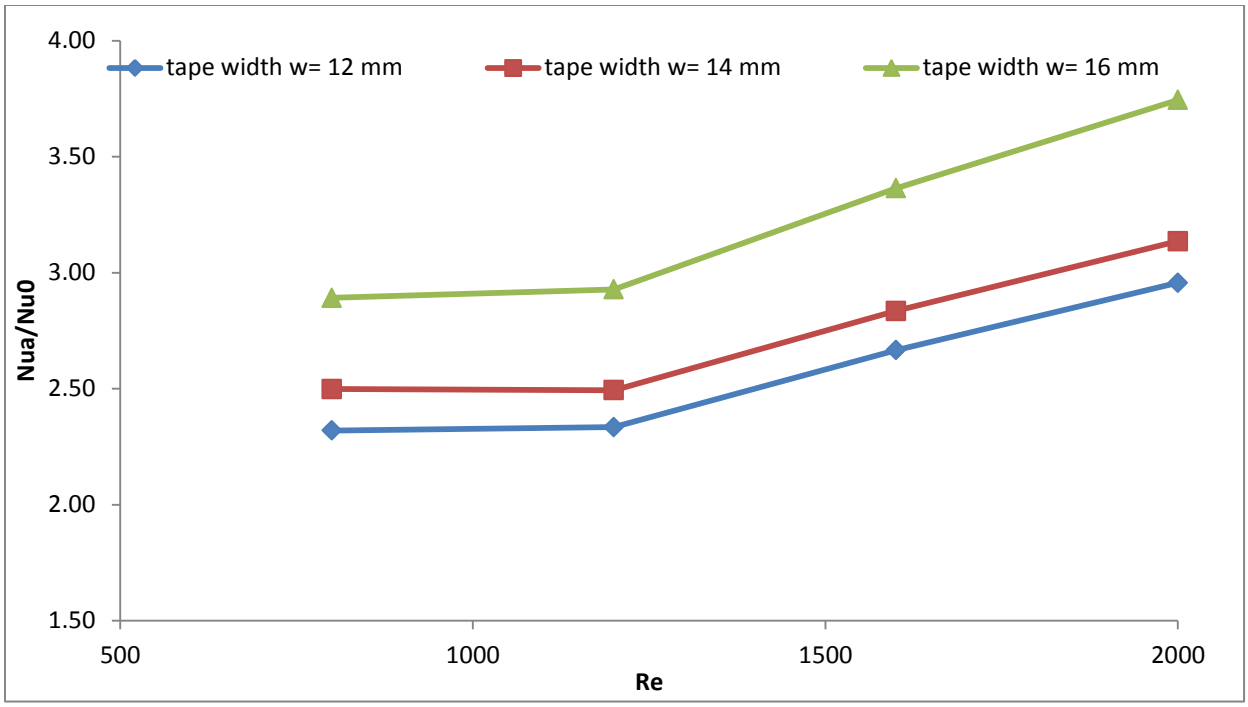

Fig.6.5. Variation of $Nu_{a/}Nu_0$ with Reynolds number in laminar regime, twist ratio y=3(RWTT)

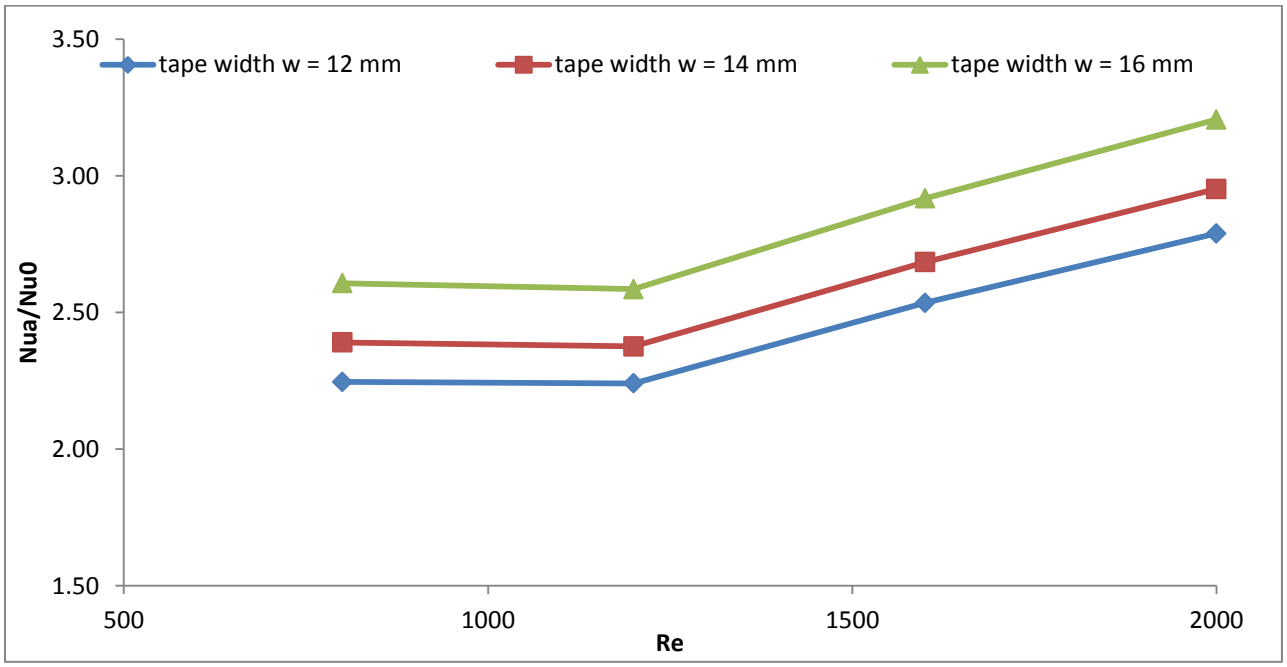

Fig.6.6. Variation of $Nu_{a/}Nu_0$ with Reynolds number in laminar regime, twist ratio y=4(RWTT)

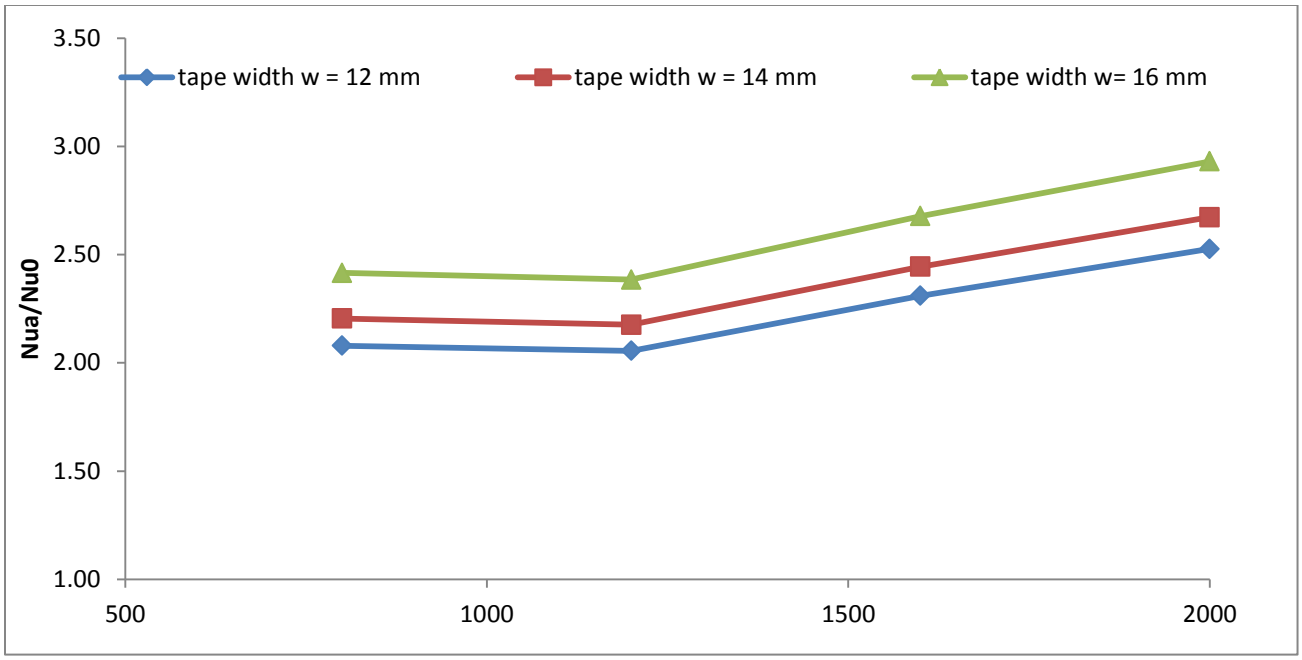

Fig.6.7. Variation of Nu_a/Nu_0 with Reynolds number in laminar regime, twist ratio y=5(RWTT)

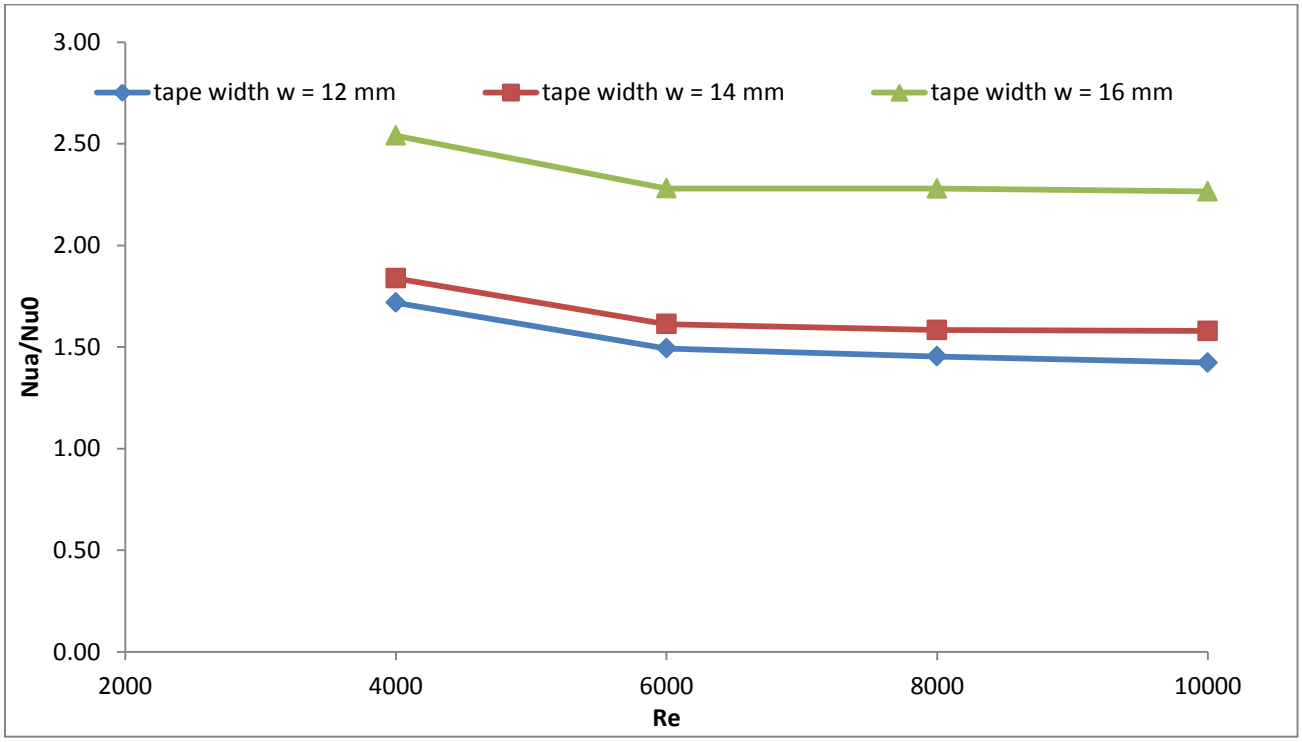

Fig.6.8. Variation of Nu_a/Nu_0 with Reynolds number in turbulent regime, twist ratio y=2(RWTT)

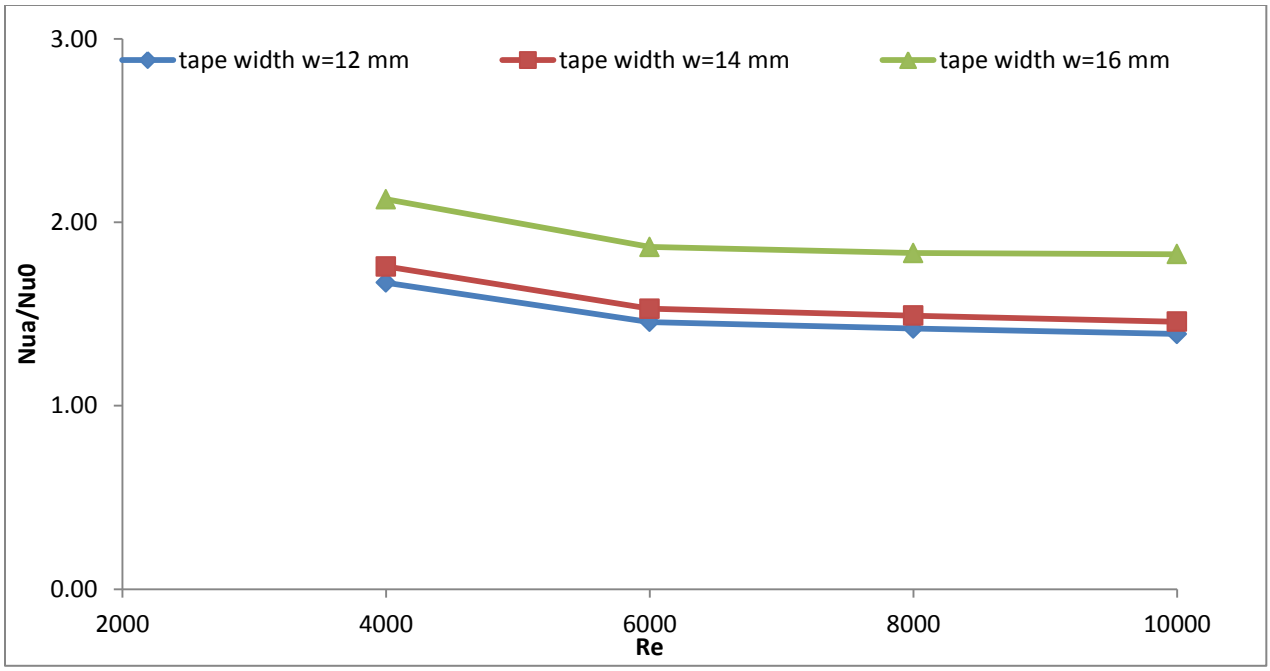

Fig.6.9. Variation of Nu_a/Nu_0 with Reynolds number in turbulent regime, twist ratio y=3(RWTT)

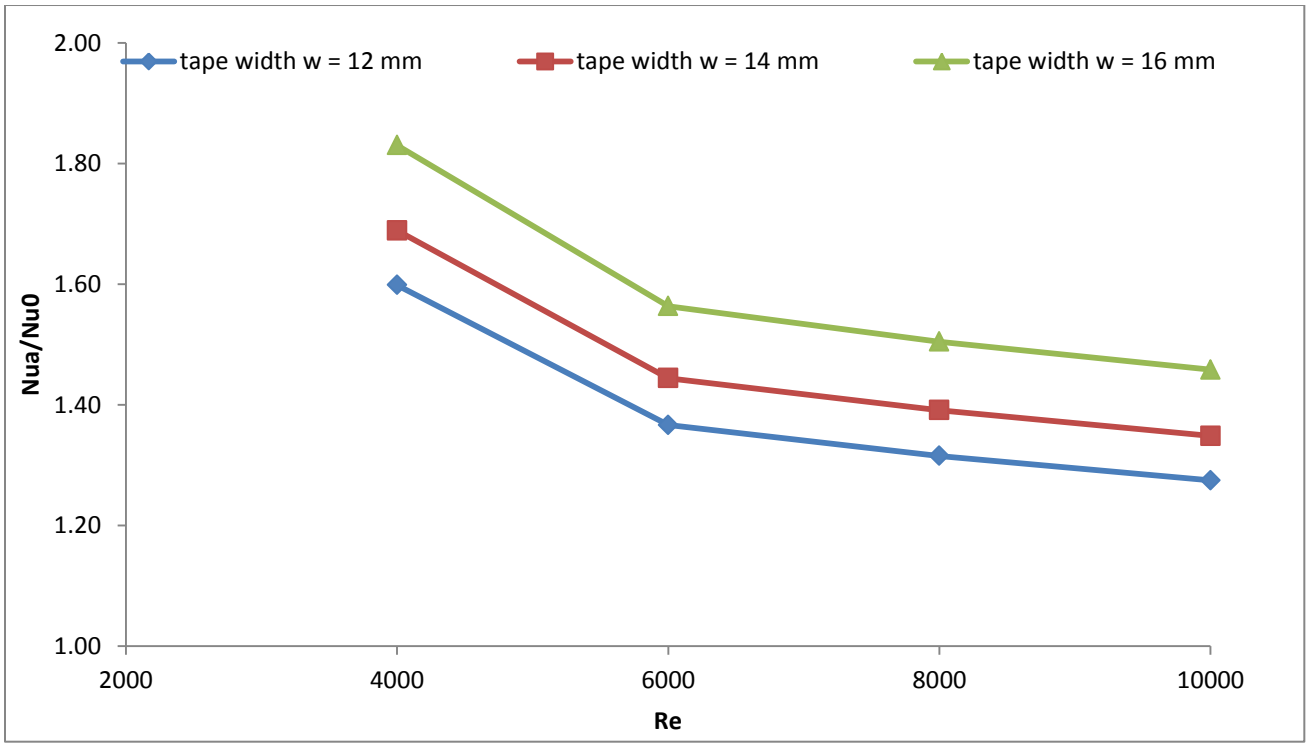

Fig.6.10.Variation of Nu_a/Nu_0 with Reynolds number in turbulent regime, twist ratio y=4(RWTT)

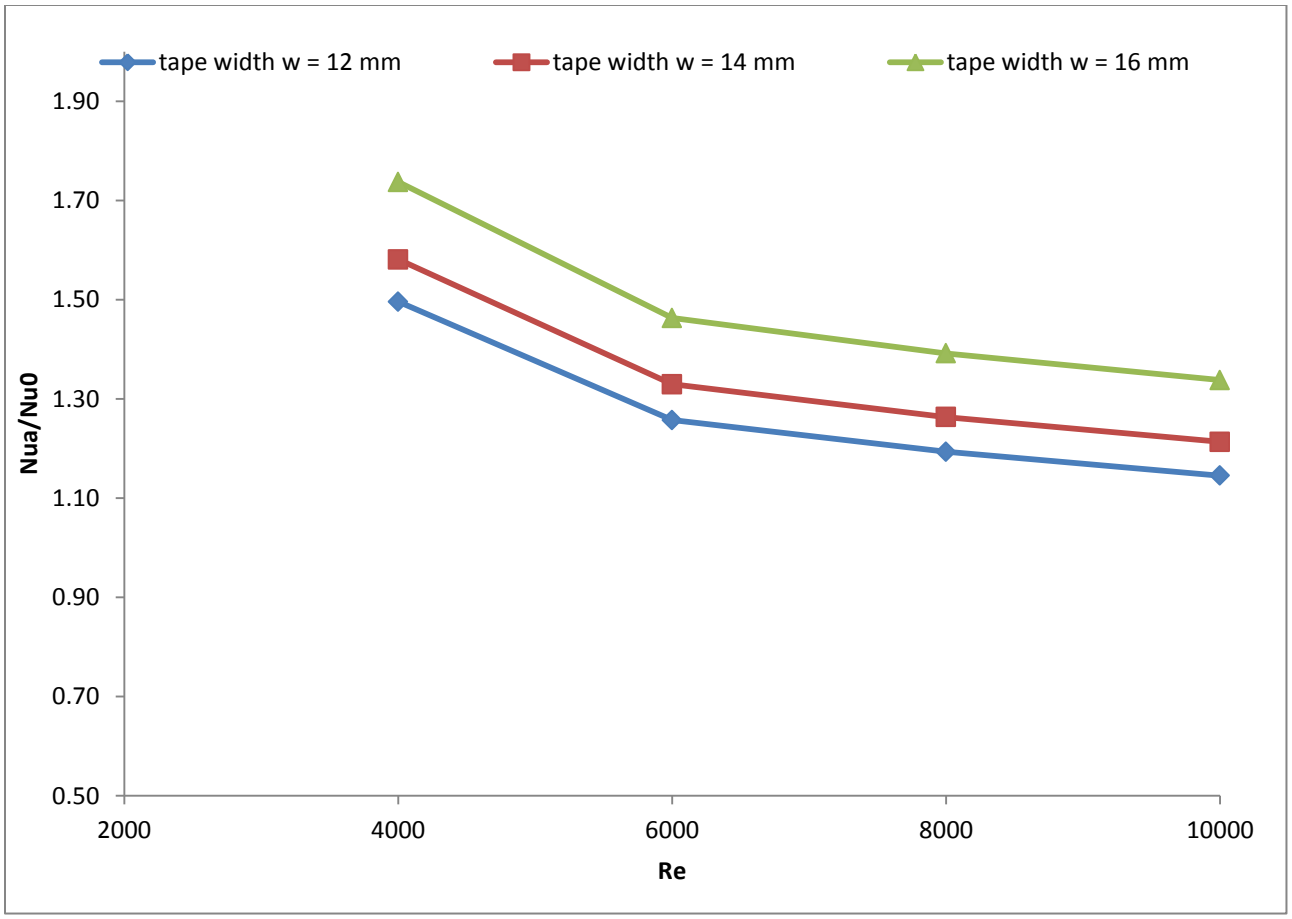

Fig.6.11. Variation of Nu_a/Nu_0 with Reynolds number in turbulent regime, twist ratio y=5(RWTT)

6.2.3. Friction factor Results

The variation of the increase in friction factor (f_a/f_0) with Reynolds number for the finned tube with RWTT of different twist ratios (y=2, 3, 4, 5) and widths of the tapes (w =12 mm, 14 mm, 16 mm) are, shown in Fig. 6.12 -6.19. Friction factor increase with increase in width of the tape, as Reynolds number increase. The corresponding values are given in Table.A.9

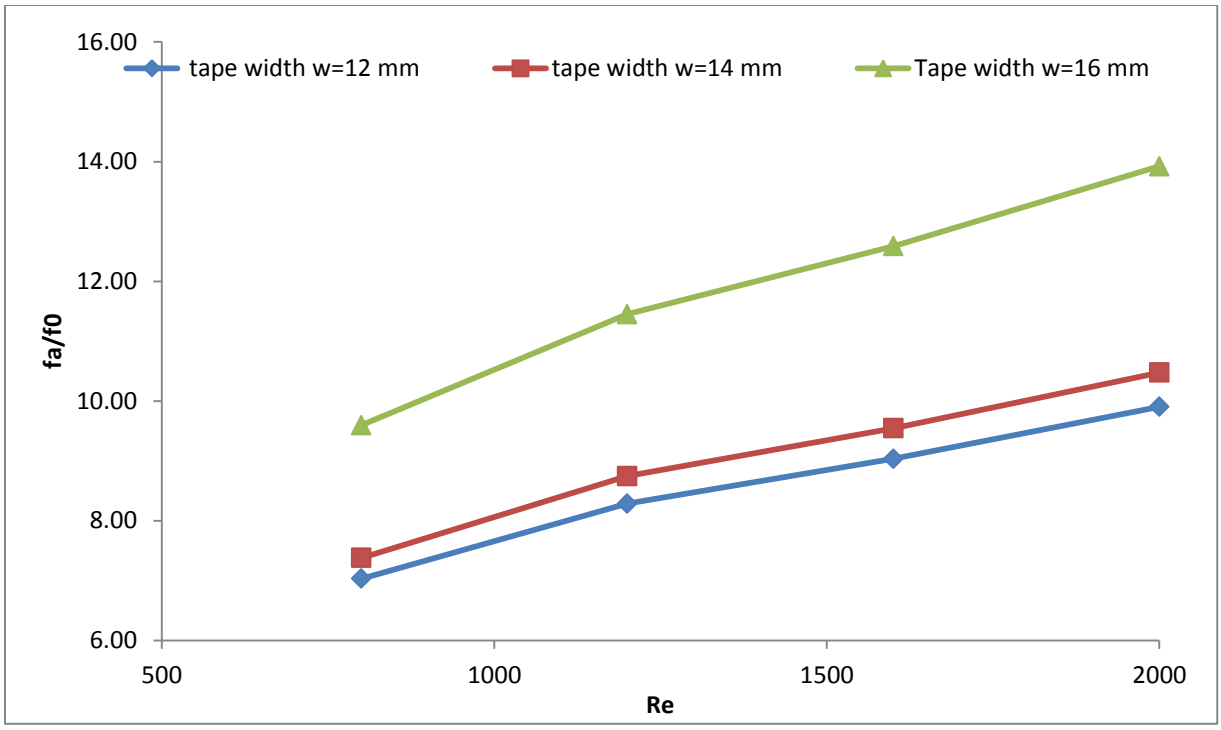

Fig.6.12. Variation of f_a/f_0 with Reynolds number in laminar regime, twist ratio y=2(RWTT)

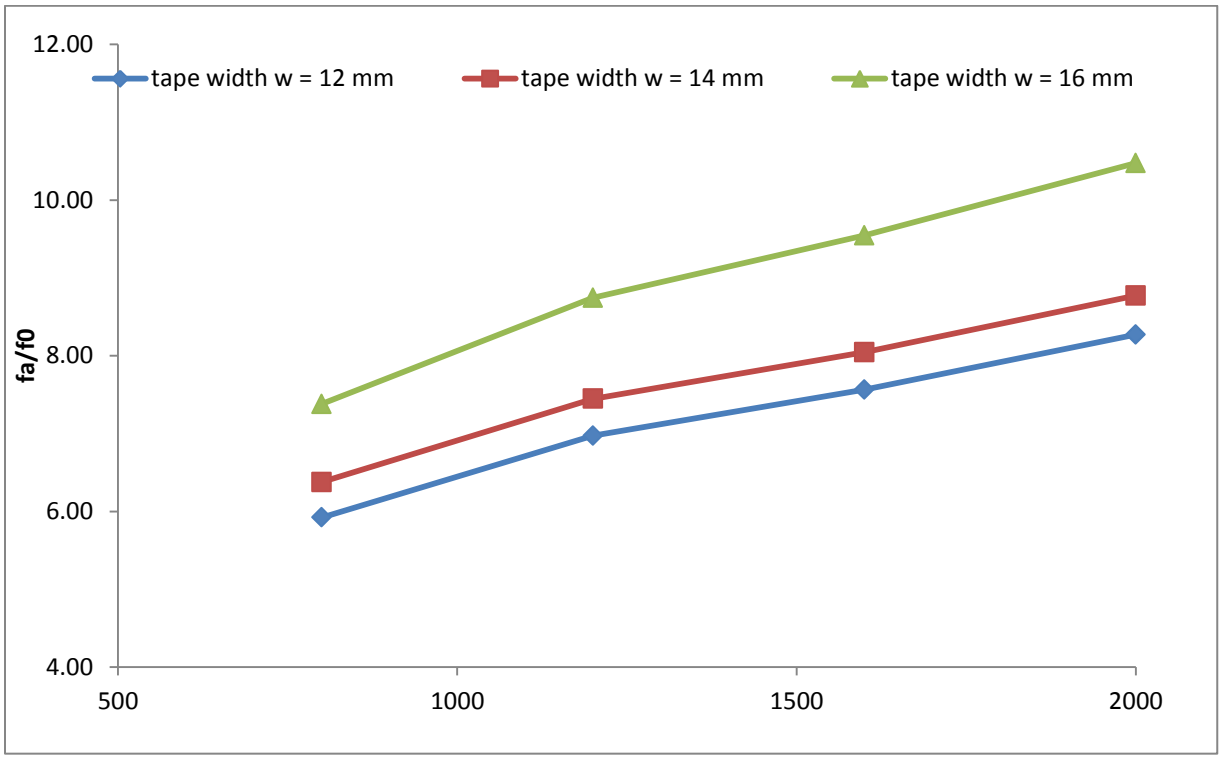

Fig.6.13. Variation of f_a/f_0 with Reynolds number in laminar regime, twist ratio y=3(RWTT)

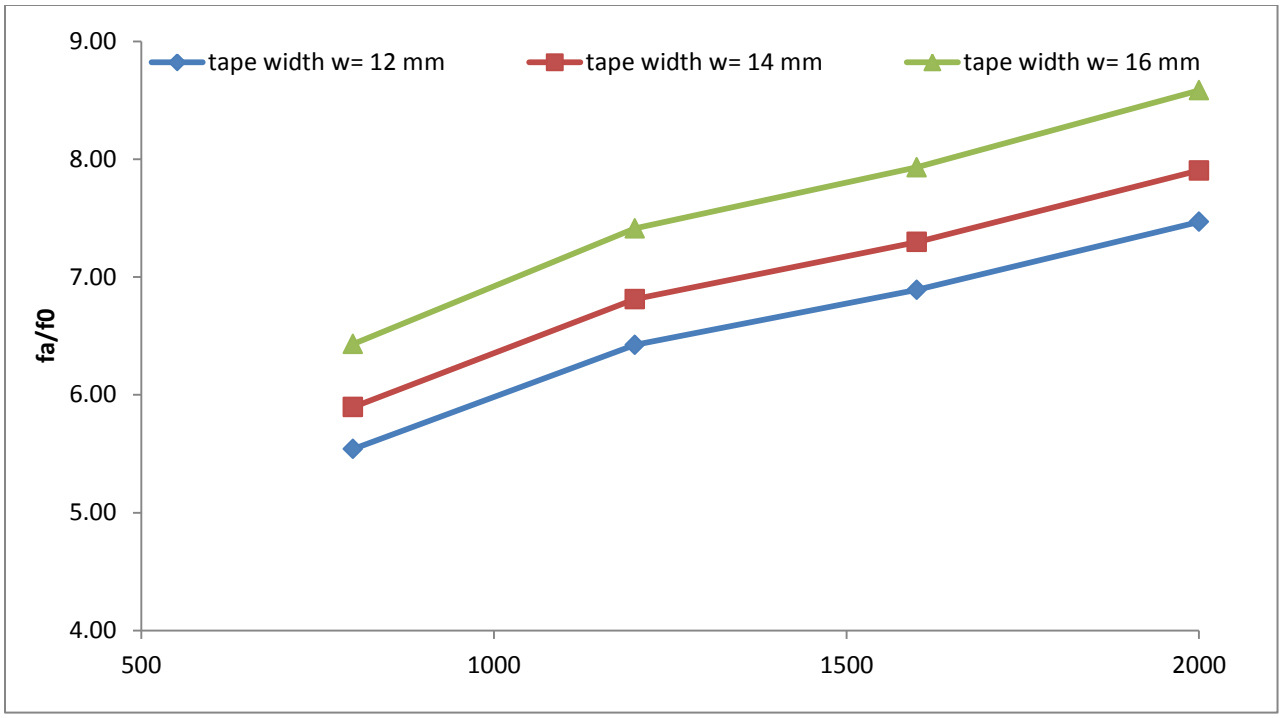

Fig.6.14. Variation of f_a/f_0 with Reynolds number in laminar regime, twist ratio y=4(RWTT)

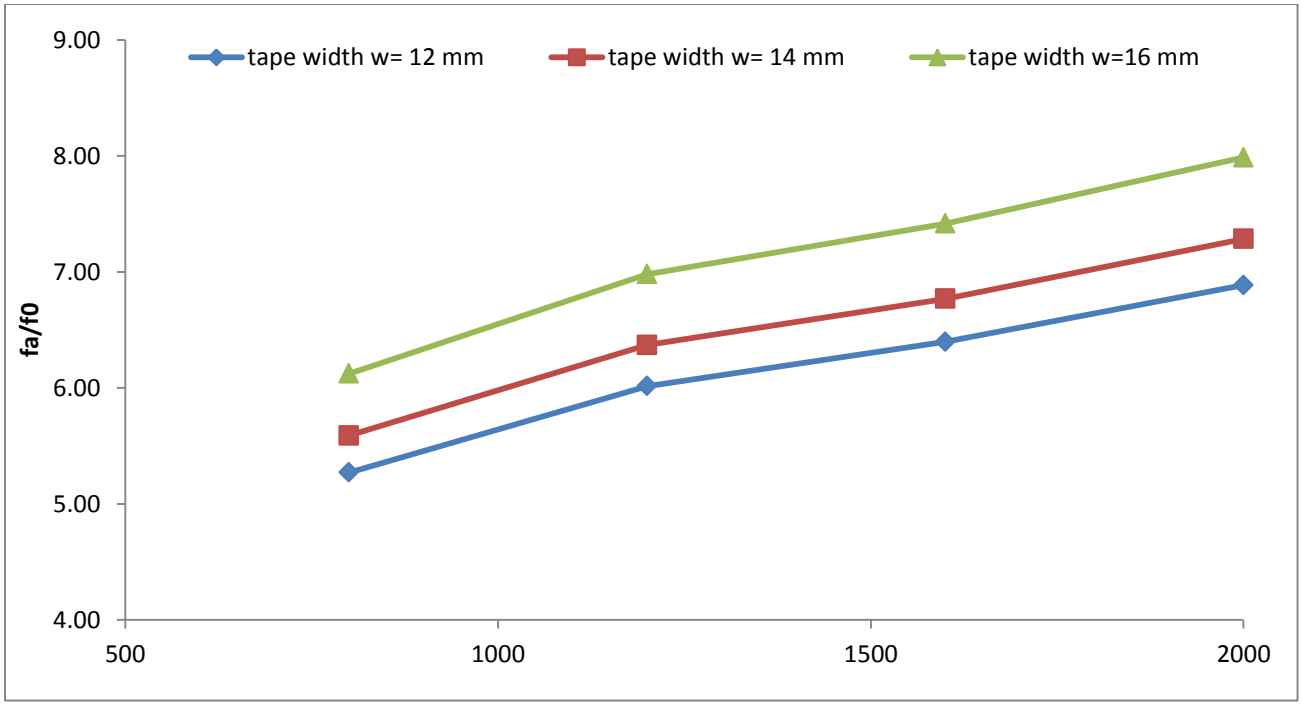

Fig.6.15. Variation of f_a/f_0 with Reynolds number in laminar regime, twist ratio y=5(RWTT)

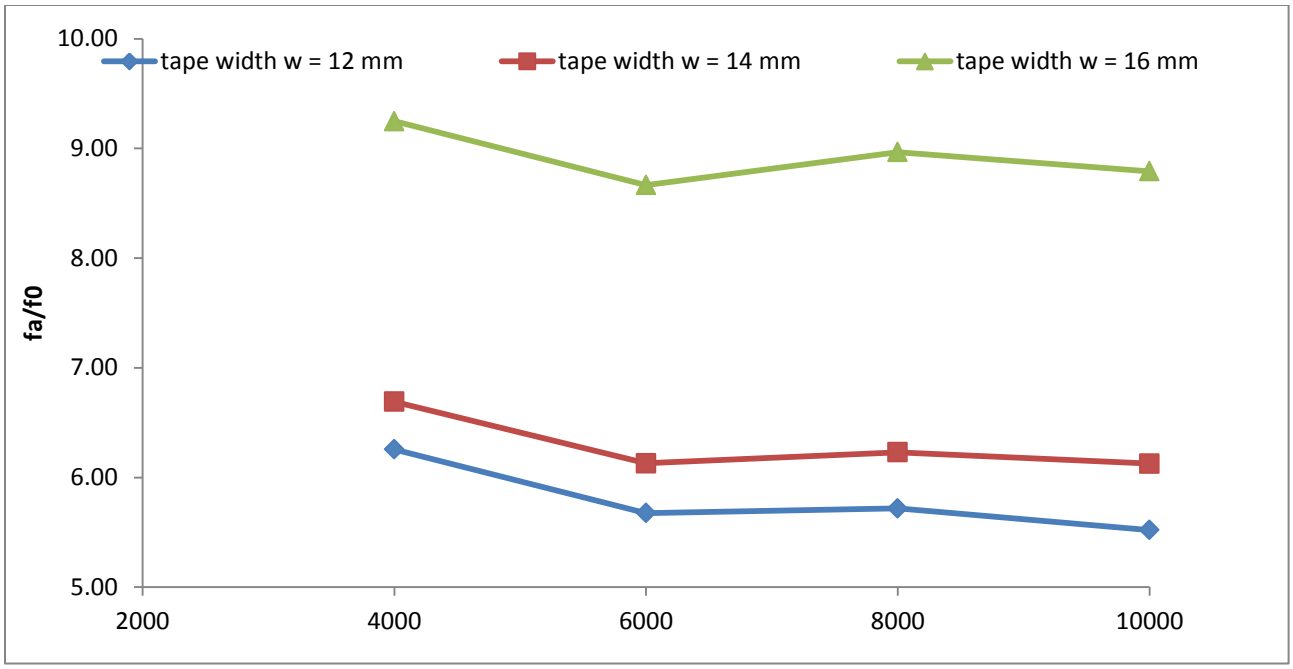

Fig.6.16. Variation of f_a/f_0 with Reynolds number in turbulent regime, twist ratio y=2(RWTT)

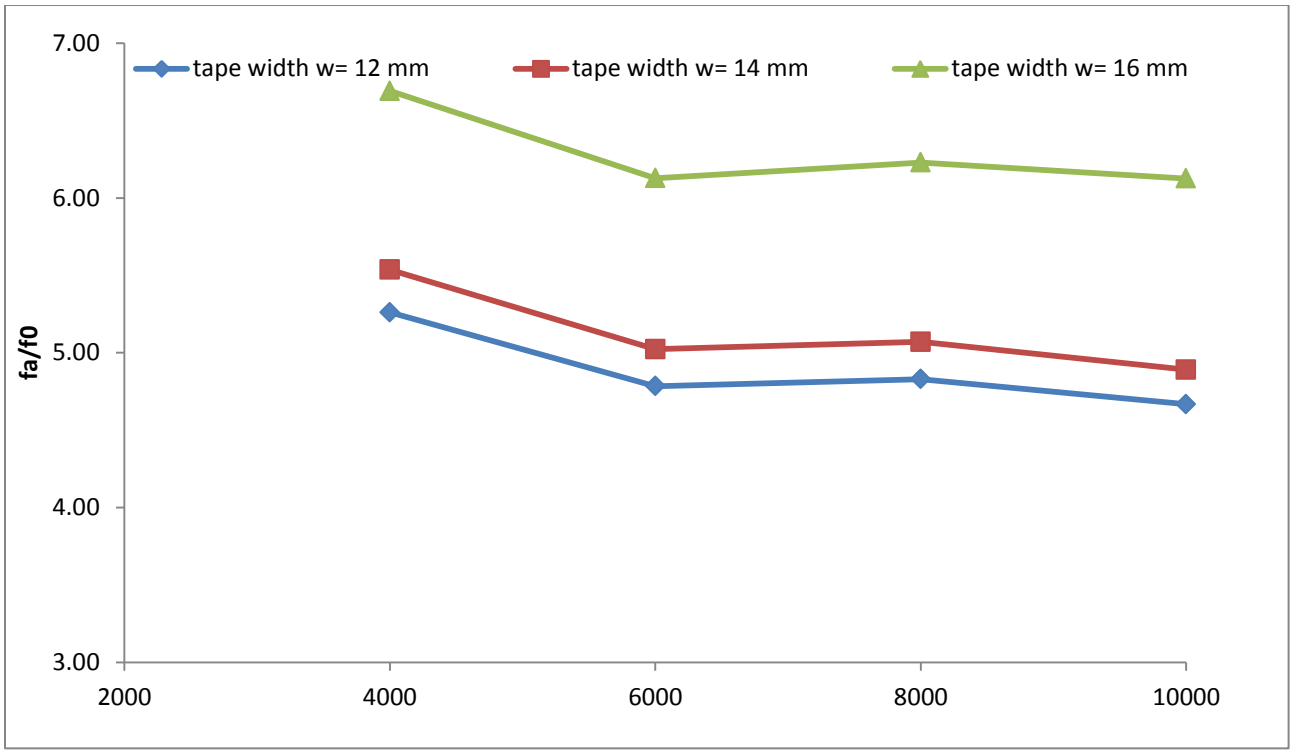

Fig.6.17. Variation of f_a/f_0 with Reynolds number in turbulent regime, twist ratio y=3(RWTT)

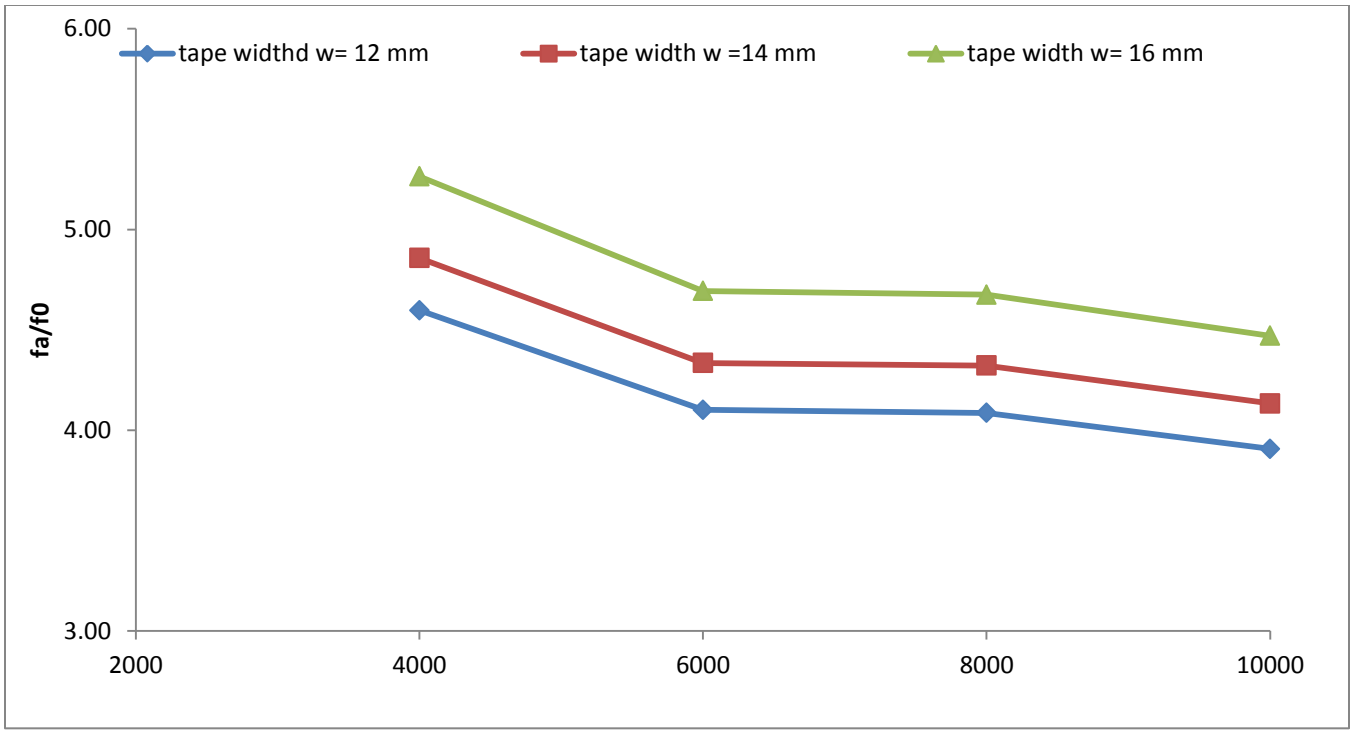

Fig.6.18. Variation of f_a/f_0 with Reynolds number in turbulent regime, twist ratio y=4(RWTT)

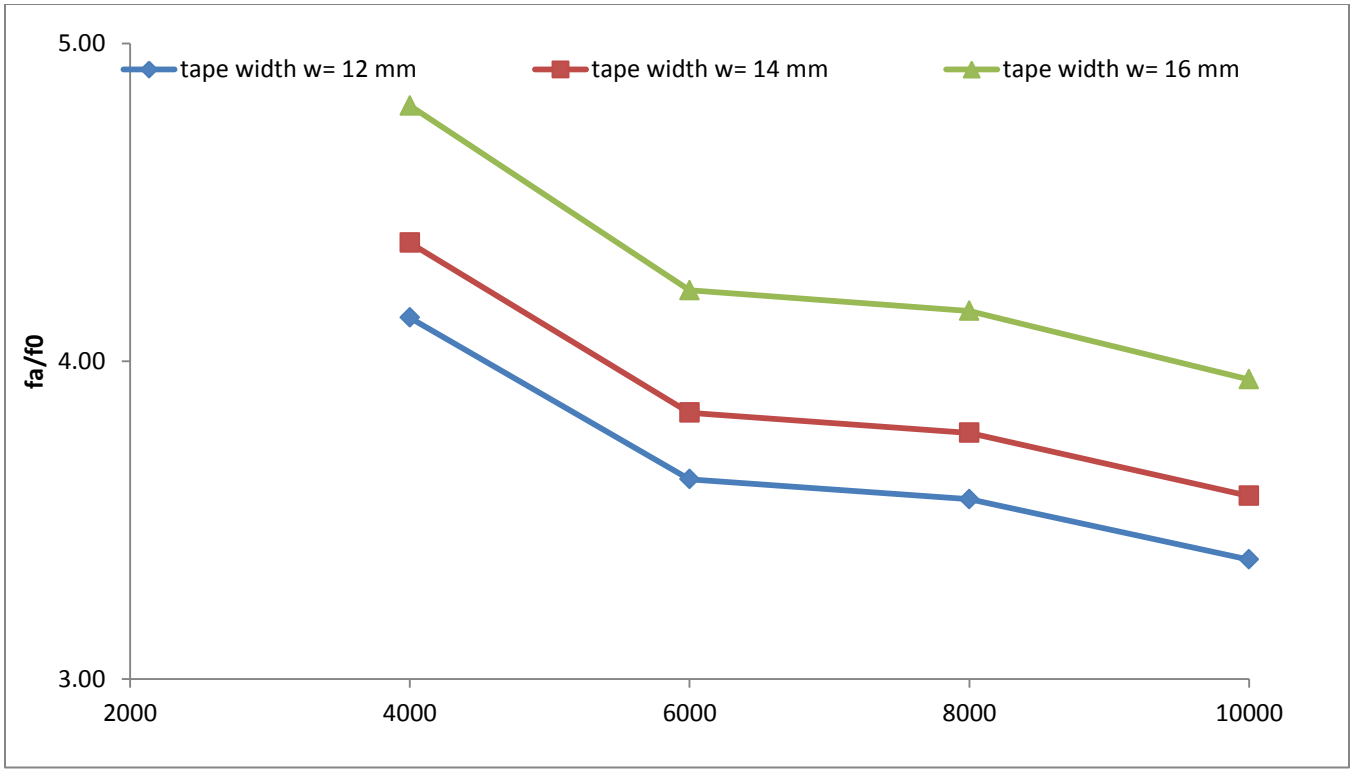

Fig.6.19. Variation of f_a/f_0 with Reynolds number in turbulent regime, twist ratio y=5 (RWTT)

6.2.5. Thermal Performance factor (η):

The Thermal Performance factor for different case are compared and shown in Fig.6.20 in laminar region Fig.6.21 is turbulent region and the related values are given in Table. A.10. In laminar region it is shows that the maximum value is 0.91 it means that there is no effect in this region. In turbulent region the thermal performance factor increase with Reynolds number increases corresponding tape widths of the, w = 12 mm, 14 mm, 16 mm.

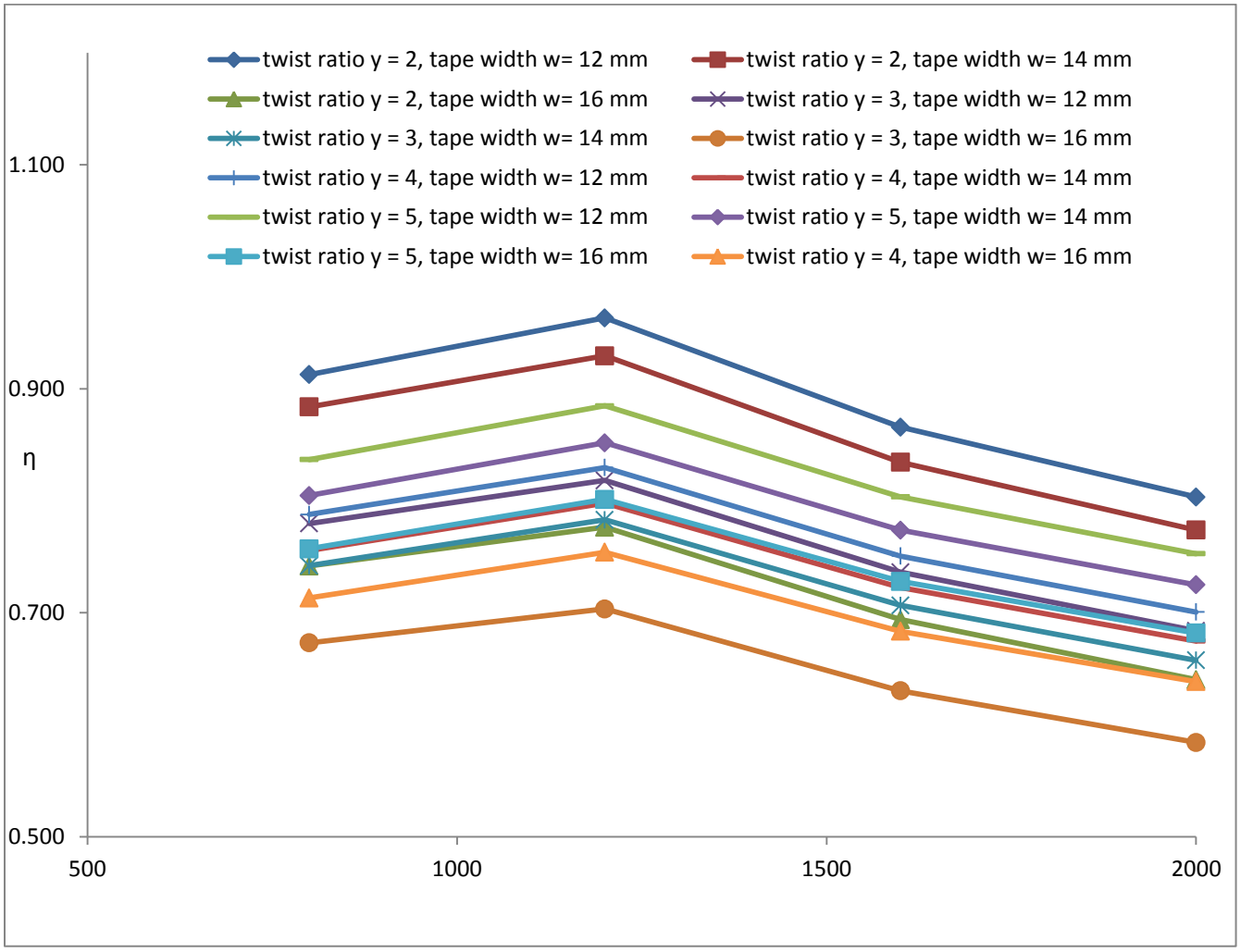

Fig.6.20. Thermal performance factor for finned tube with twisted tape inserts in laminar regime, (RWTT)

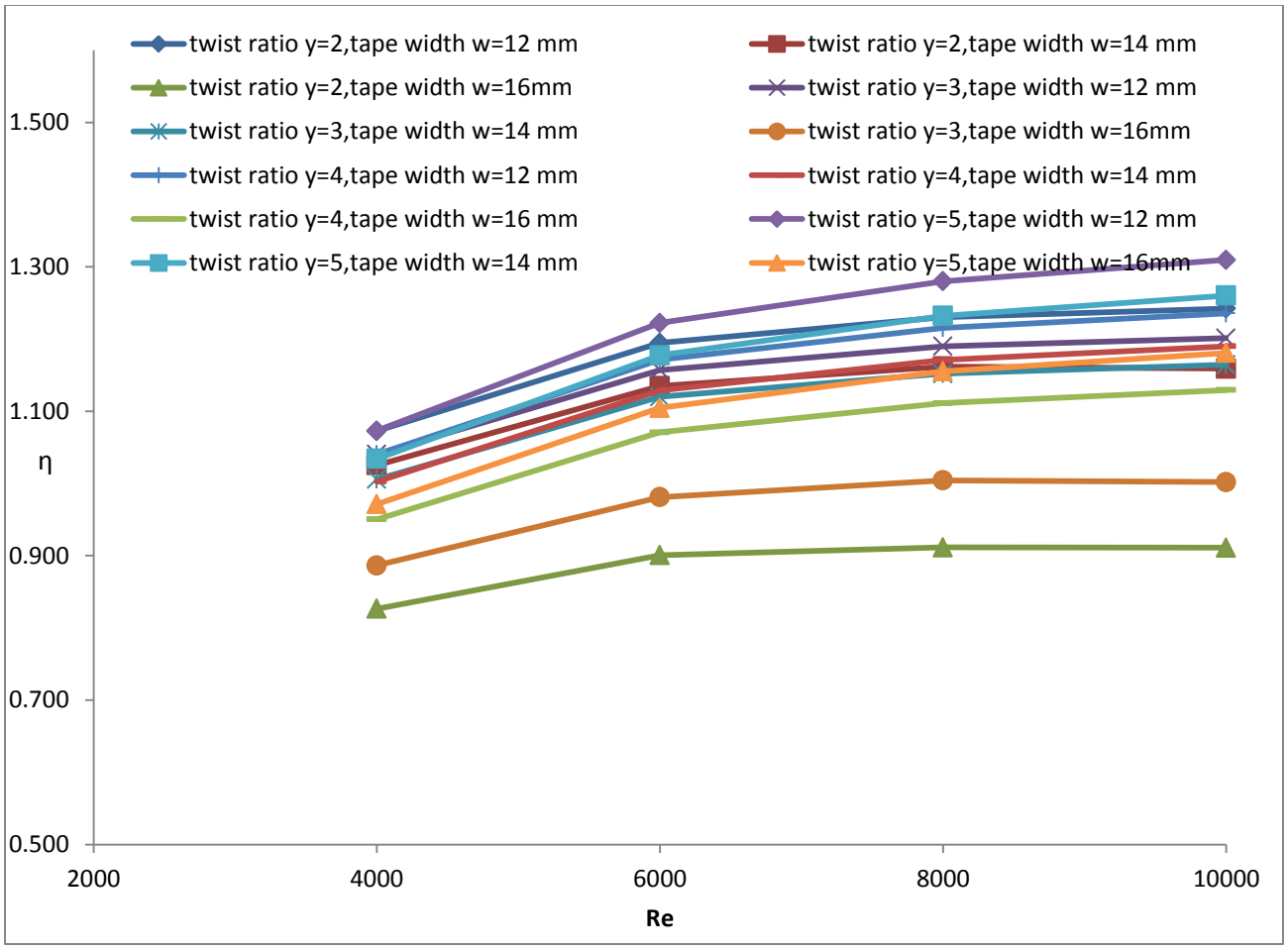

Fig.6.21. Thermal performance factor for finned tube with twisted tape inserts in turbulent regime, (RWTT)

6.3. Conclusion

It is shown that the twisted tape inserts for twist ratio (y=2) can enhance heat transfer rates up to 3.76 times at Reynolds number 2000 with tape width of 16 mm and increase in friction factors nearly 14 times in comparison with those of the plain tube. Thermal performance factor (η) was found to initially increase with increase in Reynolds number then decrease in the laminar region and increase with increase Reynolds number in the turbulent region. The maximum value of the thermal performance factor was found to be 1.31 for Twisted tape (y=5) and tape width of 12 mm at a Reynolds number of 10000

CHAPTER 7

CONCLUSION

Conclusion

The numerical analysis of heat and fluid-flows through a constant wall temperature circular plain tube and finned tube fitted with twisted tape is carried out, with the aim to investigate the effect of tape twist ratio (y=H/d) and tape width on heat transfer (Nu), friction factor (f) and thermal performance (η) behaviors in the laminar and turbulent flow regime.

The main findings can be drawn as follows.

1. Turbulent modeling was done with standard k–ε turbulence model, the Renormalized Group (RNG) k–ε turbulence model, the standard k–ω turbulence model, and the Shear Stress Transport (SST) k–ω turbulence model.

2. The CFD results of Nusselt number and friction factor are compared with those obtained from Manglik and Bergles equations. It is clearly seen that the predicted Nusselt numbers obtained from the SST k–ω turbulence models is in better agreement compared to those from other models. The SST k–ω turbulence model is valid within ±20.2% error limit with measurements for Nusselt number and ±26.4% for friction factor. Therefore this model used for further studies.

3. Plain tube with full width twisted tape inserts, (FWTT) of twist ratio, (y=2, 3, 4, 5) results show that Nusselt number and friction factor values were found to decrease with increasing in twist ratio. Twisted tape inserts for twist ratio (y=2) can enhance heat transfer rates up to 3.5 times at Reynolds number 2000 and increase in friction factors nearly 9 times in comparison with those of the plain tube. Thermal performance factor (η) was found to increase with increase in Reynolds number in the laminar region and decrease in the turbulent region. The maximum value of the thermal performance factor was found to be 1.6 for Twisted tape (y=3) in plain tube at a Reynolds number of 2000

4. Finned tube with reduced width twisted tape,(RWTT) simulation results are shown that the twisted tape inserts of twist ratio (y=2) can enhance heat transfer rates up to 3.76 times at Reynolds number 2000 with tape width of 16 mm and the corresponding increase in friction factors nearly 14 times in comparison with those of the plain tube. Thermal performance factor

(η) was found to initially increase with increase in Reynolds number then decrease in the laminar region and increase with increase Reynolds number in the turbulent region. The maximum value of the thermal performance factor was found to be 1.31 for Twisted tape (y=5) and tape width of 12 mm in a Reynolds number of 10000

REFERENCES

1. Bergles.A.E. (2001), the implications and challenges of enhanced heat transfer for the chemical process industries" Trans IChemE Vol.79 pp.437-444

2. Syam sundar, L. sharma, K.V. (2011), Laminar convective heat transfer and friction factor of Al_2O_3 nanofluid in circular tube fitted with twisted tape inserts, International Journal of Automotive and Mechanical Engineering, Volume 3, pp. 265-278

3. Adrian, B. Allan, D. K. (2003), Heat transfer enhancement. In Heat Transfer Handbook, Chapter 14, pp.1033, -1101, Wiley-interscience.

4. Bergles, A.E. Blumenkrantz, A.R. Taborek, J. (1974), Performance evaluation criteria for enhanced heat transfer surfaces. Proc. of 5th Int. Heat Conf., Tokyo, Vol. 2, pp. 239-243

5. Lokanath, M. S. (1997), Performance evaluation of full length and half-length twisted tape inserts on laminar flow heat transfer in tubes. In Proceedings of 3rd ISHMT–ASME Heat and Mass Transfer Conference, India, pp. 319–324

6. Ray, S. Date, A.W. (2001), Laminar flow and heat transfer through square duct with twisted tape insert, International journal of Heat and Fluid Flow, Vol. 22, pp. 460-472

7. Manglik, R. K. and Bergles, A. E. (1993), Heat transfer and pressure drop correlations for twisted-tape inserts in isothermal tubes: Part I: laminar flows. Trans. ASME, J. Heat Transfer, Vol.115, pp.881–889.

8. Saha, S. K. and Dutta, A. (2001), Thermo-hydraulic study of laminar swirl flow through a circular tube fitted with twisted tapes. Trans. ASME, J. Heat Transfer, Vol.123, pp. 417–421.

9. Tariq, A. Kant, K. and Panigrahi, P. K. (2000), Heat transfer enhancement using an internally threaded tube. In Proceedings of 4th ISHMT–ASME Heat and Mass Transfer Conference, India, pp. 277–281.

10. Saha, S. K. and Bhunia, K. (2000), Heat transfer and pressure drop characteristics of varying pitch twisted-tape-generated laminar smooth swirl flow. In Proceedings of 4th ISHMT– ASME Heat and Mass Transfer Conference, India, pp. 423–428.

11. Ray, S. and Date, A. W.(2003), Friction and heat transfer characteristics of flow through square duct with twisted tape insert, Int. J. Heat and Mass Transfer, Vol. 46, pp.889–902.

12. Lokanath, M. S. and Misal, R. D. (2002), An experimental study on the performance of plate heat exchanger and an augmented shell and tube heat exchanger for different types of fluids for marine applications. In Proceedings of 5th ISHMT– ASME Heat and Mass Transfer Conference, India, pp. 863–868

13. Saha, S. K. Dutta, A. and Dhal, S. K. (2001), Friction and heat transfer characteristics of laminar swirl flow through a circular tube fitted with regularly spaced twisted-tape elements. Int. J. Heat and Mass Transfer, Vol. 44, pp. 4211–4223.

14. Al-Fahed, S. Chamra, L. M. Chakroun, W. (1999), Pressure drop and heat transfer comparison for both micro-fin tube and twisted-tape inserts in laminar flow. Exp. Thermal and Fluid Sci., Vol.18, pp.323–333.

15. Liao, Q. and Xin, M. D. (2000), Augmentation of convective heat transfer inside tubes with three-dimensional internal extended surfaces and twisted tape inserts. Chem. Eng. J.Vol.78, pp. 95–105.

16. Ujhidy. A, Nemeth, J. Szepvolgyi, J. (2003), Fluid flow in tubes with helical elements. Chem. Engg and Processing, Vol.42, pp.1–7.

17. Suresh Kumar, P., Mahanta, P. and Dewan, A. (2003), Study of laminar flow in a large diameter annulus with twisted tape inserts. In Proceedings of 2nd International Conference on Heat Transfer, Fluid Mechanics, and Thermodynamics, Victoria Falls, Zambia, paper KP3.

18. Wang, L. and Sunden, B. (2002), Performance comparison of some tube inserts. Int. Commun. Heat Transfer, Vol. 29, pp.45–56.

19. Saha, S. K. and Chakraborty, D. (1997), Heat transfer and pressure drop characteristics of laminar flow through a circular tube fitted with regularly spaced twisted tape elements with multiple twists. In Proceedings of 3rd ISHMT–ASME Heat and Mass Transfer Conference, India, pp. 313–318

20. Guo, J. Fan, A. Zhang, X. Liu, V. (2011), A numerical study on heat transfer and friction factor characteristics of laminar flow in a circular tube fitted with center-cleared twisted tape, International Journal of Thermal Sciences, Vol. 50, pp. 1263-1270

21. Kumar, P. M. Kumar, K. (2012), Enhancement of heat transfer of laminar flow in a square ribbed duct with twisted tape International Journal of Engineering Science and Technology, Vol. 4, pp. 3450-3456

22. Zhang, X. Liu, Z. Liu, W. (2012) Numerical studies on heat transfer and flow characteristics for laminar flow in a tube with multiple regularly spaced twisted tapes, International Journal of Thermal Sciences Vol.58, pp. 157-167

23. 4. Manglik, R. M. and Bergles, A. E. (1993), Heat transfer and pressure drop correlations for twisted tape insert in isothermal tubes. Part 1: laminar flows. Trans. ASME, J. Heat Transfer, Vol. 116, pp. 881–889.

24 Kumar, A. and Prasad, B. N. (2000), Investigation of twisted tape inserted solar water heater heat transfer, friction factor and thermal performance results. Renewable Energy, vol. 19, pp. 379–398.

25. AI-Fahed, S. and Chakroun, W. (1996), Effect of tube tape clearance on heat transfer for fully developed turbulent flow in a horizontal isothermal tube. Int. J. Heat and Fluid Flow, Vol.17, pp. 173–178.

26. Rao, M. M. and Sastri, V. M. K. (1995), Experimental investigation for fluid flow and heat transfer in a rotating tube twisted tape inserts. Int. J. Heat and Mass Transfer, Vol. 16, pp. 19–28.

27. Sivanshanmugam, P. and Sunduram, S. (1999), Improvement in performance of heat exchanger fitted with twisted tape. J. Energy Engg, Vol.125, pp. 35–40.

28. Agarwal, S. K. and Raja Rao, M. (1996), Heat transfer augmentation for flow of viscous liquid in circular tubes using twisted tape inserts. Int. J. Heat Mass Transfer, Vol. 99, pp.3547–3557.

29. Chung, S. Y. and Sung, H. J. (2003), Direct numerical simulation of turbulent concentric annular pipe flow. Part 2: heat transfer.Int. J. Heat and Fluid Flow, Vol. 24, pp.399–411.

30. Gupte, N. S. and Date, A. W. (1989), Friction and heat transfer characteristics of helical turbulent air flow in annuli. Trans.ASME, J. Heat Transfer, Vol. 111, pp. 337–344.

31. Rahimi, M. Shabanian, S.R. Alsairafi. A.A. (2009), Experimental and CFD studies on heat transfer and friction factor characteristics of a tube equipped with modified twisted tape inserts, Chemical Engineering and Processing, Vol.48, pp.762–770

32. Murugesan, P. Mayilsamy, Suresh, K. (2010), Heat Transfer and Friction Factor Studies in a Circular Tube Fitted with Twisted Tape Consisting of Wire-nails, Chinese Journal of Chemical Engineering, Vol. 18, pp. 1038—1042

33. S. Eiamsa-ard, S. Wongcharee, K. Sripattanapipat, S. (2009), 3-D Numerical simulation of swirling flow and convective heat transfer in a circular tube induced by means of loose-fit twisted tapes, International Communications in Heat and Mass Transfer Vol.36, pp. 947–955

34. Yadav, R. J. Padalkar, A. S. (2012), CFD Analysis for Heat Transfer Enhancement inside a Circular Tube with Half-Length Upstream and Half-Length Downstream Twisted Tape, Journal of Thermodynamics, Vol.1, PP. 1-12

35. Versteeg, H. K. Malalasekera, W. (1996), Introduction to computational fluid: The finite volume method, Longman Scientific & Technical.

36. ANSYS FLUENT 12.0 Theory Guide. ANSYS, Inc. (2009)

37. Kumar, P. (2011) A CFD Study of Heat Transfer Enhancement in Pipe Flow with Al_2O_3 Nanofluid, World Academy of Science, Engineering and Technology vol. 57 pp.746-750

APPENDIX

Table.A.1. Comparison of Nu with Reynolds number in plain tube

Reynolds number, Re	Pressure drop ΔP. Pa	Friction factor, f CFD ($f \times 10^{-3}$)	Friction factor, f Correlations	% difference
800	6.04	220	200	-10.0
1200	9.46	150	133	-15.4
1600	13.18	120	100	-20.0
2000	17.15	100	80.0	-25.0
4000	65.92	9.90	8.80	-12.6
6000	131.62	8.80	8.10	-8.6
8000	226.40	8.50	7.60	-0.5
10000	330.05	7.90	7.30	-6.8

Table.A.2. Comparison of friction factor with Reynolds number in plain tube

Reynolds number, Re	Heat transfer Coefficient, h	Nusselt number CFD	Nusselt number Correlations	% difference
800	190.28	6.97	6.47	- 7.82
1200	231.14	8.47	8.82	3.91
1600	266.30	9.76	9.71	- 0.56
2000	298.14	10.93	10.46	4.50
4000	723.81	26.53	29.47	9.98
6000	1124.01	41.21	47.62	13.46
8000	1477.45	54.17	63.82	15.12
10000	1785.64	65.47	78.71	16.82

Table.A.3. Simulated and calculated values of Nusselt number at y=5

Re	Manglik and Bergles	Standard k -ϵ	percentage difference	RNG k-ϵ	percentage difference	Standard K-ω	percentage difference	SST k-ω	percentage difference
800	12.30	13.13	-6.73	13.11	-6.58	13.11	-6.58	13.11	-6.58
1200	18.57	17.95	3.34	17.95	3.31	17.79	4.16	17.80	4.13
1600	24.87	22.35	10.13	22.33	10.18	21.96	11.67	21.98	11.62
2000	31.19	26.40	15.36	25.80	17.27	25.79	17.32	25.79	17.32
4000	51.34	43.54	15.19	43.54	15.18	42.46	17.30	42.48	17.25
6000	71.01	58.74	17.28	58.75	17.27	57.28	19.34	57.31	19.29
8000	89.39	74.40	16.77	74.44	16.72	72.33	19.08	72.39	19.01
10000	106.86	87.69	17.94	87.62	18.01	85.12	20.34	85.23	20.24

Table.A.4. Simulated and calculated values of friction factor at y=5

Re	Manglik and Bergles	Standard k -ϵ	percentage difference	RNG k-ϵ	percentage difference	Standard K-ω	percentage difference	SST k-ω	percentage difference
800	0.082	0.108	-32.17	0.106	-30.56	0.103	-25.96	0.103	-25.96
1200	0.063	0.082	-29.74	0.082	-29.75	0.077	-21.66	0.077	-21.90
1600	0.053	0.073	-37.96	0.067	-27.35	0.063	-18.09	0.063	-18.30
2000	0.046	0.059	-27.49	0.054	-15.73	0.054	-15.53	0.054	-15.73
4000	0.029	0.039	-35.25	0.039	-35.23	0.035	-19.55	0.035	-19.70
6000	0.026	0.031	-18.61	0.031	-18.62	0.028	-7.43	0.028	-7.47
8000	0.024	0.028	-15.48	0.028	-15.68	0.026	-5.60	0.026	-5.70
10000	0.023	0.025	-10.09	0.025	-10.00	0.023	-0.97	0.023	-1.10

Table.A.5. Variation of Nu_a/Nu_0 with Reynolds number in plain tube with FWTT

Re	y=2	y=3	y=4	y=5
800	2.67	2.44	2.10	1.88
1200	2.99	2.72	2.35	2.10
1600	3.20	2.92	2.52	2.25
2000	3.35	3.06	2.64	2.36
4000	1.92	1.74	1.65	1.60
6000	1.67	1.51	1.44	1.39
8000	1.60	1.46	1.38	1.34
10000	1.56	1.42	1.35	1.30

Table.A.6 Variation of f_a/f_0 with Reynolds number in plain tube with FWTT

Re	y=2	y=3	y=4	y=5
800	8.77	6.09	5.14	4.67
1200	9.81	6.77	5.67	5.12
1600	10.07	6.94	5.80	5.22
2000	10.39	7.15	5.97	5.37
4000	5.59	4.39	3.84	3.54
6000	5.05	3.96	3.47	3.20
8000	4.84	3.80	3.33	3.07
10000	4.69	3.68	3.22	2.97

Table.A.7 Variation of η with Reynolds number in plain tube with FWTT

Re	y=2	y=3	y=4	y=5
800	1.30	1.33	1.22	1.12
1200	1.40	1.44	1.32	1.22
1600	1.48	1.53	1.40	1.30
2000	1.54	1.59	1.46	1.35
4000	1.08	1.06	1.06	1.05
6000	0.97	0.96	0.95	0.94
8000	0.95	0.93	0.92	0.92
10000	0.93	0.92	0.91	0.91

Table.A.8.Variation of Nu_a/Nu_0 with Re in finned tube with RWTT

	y=2			Y=3			Y=4			y=5		
Re	w=12 mm	w=14 mm	w=16 mm	w=12 mm	w=14 mm	w=16 mm	w=12 mm	w=14 mm	w=16 mm	w=12 mm	w=14 mm	w=16 mm
800	2.10	2.20	2.86	2.32	2.50	2.89	2.25	2.39	2.61	2.08	2.21	2.42
1200	2.10	2.22	2.90	2.33	2.49	2.93	2.24	2.38	2.59	2.06	2.18	2.39
1600	2.41	2.54	3.35	2.67	2.84	3.36	2.53	2.68	2.92	2.31	2.44	2.68
2000	2.67	2.83	3.76	2.96	3.14	3.74	2.79	2.95	3.21	2.53	2.67	2.93
4000	1.72	1.84	2.54	1.67	1.76	2.13	1.60	1.69	1.83	1.50	1.58	1.74
6000	1.49	1.61	2.28	1.46	1.53	1.87	1.37	1.44	1.56	1.26	1.33	1.46
8000	1.45	1.58	2.28	1.42	1.49	1.83	1.32	1.39	1.50	1.19	1.26	1.39
10000	1.42	1.58	2.27	1.39	1.46	1.83	1.27	1.35	1.46	1.15	1.21	1.34

Table.A.9.Variation of f_a/f_0 with Re in finned tube with RWTT

	y=2			Y=3			Y=4			y=5		
Re	w=12 mm	w=14 mm	w=16 mm	w=12 mm	w=14 mm	w=16 mm	w=12 mm	w=14 mm	w=16 mm	w=12 mm	w=14 mm	W=16 mm
800	7.03	7.38	9.60	5.92	6.38	7.38	5.54	5.90	6.43	5.27	5.59	6.12
1200	8.29	8.74	11.45	6.97	7.45	8.74	6.42	6.81	7.41	6.02	6.37	6.98
1600	9.03	9.55	12.59	7.56	8.04	9.55	6.89	7.30	7.93	6.40	6.77	7.42
2000	9.90	10.47	13.92	8.27	8.77	10.47	7.47	7.90	8.58	6.89	7.28	7.99
4000	6.26	6.69	9.25	5.26	5.54	6.69	4.60	4.86	5.26	4.14	4.37	4.80
6000	5.68	6.13	8.67	4.78	5.02	6.13	4.10	4.34	4.69	3.63	3.84	4.22
8000	5.72	6.23	8.97	4.83	5.07	6.23	4.09	4.32	4.68	3.57	3.77	4.16
10000	5.52	6.13	8.79	4.67	4.89	6.13	3.91	4.13	4.47	3.38	3.58	3.94

Table.A.10.Variation of η with Reynolds number in finned tube with RWTT

	y=2			Y=3			Y=4			y=5		
Re	w=12 mm	w=14 mm	w=16 mm	w=12 mm	w=14 mm	w=16 mm	w=12 mm	w=14 mm	w=16 mm	w=12 mm	w=14 mm	w=16 mm
800	0.91	0.88	0.74	0.78	0.74	0.67	0.79	0.76	0.71	0.84	0.80	0.76
1200	0.96	0.93	0.78	0.82	0.78	0.70	0.83	0.80	0.75	0.88	0.85	0.80
1600	0.87	0.83	0.69	0.74	0.71	0.63	0.75	0.72	0.68	0.80	0.77	0.73
2000	0.80	0.77	0.64	0.68	0.66	0.58	0.70	0.67	0.64	0.75	0.73	0.68
4000	1.07	1.03	0.83	1.04	1.01	0.89	1.04	1.00	0.95	1.07	1.03	0.97
6000	1.19	1.13	0.90	1.16	1.12	0.98	1.17	1.13	1.07	1.22	1.18	1.10
8000	1.23	1.16	0.91	1.19	1.15	1.00	1.22	1.17	1.11	1.28	1.23	1.16
10000	1.24	1.16	0.91	1.20	1.16	1.00	1.24	1.19	1.13	1.31	1.26	1.18